Universidade de Aveiro
2013
Departamento de Engenharia de Materiais e Cerâmica

Joel Bento Puga

Compositos de WC – (Cu, Fe, Cr, Ni) obtidos por mecano – síntese

WC – (Cu, Fe, Cr, Ni) composites attained by mechanosynthesis

Universidade de Aveiro
2013
Departamento de Engenharia de Materiais e Cerâmica

Joel Bento Puga

Compósitos de WC – (Cu, Fe, Ni, Cr) obtidos por mecano - síntese

WC – (Cu, Fe, Cr, Ni) composites attained by mechanosynthesis

Dissertação apresentada à Universidade de Aveiro para cumprimento dos requisitos necessários à obtenção do grau de Mestre em Engenharia de Materiais, realizada sob a orientação científica da Doutora Cristina Maria da Silva Fernandes Bolseira de Pós-Doutoramento e coorientação da Professora Ana de Oliveira e Rocha Senos, Professora Associada do Departamento de Engenharia de Materiais e Cerâmica da Universidade de Aveiro

o júri

Presidente

Professor Doutor Jorge Ribeiro Frade
Professor Catedrático da Universidade do Aveiro

Professor Doutor Fernando António Gaspar Simões
Professor Adjunto do Instituto Superior de Engenharia de Coimbra

Doutora Cristina Maria da Silva Fernandes
Bolseira de pós – doutoramento da Universidade de Aveiro

agradecimentos

Á Professora Doutora Ana Maria de Oliveira e Rocha Senos pela sua disponibilidade e empenho na orientação deste trabalho.

À Doutora Cristina Maria da Silva Fernandes, pela orientação e enorme apoio prestado em todas as vertentes deste trabalho e pela sua disponibilidade.

Ao Departamento de Engenharia Cerâmica e do Vidro por todas as análises e ensaios efetuados no decorrer deste trabalho.

Por fim, mas não por último, aos meus Pais por todo o esforço, paciência e amor dedicados, que me deram força e exemplo e me permitiram chegar ao final deste curso superior e sonhar com uma vida melhor, mais justa e sábia.

palavras-chave

carboneto de tunsténio, metal duro, aço, cobre, moagem de alta energia, sinterização, propriedades mecânicas

resumo

Este trabalho tem como objetivo estudar a viabilidade da substituição do ligante cobalto por cobre e aço inoxidável em compósitos de carboneto de tungsténio. Estes compósitos foram preparados com um teor de ligante de 12% pp, utilizando o método de pulverometalurgia no qual a moagem convencional foi substituída pela moagem de alta energia (MAE). Por forma a obter compósitos de elevada densidade, boa uniformidade microestrutural, e composição de fases adequada a um bom desempenho mecânico, foram otimizadas as condições de processamento das etapas de moagem de alta energia e da sinterização.

As melhores condições de moagem foram verificadas com uma velocidade de rotação de 350 rpm, um rácio de peso bolas:material de 20:1 e, dependendo da composição estudada, um tempo de moagem variável entre 8 – 10 horas.

Utilizando o processo de MAE foi possível reduzir o tamanho de partícula dos pós compósitos até à nanoescala e ainda obter uma boa uniformidade da distribuição da fase ligante. Após compactação, os pós foram submetidos a uma etapa de sinterização em vácuo num intervalo de temperaturas entre 1300 - 1500 °C, seguindo-se uma etapa de prensagem isostática a quente.

Este método permitiu obter compactos de densidade elevada e introduzir de forma eficiente até 30% de cobre na fase ligante de aço inoxidável sem se verificarem reduções substanciais da densidade dos compactos sinterizados. Os compósitos de WC-SS apresentam uma composição de fases com uma quantidade elevada de fase M_6C, formada durante a sinterização e que é favorecida nestes materiais, devido à elevada reatividade dos pós nanométricos. Contudo, a adição de cobre ao compósito WC-SS permitiu a diminuição da formação de fase M_6C. As amostras sinterizadas de WC-Cu apresentam maioritariamente duas fases distintas, W_2C e $Cu_{0.4}W_{0.6}$ e o aparecimento desta última fase depende da técnica de sinterização utilizada, convencional e sinterização em duas etapas respetivamente.

A caracterização mecânica revelou que a dureza dos compósitos de WC-SS é equivalente aos valores indicados na literatura para os compósitos de WC-Co, enquanto a tenacidade permanece abaixo dos valores de referência. No entanto, foi possível alcançar um bom equilíbrio entre a dureza e tenacidade nos compósitos de WC-(SSCu), o que poderá permitir a sua utilização em algumas aplicações dos tradicionais carbonetos cementados de WC-Co.

keywords

Tungsten carbide, hardmetal, stainless steel, copper, high energy ball milling, sintering, mechanical properties.

abstract

This work aims to study the feasibility of replacing cobalt by copper and stainless steel in tungsten carbide composite. The composites were prepared with a binder content of 12 wt% using the powder metallurgy method in which the conventional milling was replaced by high energy ball milling. To obtain a composite with high density, good microstructure uniformity and controlled phase composition, suitable for a good mechanical performance, the processing conditions of the high energy ball milling (HEBM) and sintering methods were enhanced.

Within the studied parameters, the prime milling conditions were found at the rotation speed of 350 rpm and ball-to-powder weight ratio of 20:1, varying the milling times between 8-10 hours for the studied compositions.

The HEBM process was able to reduce the particle size of the composite powders down to the nanoscale and a good binder homogenization was reached. After compacting, the powders were submitted to vacuum sintering, in a temperature range of 1300 – 1500ºC followed by HIP (hot isotactic pressing).

This procedure allowed attaining dense compacts and introduce efficiently copper in the stainless steel binder up to 30%, without substantial decrease of the sintered relative density. The WC-SS composite powders show a significant amount of M_6C phase formed during sintering, endorsed by the high reactivity of the small powder particles and the appearing of the M_6C phase. Adding copper to the WC-SS composite allowed the decrease of the M_6C phase formation. The WC-Cu sintered samples revealed two distinct major phases, W_2C and $Cu_{0.4}W_{0.6}$ and their appearance depends on the applied sintering technique, in the case of being conventional or two stages sintering, respectively.

The mechanical characterization revealed that the hardness of the WC-SS compacts is equivalent to the reported values in the literature for WC-Co. On the other hand, the fracture toughness remains below the reference values. Nevertheless, it was possible to attain a good balance between hardness and fracture toughness in the WC-(SSCu) composites, which make them promising candidates for substituting the traditional WC-Co composite.

Table of Contents

List of Figures

List of Tables

Chapter 1

Introduction

1. Introduction

Tungsten carbide (WC) composites are considered one of the oldest and most successful powder metallurgy products. The production of these composites dates back to 1923, still they have a wide field of application; from the oil and gas, mining and pharmaceutical industries to specific applications in the engineering field [1, 2]. In 2003 the global market was estimated at $ 12 billion [3-5].

The success of these materials is in large part due to its mechanical properties, which result from the combination of a hard phase, brittle and abrasion resistant (WC) with a ductile phase, usually cobalt (Co). However, the use of cobalt has been increasingly equated, since its reserves are located in geopolitically unstable areas (in 2009, 49 % of cobalt came from the Democratic Republic of Congo), and thus frequent fluctuations occur in supply causing price inflation, forcing companies and suppliers to increase stocks of this raw material, thereby increasing the operating costs [5]. On the other hand, the authorities have also alerted to the cobalt toxicity, representing risks for the handlers, which may result in short-term implementation of restrictive legislation in the use of this element. In parallel, there is also the need to avoid the restrictions of the initial patent WC-Co. Taking into account the current state in the development of WC composites based materials, the investigations in this field lays on the following four main topics:

a) development of a new material with superior properties;
b) modification of existing material with the addition of new elements;
c) improving the processing of existing materials;
d) development of new processing methods.

This work will focus on the last three threads. The modification of the existing material by total replacement of cobalt by alternative binders based alloys, Cu, Fe, Ni, and Cr (with the Fe , Ni and Cr introduced in the form of stainless steel), aiming to improve the properties: toughness, hardness and oxidation resistance of cemented carbide based on WC. The development and improvement of the processing steps of these composites will be focused in the milling/homogenization step of the powders, applying the high energy milling to reduce the particle size and simultaneously promote the mechano-synthesis of the binder phase. In comparison to the conventional milling, the high energy ball milling present

benefits in terms of time consumed and homogeneity of the mixture. Moreover, it is more environmentally friendly since no harmful effluents are generated.

It is significant to note that this type of milling significantly reduces the grain size, allowing to obtain a composite with superior mechanical properties [6]. It is also expected that the substitution of cobalt for stainless steel and copper would result in composites with interesting properties from the mechanical, thermal and corrosion resistance point of view. Previous studies conducted by Marques et al. [7, 8] showed that the use of stainless steel as a binder in the composite WC allows to obtain materials with high hardness and toughness along with superior oxidation resistance.

Copper and stainless steels presents higher resistance to corrosion and ductility than cobalt, and, at high temperatures, copper does not react to form carbides [9]. In addition, the high thermal conductivity of copper may be advantageous for the dissipation of heat during service of cutting tools, drills, among others. Furthermore, it is expected that the addition of copper to stainless steel, in amounts exceeding 1 wt%, will improve atmospheric corrosion and stress corrosion [10, 11].

However, the molten copper has poor wettability in WC surfaces, limiting the densification during sintering and the spreading of the binder among WC particles, thereby compromising the properties of the composite. The mechano-synthesis of the mixture, binder and WC powders, will decrease the particle size and improve the binder distribution in the composite, contributing positively to increase the sinterability. In order to enhance the wettability of copper on WC, some alloying elements such as iron, nickel, and chrome will be added to copper. These elements, added as a selected stainless steel (SS) powder, are considered wet well the WC surfaces and are expected to improve the wettability of the Cu based binder.

Taking into account these considerations, the main objective of the proposed work is to explore the feasibility of Cu-SS binders as alternatives to cobalt in WC-based composites, using high energy ball milling to homogenize and promote the mechano-synthesis of the binder phase. Composites with high density, good microstructural uniformity, controlled grain size and phase composition suitable for good mechanical performance are investigated

Chapter 2

Literature review

2. Literature review

2.1 Cemented tungsten carbides

Cemented tungsten carbides are composites by one or more hard ceramic phases (WC or W_2C) bonded with about 5 – 20 wt % of a ductile metal phase, normally Co or Ni, via liquid-phase sintering. The schematic microstructure of this material is shown in Figure 1.

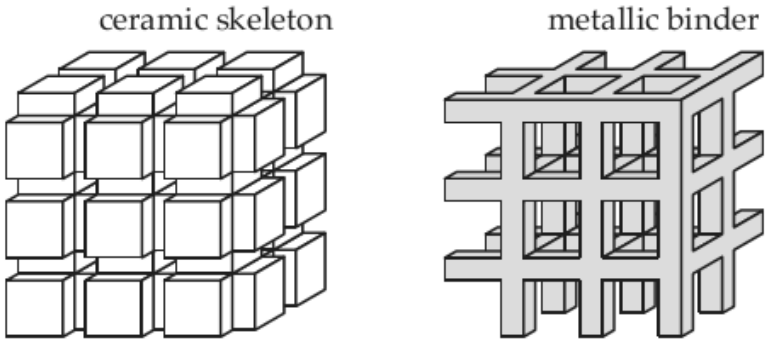

Figure 1 - Typical structure of Cemented Tungsten Carbides [12].

The development of cemented tungsten carbide, was driven to the necessity of replacement of the costly diamond wire drawing, during the First World War in Germany [13]. The first WC alloy (WC – Co) is reported to K. Schroter of Osram Studiengesellschaft Laboratories. After the successful application of cemented carbides in manufacturing dies, this type of materials draw the attention of the scientific community and was used for the development of new and better cutting tools, wear parts and machine components [14]. Most of the further developments were modifications of the Schröter's process, including replacement of part or all of the WC by other carbides, such as tantalum carbide (TaC), titanium carbide (TiC), and/or niobium carbide (NbC), as well as modifications in the microstructure of those composites [15] and in the last 40 years is being made some efforts in the substitution of Co as binder phase.

2.1.1 Classification

There are two types of composites made by the combination of a metal and a ceramic; cemented carbides and cermets:

Cemented carbides – are the carbides formed with the metals of the fourth and the sixth group of the table of elements, and they are one of the two types of composites constituted by metal and ceramic materials. These materials are also known by hardmetals in the industrial field.

Cermets - those are the nitrides, carbonitrides, borides and silicides of the group metals previously mentioned. They are formally designated as “a heterogeneous combination of metal(s) or alloy(s) with one or more ceramic phases and in which there is relatively little solubility between metallic and ceramic phases at the preparation temperature” [16] .

Cemented carbides can be classified by the tungsten carbide/binder content and by the WC grain size (Table1).

Table 1 - Classification of WC composites based on grain size distribution. [16]

Definition	Grain size (μm)
Nano	< 0.2
Ultrafine	0.2 – 0.5
Submicron	0.5 – 0.8
Fine	0.8 – 1.3
Medium	1.3 – 2.5
Coarse	2.5 – 6.0
Extracoarse	>6.0

In terms of the WC/binder classification, those can be subdivided in two different categories; WC-Co grades and alloyed grades.

- **WC-Co grades**

Straight grades, occasionally referred to as unalloyed grades, are nominally pure WC-Co composites. They contain 3-15 wt % Co, for cutting tool grades and up to 30 wt % Co, for wear resistant parts as depicted in Figure 2. Straight grades are used for machining cast iron, nonferrous alloys, and non-metallic materials, but generally not for the machining of steel [15, 16].

The relation between the WC grain size and WC/Co content, has great impact in the composite properties and so determines the application of these materials. Figure 2 shows this relation.

Nano, Ultrafine and Submicron grades - Grades with Co content in the range between of 3-10 wt% and grain size below 1 µm have the highest hardness and compressive strengths, combined with high wear resistance. These grades are used in a wide range of wear parts applications and in cutting tools designed for metallic and non-metallic machining for which a combination of high strength, high wear resistance and sharp cutting edges are essential [17].

Fine and Medium grades - The grades with binder contents between 6-30 wt% and grain sizes of 1-3 µm are used in wear parts and cutting tools when an element of improved strength and shock resistance is required [17].

Medium, Coarse, and Extra Coarse grades - Grades with binder contacts between 6-15 wt% and grain sizes above 3 µm are used in oil & gas and mining applications where resistance to high impact stresses and to abrasive wear are required [17].

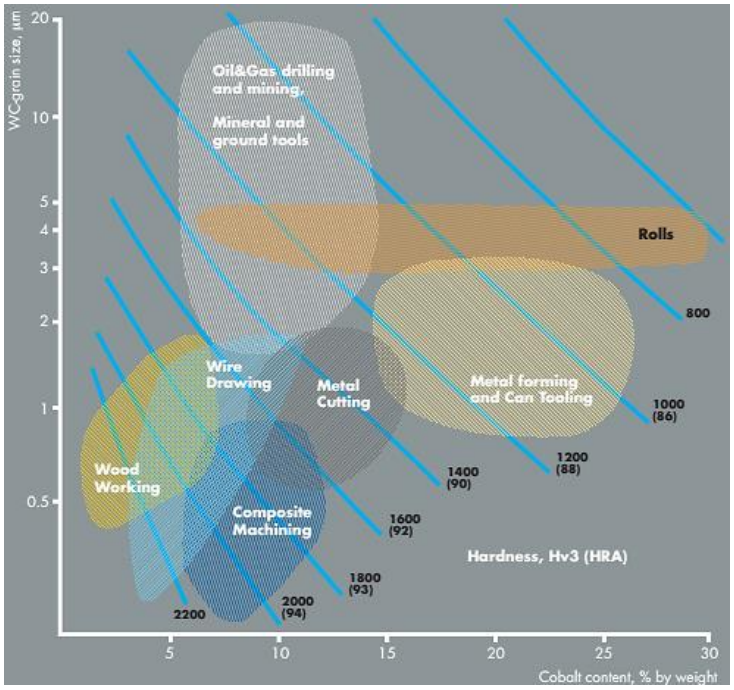

Figure 2 - Applications of WC/Co determined by its grain size and WC/Co content [18].

- **Alloyed grades**

Alloyed grades are also referred to as steel cutting grades, or crater resistance grades, which have been developed to prohibit cratering during the machining of steel. The basic compositions of alloyed grades are 3-12 wt % Co, 2-8 wt % TiC, 2-8 wt % TaC, and 1-5 wt % NbC [15, 16].

2.2. Cemented carbide phases

2.2.1. Hard phase – Tungsten carbide

The discovery of Tungsten Carbide is attributed to Henri Moissan, a Nobel Laureate (1906) and the inventor of electrical furnace. It was in his laboratory at the School of Pharmacy at the University of Paris, that the two forms of Tungsten Carbide were discovered, firstly W_2C in 1896 by H. Moissan and two years later (1898) WC by P. Williams [19]
WC as a refractory carbide is hard, wear resistant, have high melting (>1800 ºC) and high degree of chemical stability. Besides the great academic and scientific interest in these materials, refractory carbides are useful in a numerous applications such as cutting and drilling tools, oxidation – resistant gas burners, bearings, and countless others.

2.2.1.1. WC - Phase equilibria, crystal structure and properties

The compounds existing in the W–C system are W_2C and WC (Figure 3). Both compounds have several polymorphic modifications, stable in different temperature and composition ranges. The major phase is the higher tungsten carbide δ-WC (WC). This phase is the most technically important, since is the only binary phase stable at room temperature.

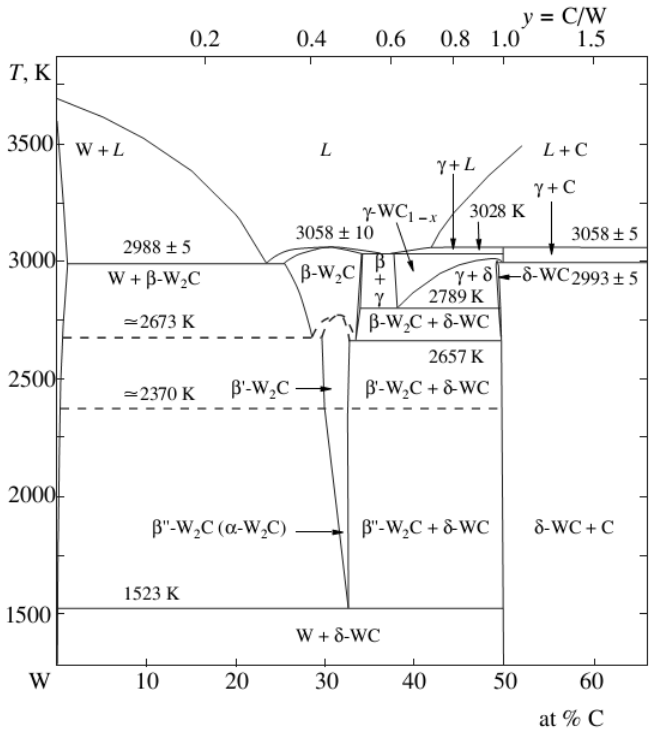

Figure 3 - Phase diagram of the W–C system [20].

The monocarbide WC, has a simple hexagonal structure, with lattice parameters a = 0.2906 nm, c = 0.28375 nm [20]. The W atoms occupies the 0,0,0 position and the carbon atom is located in the $\frac{1}{3}$, $\frac{2}{3}$, $\frac{1}{2}$ position or in the $\frac{2}{3}$, $\frac{1}{3}$, $\frac{1}{2}$ position resulting in a non-centrosymmetric crystal structure (Figure 4) [21].

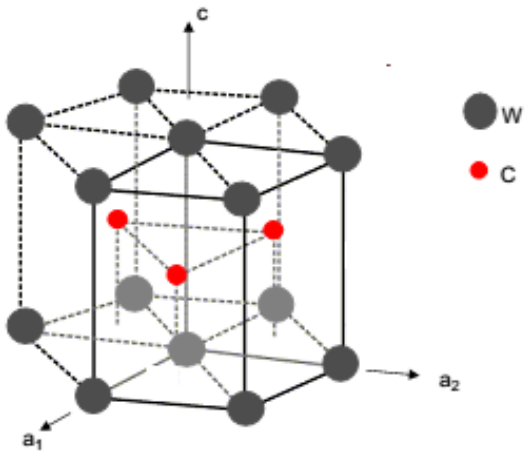

Figure 4 - Schematic image of the crystal structure of WC [21].

Some of the properties and other characteristics of the WC are resumed in Table 2

Table 2 – Properties and characteristics of Tungsten Carbides [13].

Phases	WC (also called δ-WC) W_2C (subcarbide β-WC) γ-WC_{1-x} (unstable, forming only above 2510 ºC)
Crystal structure and lattice parameters (nm)	WC: hexagonal, a = 0.2907, c = 0.2837, c/a = 0.976 W_2C: hexagonal, a = 0.3001, c = 0.4736, c/a = 1.578
Composition	Narrow range of homogeneity, δ-$WC_{0.98}$-$WC_{1.00}$
Molecular weight	WC: 195.86 g/mol W_2C: 379.71 g/mol
Colour	WC: Gray
X-ray density	WC: 15.8 g/cm^3 W_2C: 17.2 g/cm^3
Melting point	WC: 2785ºC W_2C: 2715ºC
Specific Heat (C_p)	WC: 39.8 J/mol K
Heat of Formation ($-\Delta H^o_f$)	WC: 37.7 kJ/g-atom metal at 298 K
Thermal expansion	WC: a = 5.2×10^{-6} ºC^{-1}, c = 7.3×10^{-6} ºC^{-1}
Vickers Hardness **Young's Modulus of Elasticity** **Poisson's Ratio** **Transverse rupture strength**	WC: 22 GPa WC: 620-720 GPa WC: 0.18 WC: 550 MPa
Oxidation resistance	WC: Oxidation in air starts at 500-600 ºC
Chemical resistance	WC is resistant to acids and not attacked at room temperature by mistures of HF and HNO_3, but attacked by these acids at elevated temperature. Attacked by chlorine above 400 ºC and by fluorine at room temperature. Stable in dry hydrogen until the melting point. W_2C is less stable than WC and reacts with Murakami's* reagent.

Test temperature is 20 ºC unless otherwise is stated. *(10g NaOH: 10g $K_3Fe(CN)_6$: 100 ml H_2O)

During the processing and the time of service of the WC and the WC cemented carbides it is important to take into account eventual oxidation effects. As shown in Table 2 the oxidation resistance in air is good at room temperature, but at temperatures higher than 500 ºC a oxide layer is formed [16]. Two stable tungsten oxides, WO_2 and WO_3, can be formed, being the WO_3 the most thermodynamically stable at low temperatures and atmospheric pressures. The following equations resume the oxidation processes in air and in aqueous medium [16]:

$$WC\,(s) + \frac{5}{2}O_2\,(g) \rightarrow WO_3\,(s) + CO_2\,(g) \quad \textbf{(1)}$$

The oxidation resistance of WC in water is good, and even with pre-oxidation exposure the WC is resistant to further oxidation in aqueous media. The main product of reaction from WC and water is WO_3 [16]:

$$WC\,(s) + 3H_2O\,(l) \rightarrow WO_3\,(s) + CH_4\,(g) + H_2\,(g) \quad \textbf{(2)}$$

It is this combination of technological properties and the chemical stability which underlie the wide use of tungsten carbide in the production of wear-resistant hard alloys, which are basic components of tool materials. These considerations, lead one to believe that at least for the short term, WC will be the principal hard phase in new cemented carbide systems under consideration for further development [16].

2.2.2. Binder Phase

The metallic binder phase can be constituted by a single element as in the traditional WC–Co and WC-Ni composites or by the combination of several elements WC-(Co,Ni), WC-(Co,Ni,Fe). The apparent superiority of cobalt relatively to other binders is related to its best commination characteristics in milling, superior wettability in WC, and higher solubility at sintering temperatures. But, because of the relatively high cost of cobalt, scarcity of supply and toxicity, attempts have been made to develop cemented tungsten carbides without Co [7]. Therefore in 1991 Farood et.al [22] attempt the substitution of Co by stainless steel (Fe,Cr,Ni) proving to be feasible. More recently in 2010, Marques et al. [7, 8] showed that the use of stainless steel in substitution of Co as a binder in the composite WC allows to obtain materials with high hardness, in a range 1250 – 1600 HV30 and high toughness 9.5 – 13.7 MPa.$m^{1/2}$ (depending the amount of binder phase 6 – 15 wt.% used), showing that SS can be a good alternative to Co in WC composite materials.

In this work the metallic binder phase studied is comprised by SS and copper to form a WC-(Cu,Fe,Cr,Ni) composite. It is expected that the addition of copper to stainless steel will improve ductility, fracture toughness, oxidation/corrosion resistance and thermal conductivity. Some physical and mechanical properties of the mentioned metallic elements are summarized in Table 3.

Table 3 - Physical and mechanical properties of Cobalt, Copper, Chromium, Iron and Nickel

Physical / Mechanical properties	Co	Cu	Cr	Fe	Ni
Density ($g.cm^{-3}$)	8.90	8.93	7.19	7.87	8.91
Crystal Structure	HCP	FCC	BCC	BCC/FCC	FCC
Melting point (ºC)	1495	1083	1907	1538	1455
Young's modulus (GPa)	209	130	279	211	200
Tensile strength (MPa)	235	455	270	415	462
Hardness, Vickers (MPa)	1043	369	1060	608	638
Thermal conductivity ($W.m^{-1}.K^{-1}$)	100	400	94	80	91

2.2.2.1. Stainless steel.

Stainless steels are ferrous metal alloy with low carbon content and with a minimum content of 10.5 % of Chromium (Cr), allowing the formation of a protective, auto-regenerative oxide film, which is why this group of steels are called stainless.

The group of alloys which today make up the family of stainless steels had their beginning in the years 1900 to 1915. Over this period research work was published by metallurgists in France and Germany on ferritic, martensitic and austenitic stainless steels. The commercialisation of those began in 1920, in the USA and Germany.

- **Classification of Stainless steels**

The criterion for the stainless steel classification, based upon the nature of their metallurgical structure is unusual amongst other metallic alloys [23]. Depending on the exact chemical composition of the steel, the microstructure may be made up of the three following stable phases, austenite, ferrite, or a "duplex" mix of these two. The phase martensite is created when some steels are rapidly quenched from a high temperature, or a structure hardened by precipitated micro-constituents [23]. The relationship between the different families is as shown in Figure 5.

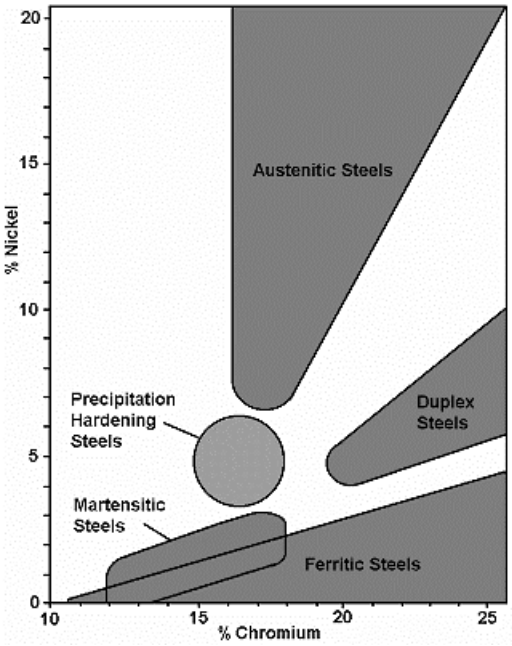

Figure 5 – Families of Stainless Steels [23]

- **Austenitic Stainless Steel AISI 304 L - crystal structure, phase equilibria and properties.**

Austenitic stainless steels are the most common stainless steels and constitute about 65–70% of the total stainless steel production. Their austenitic face centred cubic lattice (FCC) structure with a density of 7.9 g.cm^{-3}, is very tough and ductile down to absolute zero, they possess also high corrosion resistance and toughness at elevated and ambient temperature [24]. Some of these and other properties are summarized in Table 4.

Table 4 – Physical and Mechanical properties of the AISI 304 L stainless steel [25]**.**

Physical / Mechanical properties	
Density (g.cm^{-3})	7.9
Cristal structure	FCC
Melting point (ºC)	1480
Young's modulus (GPa)	193 - 200 GPa
Tensile strength (MPa)	480
Hardness, Vickers (MPa)	158
Thermal conductivity (W.m^{-1}.K^{-1})	16.2

AISI (American iron and steel institute) uses 3 digits for code for stainless steels classification. Figure 6 resumes some of the stainless steels families and the effect of the alloying elements on their properties.

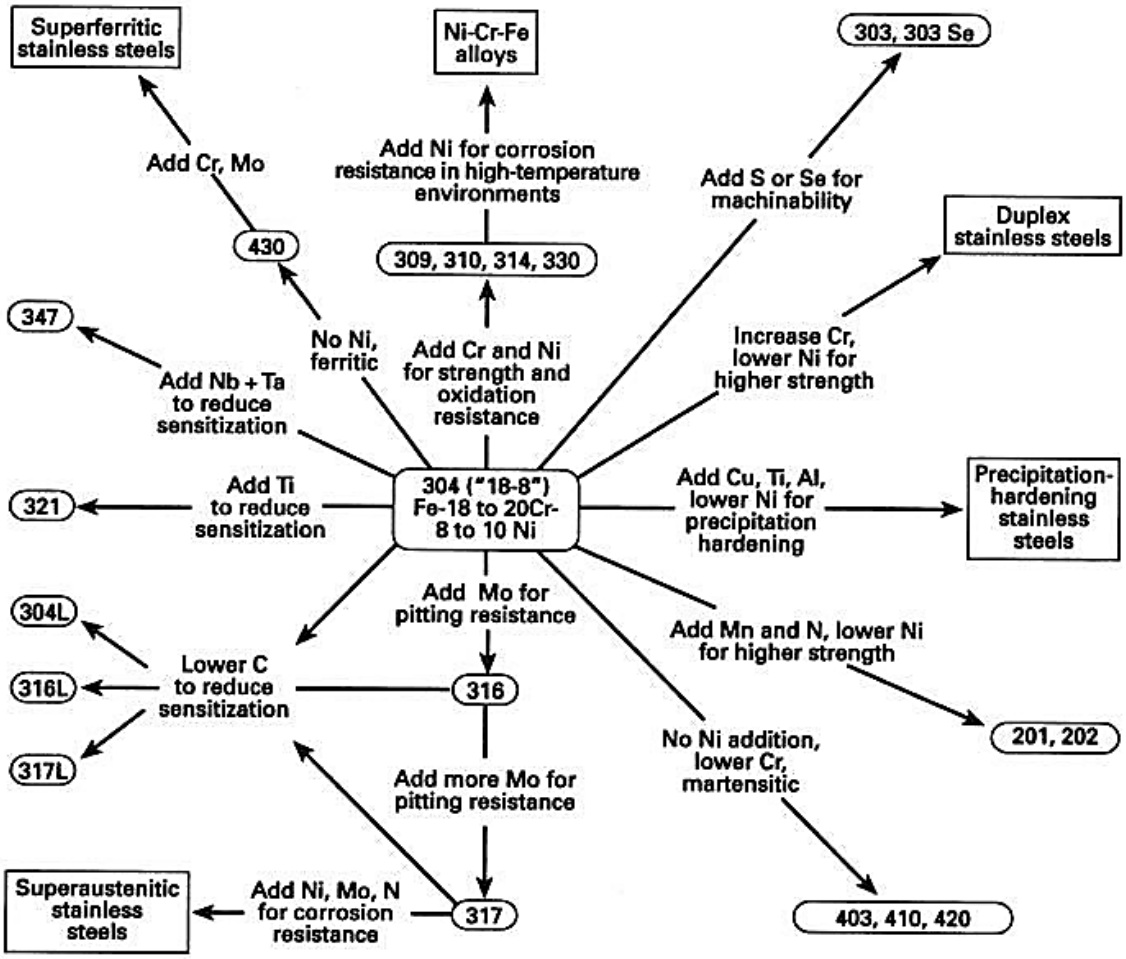

Figure 6 - Family of stainless steel alloys with compositions and properties specification [24]

In general, austenitic stainless steels are Fe–Cr–Ni–C and Fe–Cr–Mn–Ni–N alloys containing 16–26% Cr, 0.75–19.0% Mn, 1–40% Ni, 0.03–0.35% C, and sufficient N to stabilize austenite at room and elevated temperatures [26].

The 3xx (Cr–Ni) types contain high amounts of Ni and up to 2% Mn. Mo, Cu, and Si may be added to increase corrosion resistance. Ti and Nb may be added to decrease the sensitivity of intergranular corrosion. The addition of Mo and N may increase halide pitting resistance; Si and Cu may be added to increase resistance to stress corrosion cracking. S and Se may be added to certain series to enhance machinability. Nitrogen is added to increase yield strength [26].

Figure 7, shows the Fe-Cr-Ni ternary phase diagram, with the isothermics liquidus surface lines and with the respective chemical composition lines for the AISI 304L stainless steel. Observing this diagram, it is noticeable that at the composition of the AISI 304L stainless steel, the liquidus line is located at 1480 ºC. It is perceptible too, that the addiction of Cr and Ni on the original composition of these stainless steel leads to the diminution of the liquidus formation temperature.

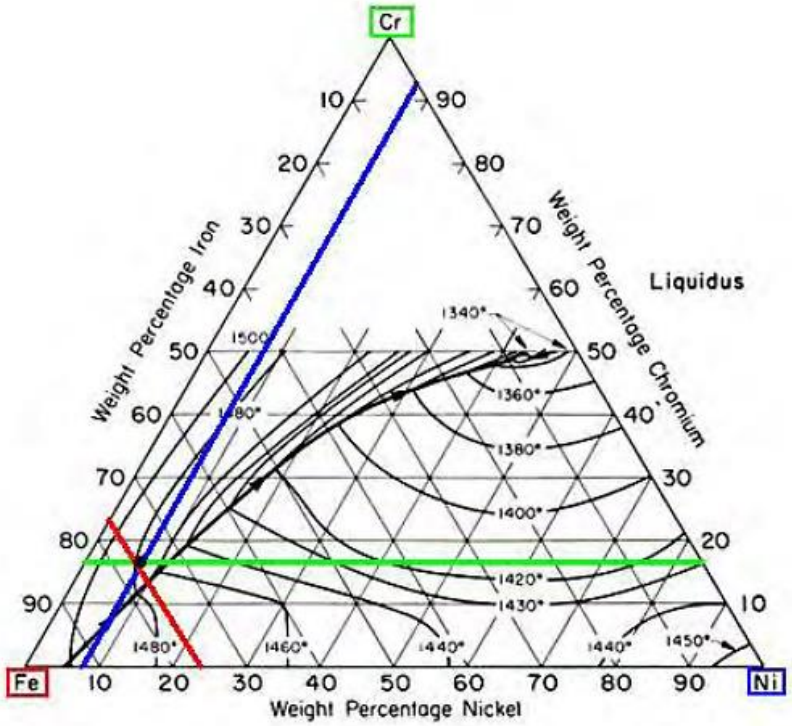

Figure 7 - Fe-Cr-Ni ternary phase diagram with Fe-18Cr-8Ni representation [8]

2.2.2.2. Copper and Copper alloys

Copper was discovered by man 10.000 years ago. The discovery of copper – tin alloy and its uses lead to the *Bronze Age,* which began in the Middle East before 3000 B.C and ended 1800 years later in 1200 B.C after which iron technology (the *Iron Age*) become common [27].

In our days, copper and copper alloys continue to be one of the major groups of commercial metals. They are widely used due to their excellent electrical and thermal conductivities, outstanding corrosion resistance, good strength, good fatigue resistance and ease of production [27]. Pure copper is extensively used for cables wires and electrical contacts.

Copper and some bronzes, brasses and cupronickels are used for radiators, heat exchangers, panels of solar energy, and due to their corrosion resistance they are usually use as pipes, valves, etc.

- **Classification**

Copper and copper alloys are usually categorized in accord to the elements and the amount of alloying elements present. The elements most commonly alloyed with copper are aluminium, tin, silicon, zinc and nickel, but other elements can be added in small quantities with the goal to improve certain material characteristics. Copper and its alloys are so divided in nine major groups [27]:

- Coppers, contain a minimum of 99.3% Cu
- High – copper alloys, which contain up to 5% of alloying elements
- Copper – zinc alloys (brasses), contain up to 40% Zn
- Copper – tin alloys, which contain up to 10% Sn and 0.2% P
- Copper – silicon alloys, which contains up to 3% Si
- Copper – nickel alloys, which contains up to 30% Ni
- Copper – zinc – nickel alloys, which contain up to 27% Zn and 18% Ni
- Copper – aluminium alloys, contains up to 10% Al
- Special alloys, which contain alloying elements to enhance a specific property or characteristic, for example corrosion resistance.

The alloys that don't fit in these nine groups are identified by their Unified Numbering System (UNS) designation. This designation consists in a five number code followed by the prefix letter "C" (i.e C1xxxx to C7xxxx wrought alloys of copper, C8xxxx to C9xxxx for cast alloys).

- **Copper crystal structure, phase equilibria and properties**

Copper is non-polymorphous metal with face centred cubic (FCC) lattice (Figure 8) and an atomic radius of 1.35A. Pure copper has a melting temperature of 1083 °C, density of 8.9 $g.cm^{-3}$, thermal conductivity of 400 $W.m^{-1}.K^{-1}$. The metal alloying decreases its conductivity [28].

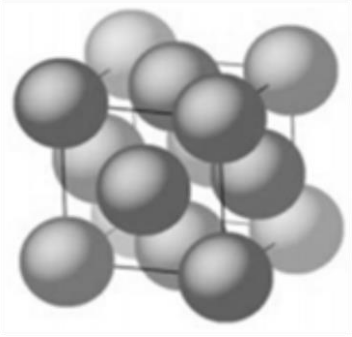

Figure 8 - Coppers crystal structure [29]

The high-purity copper generally contains from 0.01 to 0.05% oxygen due to his manufacture, where air is injected into the molten copper to oxidise impurities. As a result, oxygen is absorbed by the copper. The binary phase diagram of Cu – O in Figure 9 shows that the copper-oxygen system is a simple eutectic system. Solidification begins with the formation of nuclei on cooling below the liquidus temperature (1083 ºC). As the temperature is going down, these nuclei, which are essentially pure copper, starts to grow, causing the liquid to become richer in oxygen. The composition of the liquid follows the liquidus curve until, the eutectic point at 1066 ºC, the liquid remaining between the primary grains solidifies at constant temperature to form the eutectic composed of pure Cu and Cu_2O.

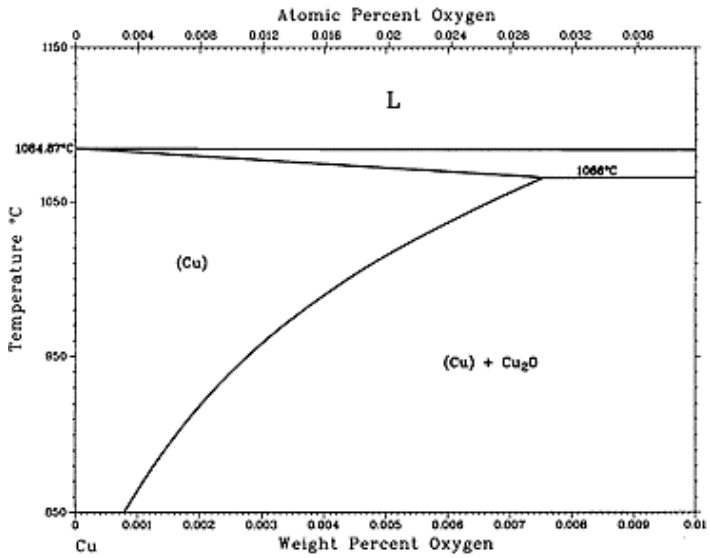

Figure 9 - Binary phase diagram of Cu - O system [30].

In Table 5 it is provided some more data about the copper physical, mechanical and thermal properties.

Table 5 – Copper physical, mechanical and thermal properties [31]

Physical properties	
Density (g.cm^{-3})	8.93
Cristal structure	FCC
Mechanical properties	
Young's modulus (GPa)	130
Poisson's ratio	0.343
Shear modulus (GPa)	46
Elongation at break (%)	60
Hardness, Vickers (MPa)	369
Yield tensile (MPa)	33.3
Thermal properties	
Melting point (ºC)	1083
Thermal conductivity (W.m^{-1}.K^{-1})	400
Thermal expansion (µm.m^{-1}.K^{-1}) (25 ºC)	16.5

- **The effect of alloying elements in copper**

As in other metal systems, copper can be intentionally alloyed to improve its properties (strength, corrosion resistance, wear resistance, machinability and colour). In Figure 10a it is possible to visualize the effect of the elements in the referred properties. In Figure 10b it is depicted the solubility of some copper alloying elements.

a)

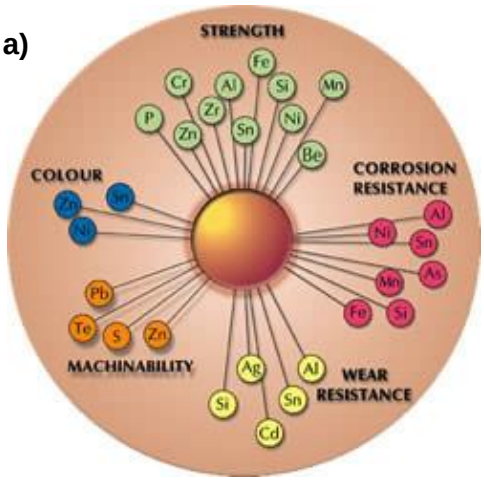

b)

Element	Solubility at 20 ºC, wt%
Co	0.2
Cr	0.03
Fe	0.14
Ni	100
O	0.0002
P	0.5
Sn	1.2

Figure 10 – a) Effect of alloying elements in copper [25]. **b)** Solubility of some copper alloying elements

However, as it was mentioned before, it should be noticed that the addition of elements also degrades the electrical and thermal conductivity, depending on the alloying element, its concentration and location in the microstructure (solid solution, precipitated, dispersoid) [27].

2.2.3. Other phases

Tungsten carbide shows low tolerance to carbon deviations from de stoichiometric WC phase. If deviation occurs, it may lead to the formation of additional phases. The increment of the carbon contents will form graphite and with the decrement of the carbon contents η phase (M_6C, $M_{12}C$), and may form [32]. In Figure 11 it is depicted the vertical section of the ternary W-C-Co phase diagram, that illustrates the influence of the carbon content on the formation of the η phase and graphite. These phases are most often not desirable, due to the degradability of some mechanical properties.

The formation of η phase increases the wear abrasion resistance and the hardness but the toughness of the composites is greatly sacrificed [33]. On the other hand, appearance of free graphite in the microstructure, decrease the hardness and the transversal rupture strength [34]. One way to minimize or avoid the formation of these undesirable phases is to control the oxygen present in the atmosphere, during the sintering process, or add carbon to the mixture, helping to adjust the balance of carbon content and obtain the desired composition of the final product.

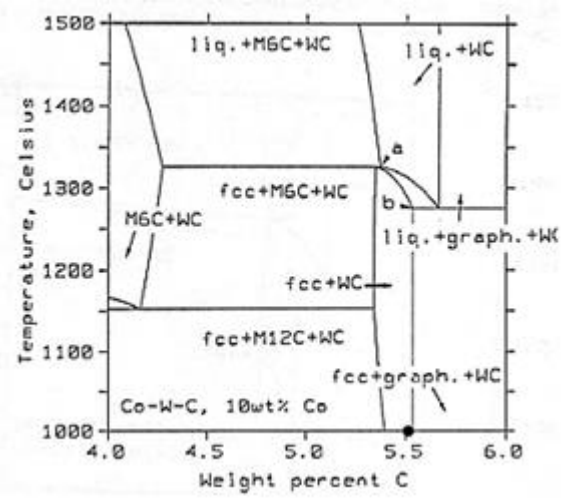

Figure 11 – Vertical section of the ternary W-C-Co, calculated at 10 wt.% Co [35, 36]. The black dot on the composition axis marks the stoichiometric composition (5.5 wt.% C).

As mentioned there are two types of η phase that can be obtained – the $M_{12}C$ that has a constant composition and the M_6C that shows variable composition within the range of $M_{3.2}W_{2.8}C$ and M_2W_4C (M = Co, Fe) [16]. The $M_{12}C$ type is formed during cooling in the solid state, it is distributed in small grains through the matrix and is consequently less embrittling than the M_6C [37], that is in equilibrium with the liquid phase and is formed through the nucleation and growth during the sintering process. However, it was proved by Pollock [38] that the η-carbide M_6C is the most stable at high-temperatures.

Reported results regarding the WC–SS system also show the formation of M_6C phase, this phase is formed during the solid state sintering at temperatures above 750ºC, before the liquid phase formation [39]. The conditions to form M_6C during heating are favoured for increasing SS amounts, decreasing Ni/Fe+Cr ratio in the binder composition, and lowering the carbon content. However, some phase dissolution arises when the liquid phase is formed, at temperatures near 1200ºC, releasing binder elements to create more liquid phase [39]. During cooling, precipitation of M_6C from the liquid is expected to occur. In this system the composition of the M_6C was recently reported by Fernandes et.al [40] to be $(Fe_{2.6}Ni_{0.2})(Cr_{0.6}W_{2.6})C$.

2.3. Phase diagrams

Phase diagrams are an important tool in the study and development of cemented tungsten carbides. They allow us to predict the thermal behaviour of the compositions, i.e., equilibrium phases at a given temperature, and eutectic temperatures which will be very useful, namely to establish the sintering conditions.

In this work the following phase diagrams, W-C-Fe-Ni, W-C-Fe-Cr and W – Cu are relevant. It would be also desirable the study of W-C-Fe-Cr-Ni, W-C-Cu and W-C-Cu-Fe phase diagrams, but they were not found in the literature.

2.3.1. W-C-Fe-Ni system

The substitution of Co for Fe plus Ni in the hardmetals was already investigated. This composite shows satisfactory properties that are associated with an accurate control of the

composition, in order to guarantee the absence of M_6C and graphite in the sintered alloy [29, 41]. This means that at the sintering temperature the global composition of the system should fall inside the WC + liquid region of the respective phase diagram. During cooling, the composition should fall within the FCC+WC region and not precipitate graphite or M_6C [16]. So, in order to achieve satisfactory results one should be able to accurately define the region of critical carbon contents once the Fe:Ni ratio has been selected [16].

Agte [42] and Moskowitz [43] observed that, if the carbon content exceeds the stoichiometric composition, good properties were obtained and the increase of the Ni content in the initial composition decreases the necessary carbon excess to avoid the formation of the M_6C phase.

It can be seen in Figure 12 a), that stoichiometric composition of WC with Fe + Ni = 10 wt% when sintered above 1360 °C it will precipitate η-phase. Even though the alloy after cooling would arrive at a stable two-phase field WC + CFC (Fe – Ni), the η-phase formed in the sintering temperature will not be dissolved and will remain in a metastable form at low temperatures. One way to avoid the formation of η-phase at the sintering temperature will be the addition of small amounts of excess carbon in order to obtain a carbon content in the alloy of 5.6 to 5.7%. If the carbon content exceed this rage, graphite precipitation will occur. Figure 12 b) represents a projection of the WC-Fe-Ni system temperatures in the areas where graphite or η phase are in equilibrium with the liquid phase, during sintering or cooling steps. The middle area, are the one where no η-phase or graphite precipitates.

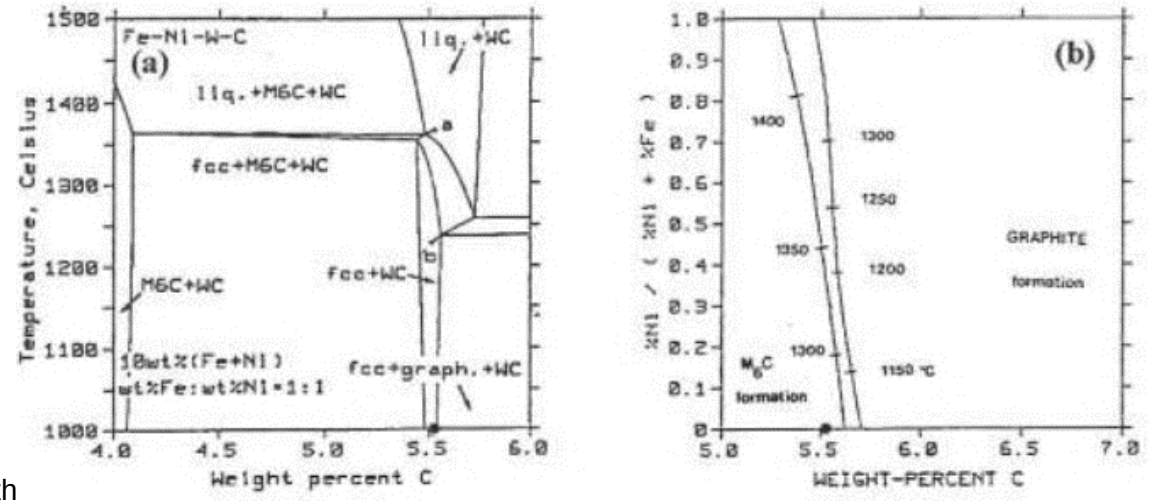

th

Figure 12 - **(a)** Vertical section of the Fe-Ni-W-C phase diagram calculated at Fe+Ni = 10 wt.% and %Fe:%Ni=1:1 [44]. **(b)** Temperature projection calculated at Fe+Ni=10 wt.%. The lines describe the compositions of a mixture of WC + liquid in equilibrium with$FCC+M_6C$ (left) or FCC + graphite (right) [44].

2.3.2. W-C-Fe-Cr

The available experimental data on the quaternary system W-C-Cr-Fe is still scarce. The first schematic diagram of the quaternary W-C-Cr-Fe system was presented by Goldschmidt [45] in the early 1950's. It was shown that Cr and W form carbides and many different types of carbide may form in steels containing these elements. The ternary M_6C carbide, also stable in the W-C-Fe system, was shown to possess a limited solid solubility for Cr.

The region of existence of the M_6C carbide was studied by Bergström [46]. Despite of M_6C he reported the existence of two additional carbides, $M_{12}C$ and M_4C, also found on the ternary C-W-Fe. The M_6C and $M_{12}C$ carbides dissolve up to 8 and 4 at.% Cr, respectively, at 1250 ºC. The maximum solubility at 1250 ºC of Cr in other phases, like Fe and W, were reported to be 10 at.% and 2 at.%, respectively. In Figure 13 are represented the isothermal sections at 1250 ºC of the W-C-Fe and W-C-Fe-Cr at Cr levels of 2 and 10 at.%. The isopleth W-C-Fe-2Cr (Figure 13b) contains the same regions as the isopleth Fe-W-C-0Cr (Figure 13a) since no phase, except WC has a Cr solubility limit below this section. The isopleth W-C-Fe-10Cr (Figure 13c) is positioned above the maximum of Cr solubility in all phases. The maximum solubility of Cr in Fe lies on this level, which implies that the four-phase tetrahedron, $M_6C+M_{12}C+\mu(Fe_3W_2)+Fe$, the three-phase volume, $M_6C+M_{12}C+Fe$, and the two-phases volumes M_6C+Fe and $M_{12}C+Fe$, touch the section only in one corner [46].

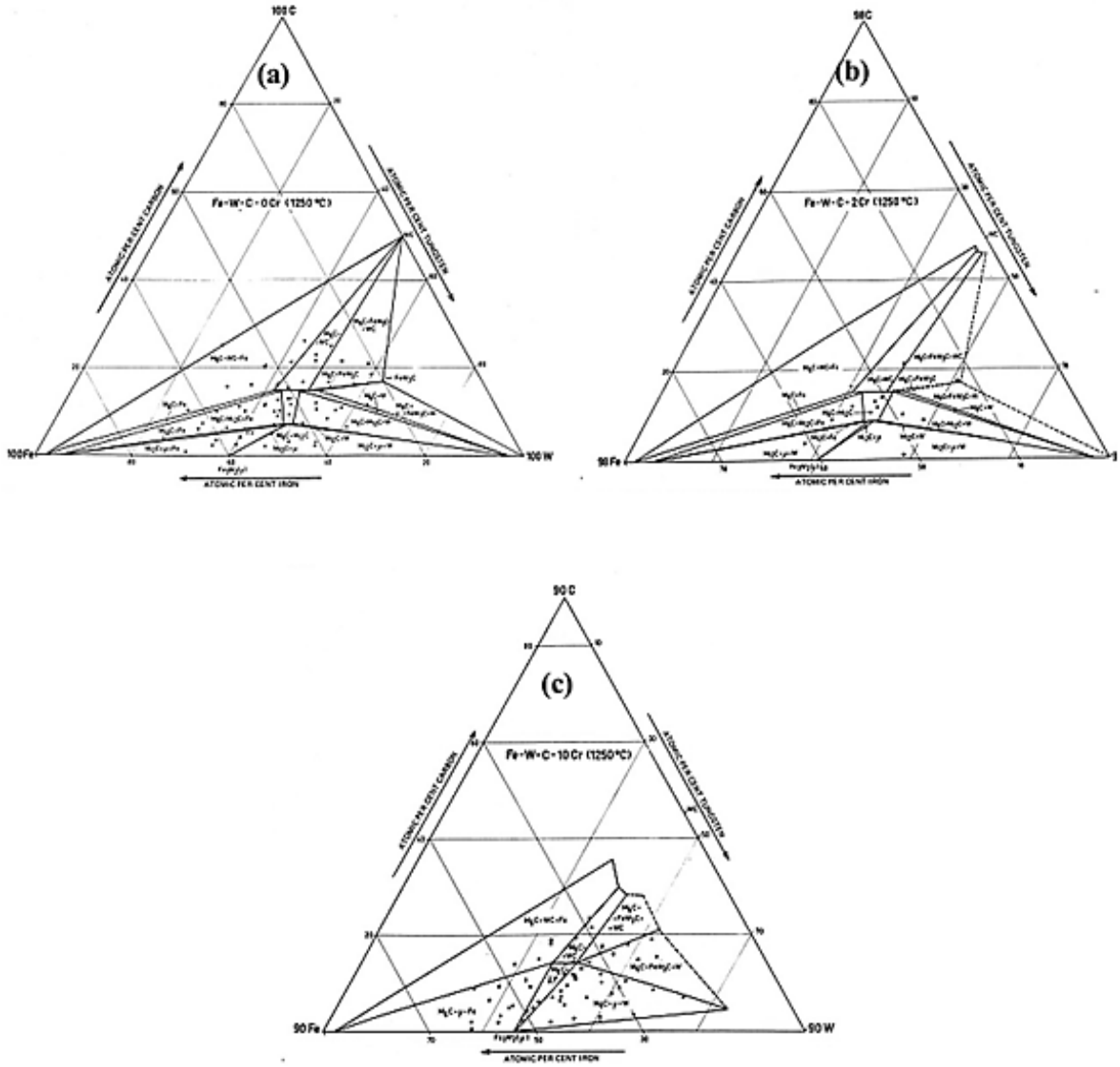

Figure 13 – a) Isopleth W-C-Fe-0Cr (1250 ºC) [46]; **b)** Isopleth W-C-Fe-2Cr (1250 ºC) [46]; **c)** Iso pleth W-C-Fe-10Cr (1250 ºC) [46].

2.3.3. W-Cu

Tungsten–copper (W–Cu) composites are promising materials for manufacture of electrical contact parts, thermal management devices, welding electrodes, due to the high thermal and electrical conductivity of copper ant to the high arc erosion, and low thermal expansion coefficient of tungsten [6].

The alloying of W and Cu proves to be difficult due to the mutual insolubility of W and Cu. The assessed equilibrium phase diagram in Figure 14 reveals that the two metals are

immiscible in both solid and liquid phases. This limitation excludes the use of conventional alloying techniques to develop full density W-Cu alloys [47].

Several alternate processing techniques have been examined to develop W-Cu composites [48]. Usually, W-Cu is alloyed through the sintering of W-Cu powder mixtures. This could be processed through solid-state and liquid-phase-sintering (SSS and LPS) techniques [47]. SSS of W-Cu may be performed at any temperature, but LPS requires a sintering temperature that is at least higher than the melting point of Cu (1083 °C). In some cases, when mechanical alloying is used, LPS may occur at lower temperatures, specifically, when the powder particle size is reduced, through welding and fracture during milling, to the nanoscale [49]. As a result, diffusion paths are decreased, which in turn, reduces the required temperature [50].

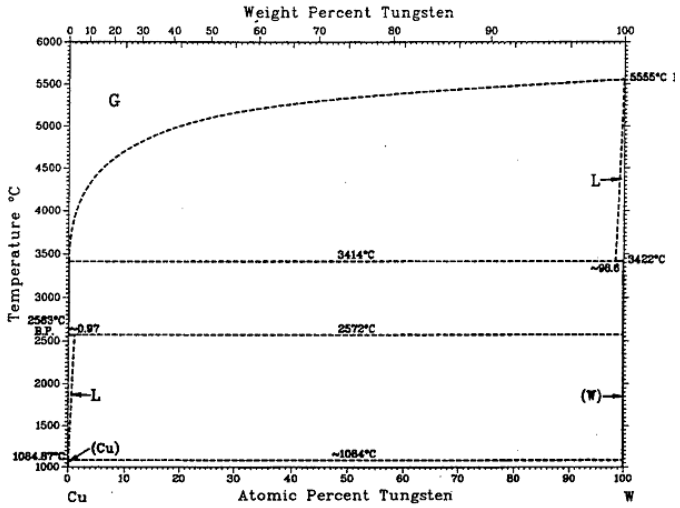

Figure 14 – W-Cu binary phase diagram [51]

2.4. Processing – General process

Cemented tungsten carbides like most of the other refractory carbides are usually manufactured by a powder metallurgy processing method. This method is composed by the following five main steps:

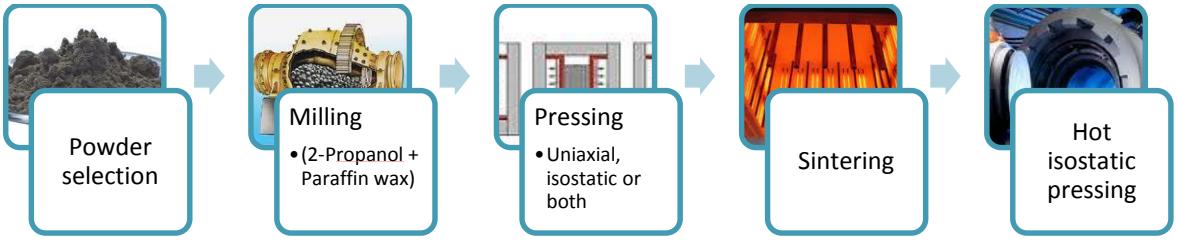

Figure 15 - Manufacturing stages of cemented WC

After the powder selection, milling process takes place. Here the powders are ball milled with a mixture of a lubricant, the paraffin wax and a lubricant solvent, e.g. 2-Propanol. The main propose of the wet milling step is to produce a homogeneous dispersion of the binder in the tungsten carbide matrix. Lubricant is added to the blended powder, mainly to reduce the friction between the powder mixture and the surfaces of the apparatuses and also as a mean to help the pressing of the mixture powders.

The milled powders are uniaxially pressed, with pressures between 150-990 MPa, and/or in the almost same rage of pressure, isostatically pressed until the compact obtain a green density in a range of 45 – 65%. The composite powders can be pressed directly into specified final shapes or they may be pressed into blocks and later shaped.

Following the pressing process the composite is pre-sintered in a gap of 600 - 900 °C. This step must remove the lubricant and provide mechanic consistence to allow further shaping. Sintering is normally conducted in vacuum or H_2 atmosphere at temperatures between 1350 °C and 1600 °C. After this step, if the samples are not completely densified they can be submitted to a HIP (hot isostatic pressure) in order to totally close some reminiscent porosity. In alternative, modern sinter-hip furnaces allow the combination of the three sintering processes mentioned, pre-sintering, sintering and HIP in one step which helps to increase the speed of the entire sintering cycle.

In this work it is proposed to investigate the use of mechanical alloying, a high energy milling process, for the hard metal production. Therefore, it will be especially important a more detailed understanding about the milling and the sintering processes.

2.4.1. Mechanical alloying

Mechanical alloying (MA) is a powder processing technique, developed in the International Nickel Company (INCO) by John S. Benjamin and his colleagues in 1966. This method allows production of homogeneous materials starting from blended elemental powder mixtures [52].

The term MA is applied to the processing of metal powders (of different metals or alloys) in high-energy ball mills and describes the process where mixtures of powders are milled together to obtain a homogeneous alloy, accomplished through a repeated cold welding, fracturing, and rewelding of powder particles, during milling [52]. In this process, small quantities of the powder mixture is loaded into a container along with the grinding media, being agitated at a high speed for a pre-determined time frame, until the composition of every powder particle is in the same [53]. In some cases, dispersant agents, like hexane or toluene, can be added to avoid the formation of clusters.

In Figure 16 it is shown the effects of a single collision on each type of constituent powder particle. The impact of the grinding balls causes the ductile metal powders to flatten and work harden. The brittle powder particles get fractured and are refined in size. [52].

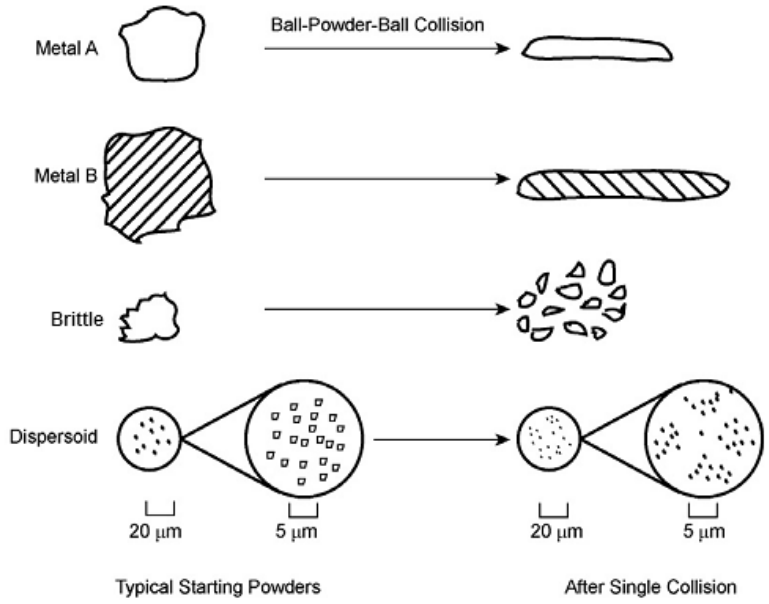

Figure 16 - Effects of a single collision on each type of constituent powder particle [52]

Whenever two grinding balls collide, a small amount of powder is trapped in between them. Typically, around 1000 particles with an aggregate weight of about 0.2 mg are trapped during each collision (Figure17) [52]. During this process the morphology of the constituent powders change significantly: in the case of cemented tungsten carbides, composed by the combination of ductile–brittle components, the ductile metal powder particles initially get flattened by the ball–powder–ball collisions, while the brittle phase particles get fragmented. These fragmented particles tend to become occluded by the ductile constituents and trapped in the ductile phase [52]. The brittle constituent is closely spaced along the interlamellar spacing. With further milling, the ductile powder particles get work hardened

and refined. If the brittle particles are insoluble in the ductile matrix, they start to be uniformly dispersed in the matrix. On the other hand, if they are soluble, they get alloyed.

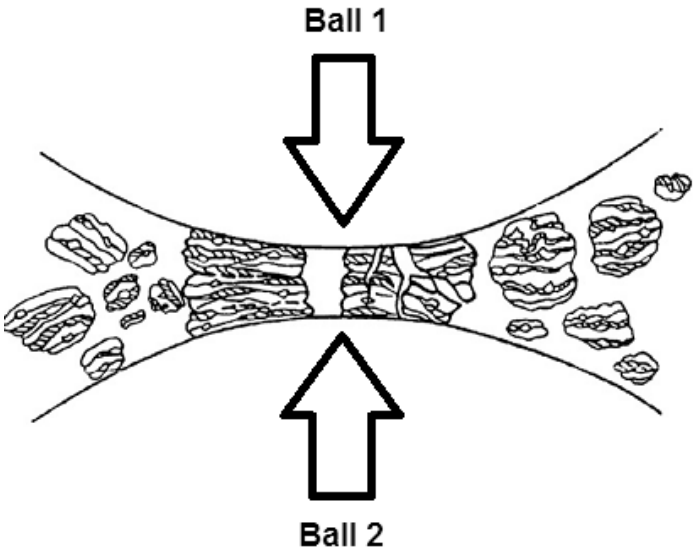

Figure 17 - Ball-powder-ball collision of powder mixture during mechanical alloying [53]

2.4.1.1 Factors affecting the MA process

The MA process is a complex process and is significantly affected by a number of factors. The more complete the control and monitoring of the milling conditions, better the end product will be.

The most important parameters that influences MA process are: raw materials, milling time and speed, ball-to-powder weight ratio (BPR), milling atmosphere and types of mills. Table 6 summarizes the milling parameters influencing MA.

Table 6 – Summarization of the milling parameters influencing MA

Parameters	Values	Observations
Raw materials	Powders size 1 – 200 µm	Initial powder particle size is not critical, since in most cases, the powder particle size decreases exponentially with time and reaches a small value of a few microns only after a few minutes of milling [53].
Time and speed	Time: The necessary to achieve a stable state between the fracturing and cold welding of the powder particles Speed: Generally between 200 – 600 RPM	The two most important variables in MA. Time required is dependent on the type of mill, the BPR and the temperature of milling [53]. Powder should be milled just for the required duration and not any longer, due to the increment of contaminations and formation of undesirable phases. The faster the mill rotates, faster will be the average particle size reduction. Therefore, for high speeds, the temperature of the container may reach a high value. Limiting speed rotation.
Ball-to-powder weight ratio (BPR)	1:1 to 220:1. Most frequently 10:1 and 20:1	At a high BPR, the number of collisions per time unit increases and consequently more energy is transferred to the powder particles, thereby the rate of alloying is increased [53]. The BPR also has substantial effect on the time required to achieve a milled powder particular phase, for a higher BPR the time required is reduced.
Milling atmosphere	Inert gases: Argon of Helium	The major effect of the milling atmosphere is the contamination of the powder. Very fine powders have relatively large surface areas, highly reactive not just with O_2 but also with other gases such as hydrogen or nitrogen [54-56]. High-purity argon is the most common atmosphere to prevent oxidation and/or contamination of the powder.
Type of mills	Shaker attritor, drum, planetary and horizontal mills	There are several types of mills for MA and they differ in their capacity, speed of operation, efficiency of milling, additional arrangements for cooling or heating and their ability to control the operation. The one used in this work is depicted in Figure 18a, Figure 18b describes it working principle.

As mentioned before, planetary ball mill was used in this work. The name “planetary“ drives from the planet-like movement of its containers. The special drive mechanism origins the combination of the two movements, rotation and translation. Since the rotation and translation of the containers is made in opposite directions, the centrifugal forces alternately act in like and opposite direction. This makes the gridding balls develop a friction effect in the material powders on the track down in the inside wall of the container, followed by an impact effect, caused by the material being ground and the gridding balls lifting and traveling freely through the inner chamber of the container and colliding the opposite inside wall [53], as is depicted in Figure 18b.

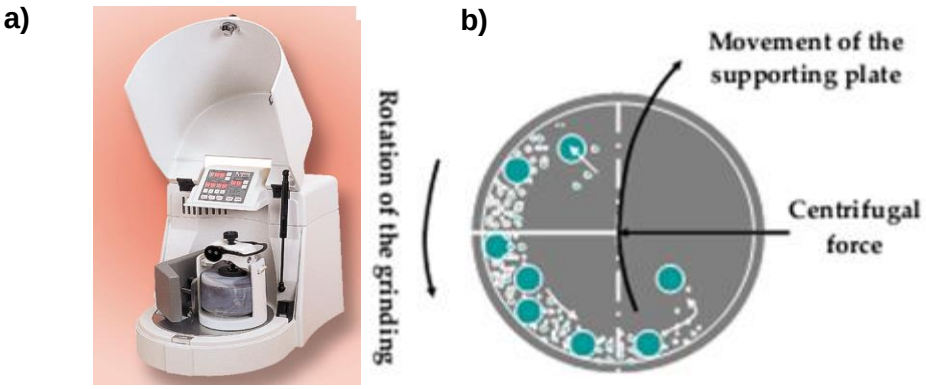

Figure 18 – High energy ball milling apparatus. **a)** Fitsch Pulverisette 6. **b)** schematic representation of the displacement of the milling media inside the vessel.

2.4.2. Sintering process

After compaction, cemented carbides are sintered in a temperature range between 1350 – 1600 ºC. Figure 19a shows a micrograph of a WC-Co, the grey WC hard phase and the dark Co matrix. At this temperatures significant microstructural changes occur, driven by the reduction of the interface energy stored in the WC-binder, WC-gas, WC-WC, binder-gas, binder-binder interfaces [57]. The differences in interface energies and the anisotropic nature of the WC crystal structure are responsible for the characteristic trigonal shape of the WC grains (Figure 19b) [58].

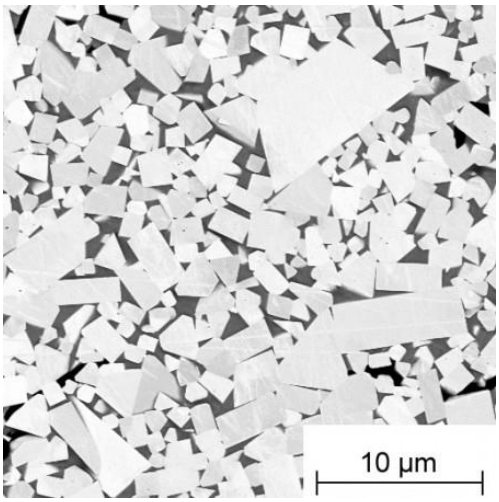

Figure 19 - a) micrograph of WC/Co showing the WC hard phase surrounded by the dark shade of Co matrix**.**

The sintering process of this type of material usually involves the combination of solid state and liquid phase sintering, due to the presence of a eutectic point in the WC-binder system (liquid phase sintering),

2.4.2.1. Solid state sintering

Solid state sintering occurs below the eutectic temperature (1310 ºC for WC – Co systems). In this step a certain amount of the hard phase is dissolved in the still solid binder. New phases and material transport may occur through surface and bulk diffusion, decreasing porosity by re – arrangement of the particles.
For the case of submicron and finer WC particles, densification is more rapidly achieved and high densities (> 85% of the theoretical one) may well be obtained even before the formation of the liquid phase [59], as is depicted in figure 20.

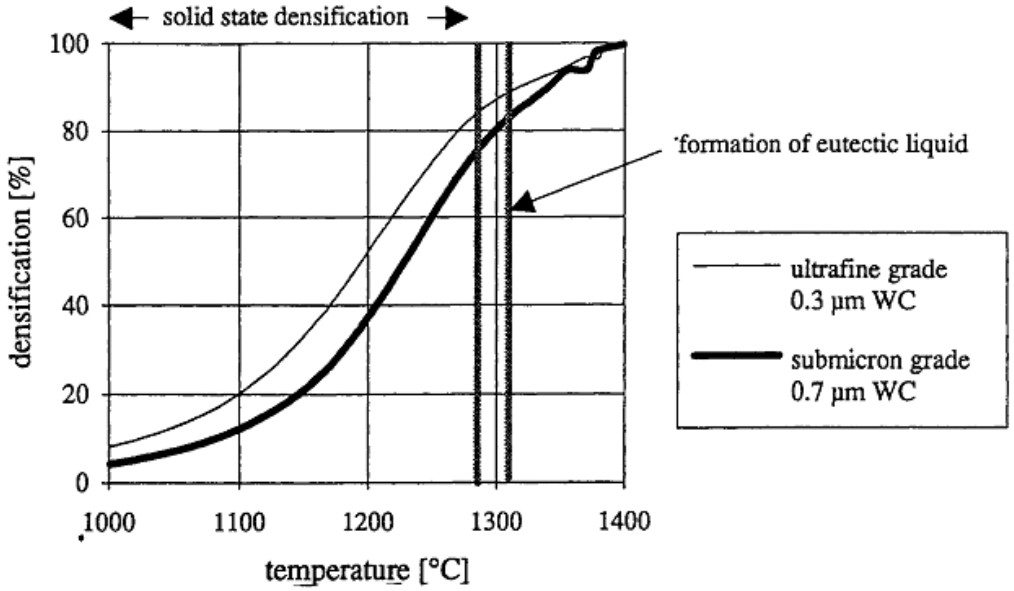

Figure 20 - Densification of WC/10 %wt Co hard metals based on ultrafine and submicron WC [60].

Moreover, in situ studies conducted by Froschauer and Fulrath [61] showed the microstructural evolution of submicron hardmetal grades (< 0.8 µm) and confirmed that rearrangement in the solid state is the main densification process. The smaller the grain size, the larger the interfacial area of the compact, and higher it is the stored interfacial energy. As a result, sintering starts earlier for fine-grained cemented carbides and the relative contribution of solid state shrinkage to the global densification increases. Therefore,

densification in solid state can be compared to the a rearrangement process in the first stage of the liquid phase sintering [62]. As is depicted in Figure 21, solid state sintering occurs in two stages.

- **The first stage** starts at temperatures above 0.5 $T_{melting}$ (650-710ºC), here, highly dispersed Co particles begin to behave like a viscous mass, spreading by wetting onto the surrounding WC particles immediately after degassing and surface oxide reduction [63]. This process, is schematically represented by stage 1 in Figure 21a). In this first part of the sintering process, the heating rate should be low, allowing the proper de – waxing of the binder and removing the outgassing adsorbed gases and some gaseous reduction products that may take place, while the material still have open porosity.

- **The second stage** of the solid state sintering usually starts at temperature between 1050-1100ºC. At these temperatures, a certain particles rearrangement results in local dense areas comprising a large number of WC grains. Concurrently, some micropores or pores are also formed as a result of fluctuating densification due to heterogeneous Co binder distribution as well as differences in green density, WC specific surface area or grain size [63]. For temperatures above 1050-1100ºC, densification continues by creep of the WC-Co mixture into the existing micropores and pores [63].

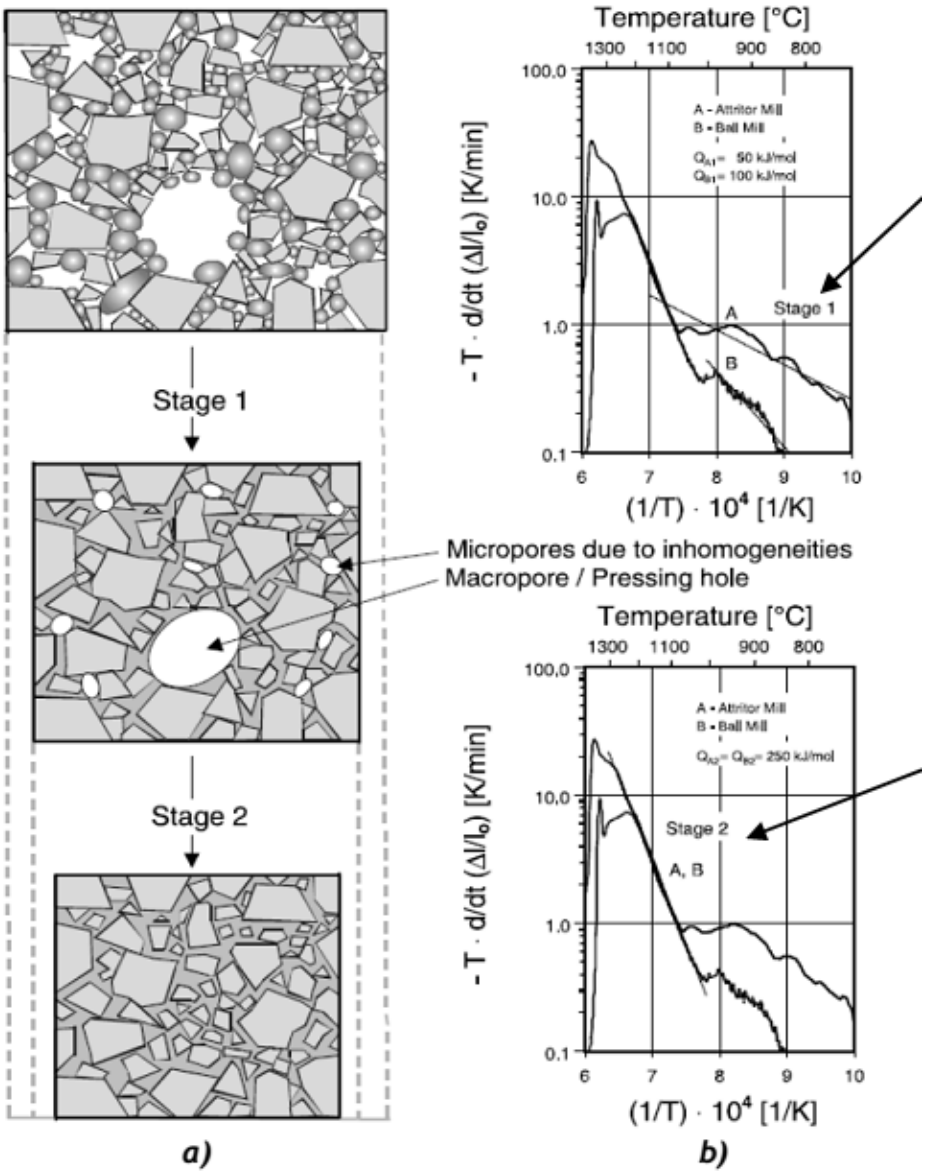

Figure 21 - a) Schematic representation of the two initial stages of the solid state sintering, and **b)** shrinkage rate vs. temperature graph, showing the two stages Arrhenius related activation energy [64]

2.4.2.2. Liquid phase sintering

Above the ceramic – metal eutectic melting point temperature, the liquid phase sintering (LPS) takes place. The densification process at this stage proceeds with the accommodation of the WC particles, with cooperation from the contact flattening of the carbide particles, dissolution of small grains and re-precipitation on large grains as well as by coalescence via grain boundary migration [63, 65].

Through typical coalescence and Ostwald-ripening process, WC dissolves at the solid-liquid interfaces with high chemical potential and re-precipitates over other particles with lower chemical potential, this process ultimately leads to the availability of the liquid phase for fill the pores. The amount of solid dissolving in the liquid is inversely related to the WC particle size [66]. This extensive dissolution-precipitation process, allows the bigger grains to grow, sacrificing the small ones. Thus, liquid-phase sintering is usually marked by a microstructural coarsening, leading to a WC prismatic grain shaping [67], as can be seen in Figure 22.

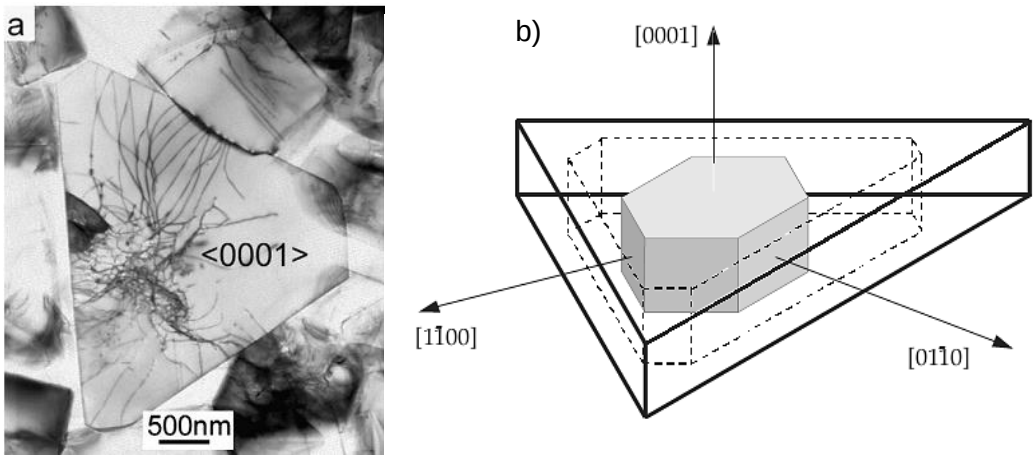

Figure 22 – Prismatic trigonal grain shape. **a)** Transmission electron microscopy micrograph of WC – 13 wt.% Co sintered at 1450 ºC – 2h. **b)** WC grain shape resulting from preferential growth along one type of prismatic planes.

The grain growth continues even during cooling, in the final solid state sintering and ends when the temperature becomes too low and the structure is frozen. The sintering time at high temperature must be long enough to reach full densification of the structure, but it should be as short as possible to limit grain growth, which is detrimental for the mechanical properties [68].

To reach full densification of the structure by liquid phase sintering three requirements must be fulfilled [69, 70]: The existence of an appreciable amount of liquid, the solubility of the solid in the liquid and high wetting. [71]. Wetting is promoted by solubility of the solid in the liquid, formation of intermediate compounds and interdiffusion [72]. It is important to have high wetting for the sinterability of a powder system, and it can be characterized by the contact angle determined by the solid-liquid-vapour equilibrium energies (Figure 23).

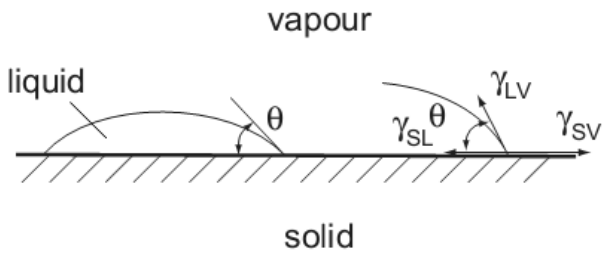

Figure 23 - Interfacial energies and the definition of a contact angle [72].

The contact angle (θ) is determined by the balance of the interfacial energies associated with each interface and given by the Young's equation [72].

$$\gamma SV = \gamma SL + \gamma LV \cos\theta \quad \textbf{(3)}$$

Where γ_{SV} is the solid-vapor interfacial energy and γ_{SL} and γ_{LV} stand solid-liquid and for the liquid – vapor interfacial energies, respectively.

If γ_{LV} plus γ_{SL} is lower than γ_{SV}, the net interfacial energy is reduced by spreading the liquid over the solid surface and creating a low contact angle characteristic of good wettability, as depicted on left side of the figure 24.

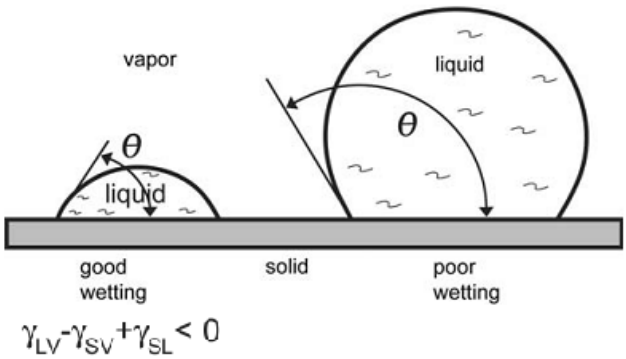

Figure 24 - Contrast of wetting behaviour for a liquid on a horizontal plane showing how a low-contact angle supports wetting while a high-contact angle resists wetting. Densification requires a low-contact angle to ensure that the grains are pulled together. (adapted from [73]).

A low-contact angle induces liquid spreading over the solid grains, providing a capillary attraction that helps densifying the system, on the other hand, high-contact angles indicates poor wetting, so the liquid retreats from the solid. This results in compact swelling and liquid exuding from pores, undermining the densification process [73].

2.4.2.3. Microstructural evolution

After milling, the WC particles are typically angular sharped, being transformed during sintering to a prismatic shape, characteristic of the WC-Co hardmetals as shown in Figure 22 and 25. Figure 25 illustrates the microstructural evolution of WC-Co with temperature.
Prismatic WC grains develop faster in fine-grained materials than in coarser ones [74] and the shape of the faceted WC grains changes with C content, the higher the carbon content, the more faceted the particles are [63, 75].
For MA processed hardmetals, the grain size of the sintered structure essentially depends on the initial size distribution, therefore on the milling conditions. The higher sinterability and chemical reactivity of ultrafine WC powders, due to their higher specific surface areas, intensifies the grain growth by coalescence in the solid state and by solution-reprecipitation in the liquid phase sintering [76, 77], potentially leading to abnormal grain-growth.

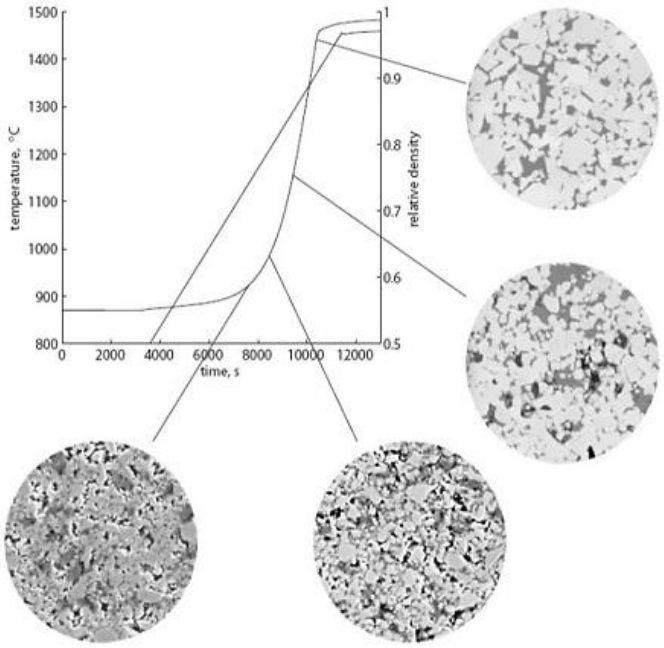

Figure 25 - Microstructural evolution of WC-Co during sintering [78]

Abnormal grain-growth has serious consequences in mechanical properties of hardmetals, since large grains act as stress concentrators, reducing the material strength. The formation of these large grains is also associated to the presence of coarser grains in fine grained powders, WC agglomerates, heterogeneous C distribution, recarburizing of the η-phase, and other defects formed during milling [63, 79].

There are several methods for limiting microstructural coarsening and abnormal grain growth. The use of sintering techniques, such as Laser Sintering (LD), Spark Plasma Sintering (SPS), Two-Stage Sintering (TSS) or through the introduction of grain-growth inhibitors in the powders mixture. Compared to conventional sintering techniques, fast sintering techniques (LD, SPS, among others) are characterized by shorter densification time at lower temperature, with a nearly insignificant grain growth. TSS is a sintering technique were the time period necessary for reach full densification at the liquid phase sintering (LPS) temperature is reduced by increasing the compact density in the solid state sintering (SSS) period. Figure 26 compares the conventional sintering cycle with two-stage sintering cycle, it is shown that the time of permanence at above the liquid formation temperatures is dramatically decreased. Yang et.al [80] showed that this technique can be effective in the abnormal grain growth suppression of hardmetals with a Co content of 8 wt.%.

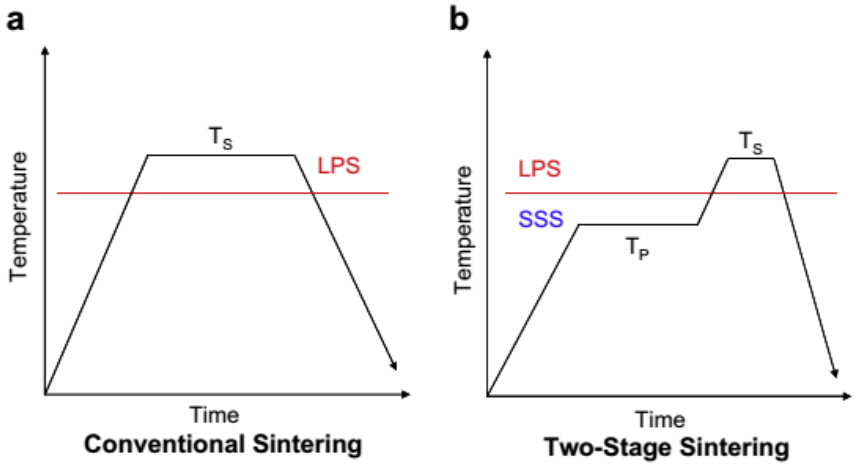

Figure 26 - Two types of thermal cycles, conventional and two-stage sintering [80].

The grain-growth inhibition is related to a reduction of the solution/re-precipitation reactions at the WC–Co interfaces [81]. The most common grain growth inhibitors are VC, Cr_3C_2 and TaC, they are used in small percentages (until 1 wt.%) accounting for their effectiveness and solubility in Co. Above this amount, no additional grain growth inhibition is usually achieved [64].

2.4.2.4. Sintering and phase formation of WC-AISI304 powder composites

The first reported case in the substitution of Co by Austenic stainless steel in hardmetals was made by Farooq et al. [22]. In that work was investigated the use of an austenitic stainless steel AISI 316 binder. More recently, results using AISI 304 SS binder added to WC by sputtering technique were reported by Fernandes et al. [1, 82, 83], it was revealed that this binder shows good sinterability characteristics due to the excellent wetting and solubility of the carbide phase in the molten binder. In 2013 Marques et al. [7], reported the behaviour of WC-AISI 304 powder composites during vacuum sintering. It was found that sintering of this composites occurs in three different stages (Figure 27). Stage I, below the eutectic temperature, within solid state sintering, Stage II with fast densification by viscous flow and Stage III dominated by solution/precipitation processes. This behaviour was also verified for WC-SS powder composites with the binder content of 12 wt.%, and it was similarly reported for WC–SS compositions prepared by sputter-coating technique [1, 82, 83]. Another important feature, confirmed by Marques et.al [7] study, was the shrinkage dependence on the binder amount; higher SS contents originate higher shrinkages. The presence of higher binder amount increases the amount of liquid phase at temperatures above the eutectic, and, consequently, the amount of shrinkage attained by viscous flow.

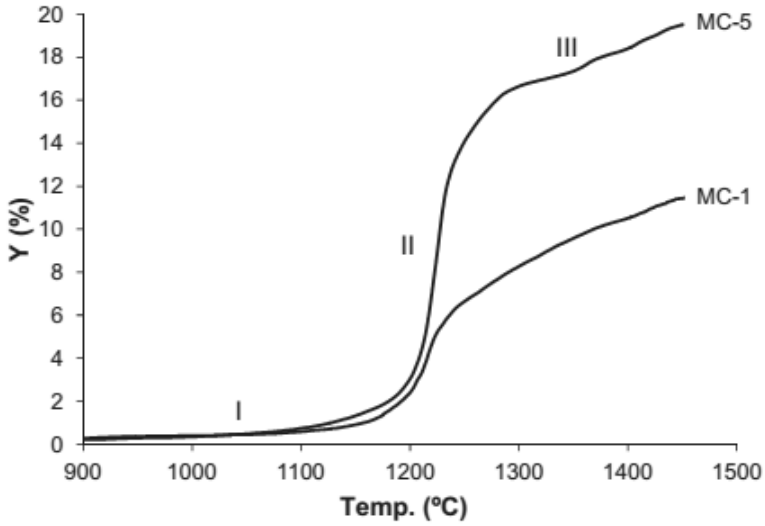

Figure 27 - Linear shrinkage vs temperature, for WC–SS compositions, calculated from the dilatometric curves at 5ºC/min. MC-5, 15 wt.% of SS binder; MC-1, 6 wt.% of SS binder [7].

Concerning the phase formation the WC–SS system shows three different phases, WC, Fe-(γ) and M_6C (eta-phase). The formation of M_6C phase is expected in WC based composites with iron rich binders, since it is predicted in the WC-Fe-Ni phase diagram (Figure 12). This phase formations occurs during the solid state sintering, at temperatures above 750ºC, before the liquid phase appearance [39]. The conditions to form eta-phase during heating are favoured for increasing iron amounts. Nevertheless, some phase dissolution arises when the liquid phase is formed, at temperatures near 1200ºC, releasing binder elements to form more liquid phase and promoting a significant shrinkage contribution by viscous flow [39], as depicted in the shrinkage curves in Figure 27. During cooling, it is expected to occur the precipitation of some M_6C [39] from the liquid phase [40].

2.5. Mechanical properties of hardmetals sintered from nanosized powders

Hardness and fracture toughness are the two most important mechanical properties of cemented tungsten carbide and other cermets. Other mechanical properties, such as flexural strength, wear resistance and impact resistance, are fundamentally related to the hardness and fracture toughness [84].

It is well known that the hardness of cermet materials is inversely proportional to its grain size and that the fracture toughness is inversely proportional to the hardness, although the relationship between the hardness and fracture toughness may not be linear when the grain sizes are extremely fine [84], as depicted in Figure 28. Therefore, a finer grain size usually results in lower fracture toughness. However, for ultrafine and nanostructured metal alloys and ceramics, it has been noted that the mechanisms of strengthening are different because of the large volume fractions of grain boundaries [84]. It is clear in Figure 28 that the mechanical behavior diverges from the normal trend for hardness versus toughness for bulk hardmetals, when grain sizes approach nanoscale. This deviation is made toward the improvement of hardness versus toughness relationship [84, 85]. The deformation mechanisms depend on grain boundary sliding and diffusion-controlled processes [86]. Grain boundaries in polycrystalline metals also impede the motion of cracks, which contributes to better fracture toughness. Therefore, it is hypothesized that the fracture toughness of WC–Co composite will improve when WC grain sizes tends to reach the nanoscale.

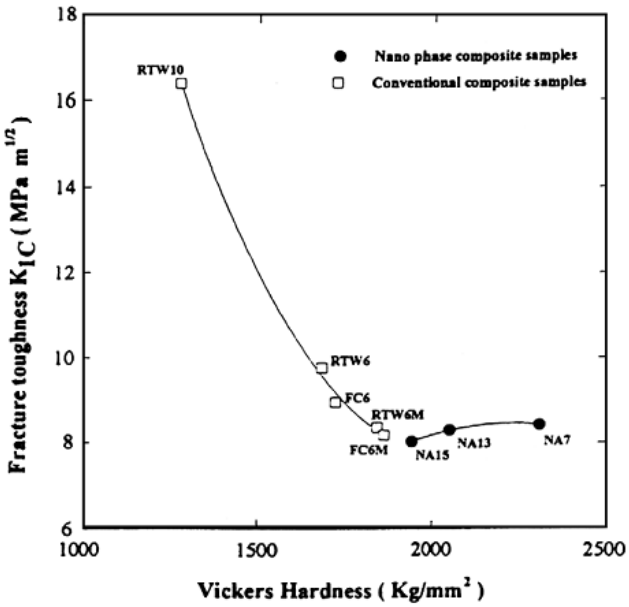

Figure 28 - Fracture toughness versus hardness of WC–Co materials comparing nano-phased composite samples to conventional composite samples [85]

In Table 7 it is summarized the hardness and fracture toughness of some hardmetals obtained by processing nanosized and microsized powders.

Table 7 - Hardness and fracture toughness of hardmetals using nanosized powders as reported in open literature

Nanosized powders				
Material	**Sintered grain size (nm)**	**Hardness[a] (HV)**	**Fracture toughness[b] (MPa.mm$^{1/2}$)**	**Reference**
WC–14 wt.% Co	97	1122	4	[87]
WC-0.6wt.%VC-10 wt.%Co	169	2084	8.8	[88]
WC–12 wt.%Co	470	1575	11.4	[89]
WC–10 wt.% Co	1000-2000	1326	-	[90]
WC-10wt.% Fe	450	1814	10.4	[91]
WC-10wt.% Ni	490	1750	11.1	[91]
Microsized powders				
WC–12 wt.% Co	3000	1320	14	[17]
WC-12 wt.% 316 SS[c]	5100	1300	12.9	[22]
WC–12 wt.% 304 SS[d]	2800	1360	13.3	[7]

[a] For convenience of comparison, the original hardness values from papers were converted to Vickers hardness values.

[b] Fracture toughness value was calculated from indentation method.
[c] AISI 316 stainless steel (68 – 74 wt.% Fe, 16 – 18 wt.%Cr, 10 -14 wt.%Ni)
[d] AISI 304 stainless steel (70 – 74 wt.% Fe, 18 – 20 wt.%Cr, 8 – 10 wt.%Ni)

Since almost all the available data in literature is based on samples that have ultrafine and submicron grain sizes at sintered state, the mechanical behaviour of hardmetals with truly nanoscaled grain sizes (<200 nm) remain not well explored. A depth research in sintering technologies and composite formulation is still needed to enable the manufacture of bulk materials with nanoscaled grain structure.

Chapter 3

Experimental procedure

3. **Experimental Procedure**

This chapter describes in detail the methods and materials used in:

- Preparation and characterization of the raw materials;
- Optimization of the high energy ball milling (HEBM) process;
- Characterization of the HEBM powders;
- Optimization of the packing and of the sintering processes;
- Mechanical, chemical, morphological and structural characterization of the consolidated samples.

The processing and characterization steps of the WC-(Cu,Fe,Ni,Cr) composites are summarized in the following flowchart.

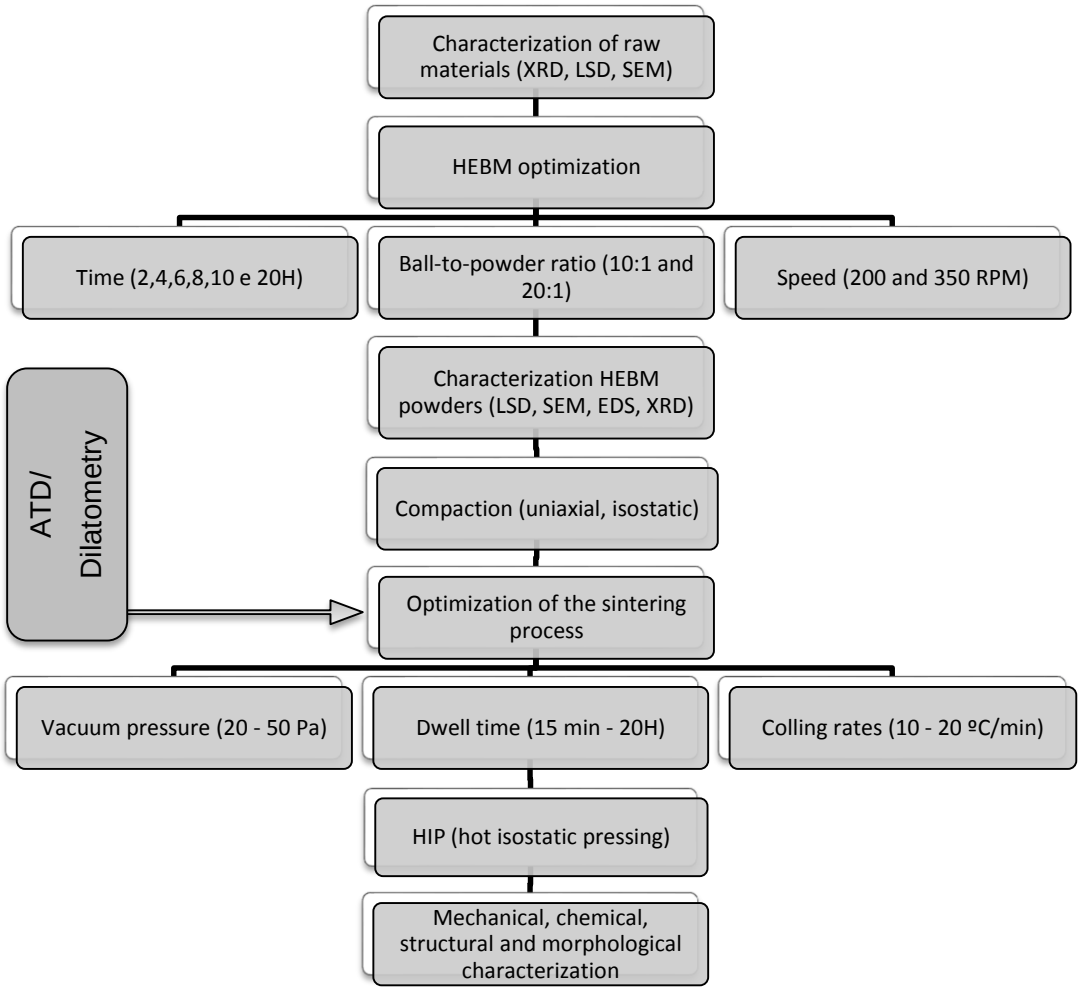

Figure 29 – Experimental procedure flowchart.

3.1. Materials

In the present investigation three different types of powders, WC, stainless steel AISI 304 (SS) and Cu were used. The WC was provided by H.C. Starck, HCST-Germany, the SS was acquired to Sandvik Osprey, Ltd., and the 99.9% pure spherical Cu was purchased to Alfa Aesar Gmbh & Co. KG. The characteristics of these powders are summarized on Table 8.

Table 8 – Properties of raw powders.

Properties	WC	Cu	SS
Chemical composition (wt.%)	93.87 (W), 6.13 (C)	99.9 (Cu)	71.15 (Fe), 18.8 (Cr), 10 (Ni), 0.03(C)
Average particle size (μm)	1	9	5
Density (g/cm^3)	15.6	8.9	7.9
Melting temperature (ºC)	2785	1083	1400 - 1455
Tensile strength (MPa)	345	33.3	460 - 1100
Thermal expansion coefficient (20 – 100ºC) (*10^{-6} K^{-1})	5.2	16.5	19.0

The AISI 304L stainless steel belongs to the austenitic family and as previously mentioned they are ternary iron alloys, with Fe, Cr, Ni and small amounts of Mn, Si, P and S. In the case of copper the remaining 0.1 wt.% is residual oxygen resultant from the refining process. For the preparation of composite powders, the amount of metallic binder was fixed at 12 wt.%.

3.2. Powder processing

The traditional processing methods applied to cemented tungsten carbides consist in the following main steps; mixture, pressing, sintering and in some cases HIP (hot isostatic pressure). In this work the mixture step, normally performed by conventional wet milling, was replaced by high energy ball milling (HEBM).

3.2.1. High energy ball milling

The HEBM was performed with the purpose of reaching better homogenization between the WC particles and the binder phase, to allow better refinement of the powder particles and increase the sinterability of the WC with Cu rich binders. The high energy ball milling used in present work was the planetary Fritsch Pulverisette 6, depicted in Figure 30.

Figure 30 - Planetary high energy ball milling Fritsch Pulverisette 6.

Before the parameters enhancement, a brief study was executed in order to evaluate the possible contamination of WC powders by the balls and the container during milling. Therefore, it was used 400 g of cemented tungsten carbide balls with 8 mm of diameter in a 250 ml AISI 303 stainless steel container. About 20 g of WC powders were subjected to the following conditions; 20h of milling at 350 RPM and a ball-to-powder weight ratio of 20:1 in argon atmosphere. After that, it was measured the weight loss of the balls and the container. It was also performed a chemical characterization by EDS of the WC powders to check possible contamination. The argon atmosphere is used to avoid oxidation of powders and gridding media during milling. To attain a proper argon atmosphere the system was purged during 2 min. and pressurized at 2 bar.
After this study, four compositions were prepared: WC, WC–12wt.% SS, WC–12 wt.% Cu and WC–6 wt.% SS + 6 wt.% Cu. These four compositions were investigated for the optimization of the following milling parameters:

- Rotation speed – 200 and 350 RPM;
- Milling time – 2, 4, 6, 8, 10 and 20 hours;
- Ball-to-powder ratio – 10:1 and 20:1.

Subsequently, the composite powders were characterized and the enhanced milling conditions were selected. Besides the compositions mentioned above, two other more compositions were studied in the further studies, WC–8 wt.% SS + 4 wt.% Cu and WC–10 wt.% SS + 2 wt.% Cu.

3.2.2. Powder compaction

In order to determine the most appropriate pressing pressure for the milled powders, a compaction study was made.

Firstly the powders were uniaxially pressed (*CARVER laboratory press – Model C*) in a stainless steel die with 10 mm of diameter during 60 seconds and using four different pressures, 200, 250, 300 and 350 MPa. The green density was achieved geometrically. After, the samples were isostatically pressed (*High pressure system U33, Institute of High Pressure Physics*) at 350 MPa during 15 min and the geometric green density was also assessed.

3.2.3. Sintering

Sintering is one of the most important stages in the powder processing, as well one of the most complex to control due to the great number of variables involved in the process.

Before starting any sintering cycle the vacuum levels of the furnace are tested and any eventual leakage are sealed. The samples were sintered in a tubular and vertical *SUPER KANT Termolab* furnace with operational maximum temperature of 1650 ºC, controlled by a *Eurotherm* DIP (derivative, integral and proportional) controller. This furnace has coupled a *Criolab* vacuum system comprising by a primary vacuum *Alcatel* pump and a *917 Pirani* pressure sensor, as is schematized in Figure 31.

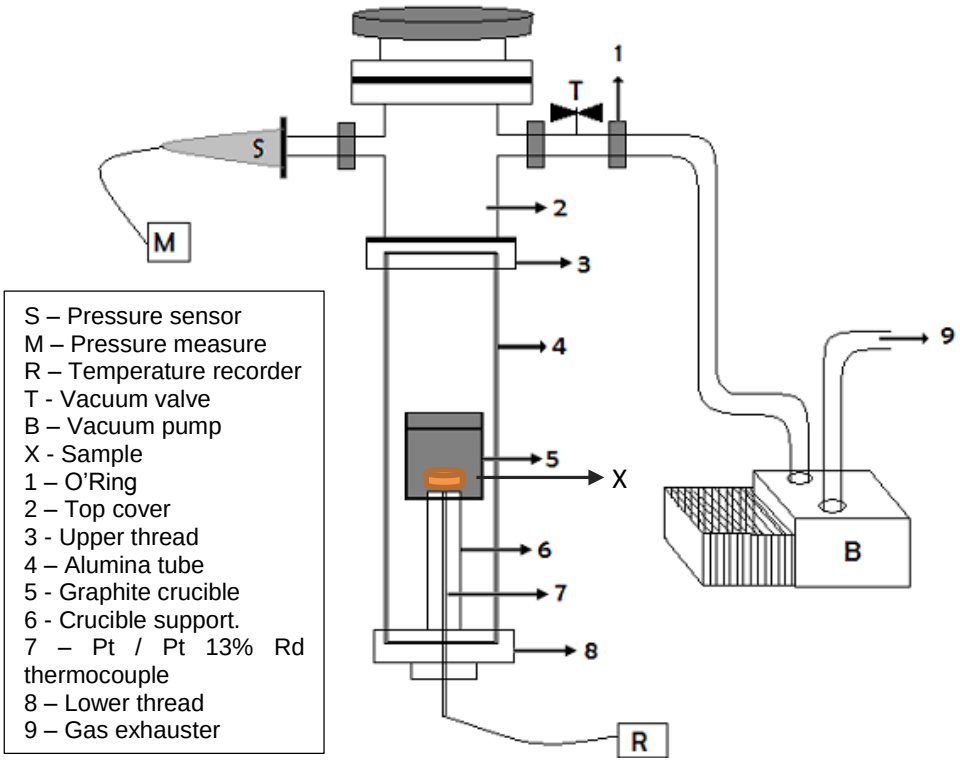

Figure 31 – Schematic representation of the furnace and vacuum system [8].

For the measurement of the temperature it was used a Pt/Pt 13% Rd thermocouple, that was in contact with the graphite crucible. Temperature and pressures during sintering were continually recorded by 2 channel *Kipp & Zonen* recorder. During the sintering cycle the vacuum pump was only turned off when the temperature was below 500 ºC to avoid eventual oxidation.

The sintering parameters, i.e., the cooling rates, sintering temperatures, dwell times and vacuum pressure were optimized. Besides the conventional sintering technique it was also tested the two-step sintering method. Table 9 shows the parameters range tested for both techniques.

Table 9 –Sintering parameters range.

Sintering temperatures (ºC)	1350 - 1500
Heating rates (ºC/min)	5 ºC
Cooling rates (ºC/min)	10 – 20 ºC
Dwell times	15 min – 20 hours
Vacuum pressure	20 – 50 Pa

3.2.4. Hot isostatic pressing (HIP)

Hot isostatic pressing (HIP) is a common technic amongst the powder metallurgy processing routes. This consolidation process allows the elimination of the remaining close porosity, enabling the attainment of near full dense samples. The HIP method combines elevated temperature with isostatic gas pressure placed together in a high pressure containment vessel favouring the sintering process.
This stage was performed in Durit Metais Duros, Lda. Facilities and the conditions used were the same for all the developed compositions; 1400 ºC, 60 MPa, in a total cycle duration of 9 hours.

3.3. Particle size analysis

The powder agglomeration, due to the high specific surface area, prevented the use of Laser Diffraction analysis. The BET (Brunauer–Emmett–Teller) technique was also attempt as a means to assess the powder particle size by the SSA (specific surface area), although for the same mentioned reason it proved to be unreliable; consequently, it was used Dynamic Light Scattering (DLS) analysis to assess the mean particle size.
For such purpose it was used the *Zetasizer Nano Zs* – Malvern Instruments*.* This apparatus applies the DLS technique to measure the diffusion of particles moving under Brownian motion, and converts these values to a size distribution using the Stokes-Einstein relationship. The suspensions were prepared with 0.02 wt% of powders sonicated for 15 min. It was tested 3 different suspension media (water, ethylene glycol and isopropyl alcohol). No significant difference were detected between the results achieved with the tested suspension media, therefore the water was the selected media for further studies.

3.4. Density determination

The apparent density was determined in green and dense samples geometrically by taking the weight, diameter and thickness.

In order to determine the relative density of each sample, it was necessary to establish the theoretical density, which depends on the sample composition, and can be calculated by the mixing rule, as

$$d_{theoretical} = \frac{1}{\sum\left(\frac{W_i}{r_i}\right)} \quad \textbf{(4)}$$

where W_i is the concentration (weight fraction) of each constituents and r_i is the theoretical density of each constituent. Table 10 resumes the theoretical densities calculated for each powder composition, assuming d_{SS} = 7.93 g/cm^3; d_{Cu} = 8.9 g/cm^3 and d_{WC} = 15.58 g/cm^3

Table 10 – Theoretical densities of the investigated compositions.

Composition	SS (wt. %)	Cu (wt. %)	$d_{theoretical}$ (g/cm^3)
WC-SS	12	0	13.95
WC-Cu	0	12	14.30
WC6SS6Cu	6	6	14.13
WC8SS4Cu	8	4	14.08
WC10SS2Cu	10	2	14.02

3.5. Thermal analysis

The thermal reactivity of the powders was evaluated by Differential Thermal - Thermogravimetric Analysis (DTA/TG) and also by Dilatometric Analysis (DA). Thermoanalytical methods, such as thermodilatometry and DTA analysis are crucial techniques to characterize the complex processes occurring during high-temperature treatment. Provides information on the shrinkage behaviour and kinetics, whereas DTA detects the fundamental thermal events, such as outgassing behaviour of the powders, melting and solidification of liquid phases [92]. This analysis assisted the optimization of the sintering process.

3.5.1. DTA/TG

The WC-SS, WC-Cu, WC6SS6Cu powders (see Table 10) milled for 20 h were analyzed using a *Setaram Labsys* equipment. The DTA/TG equipment calibration was carried out prior to sample testing using an empty alumina crucible. For each sample analysis, 10-20 mg of powder was placed in a new alumina crucible. A heating/cooling rate of 5°C min^{-1} was used from 25°C up to a 1400 ºC maximum temperature, within a flowing Argon atmosphere. However the available equipment, does not guarantee a constant flux of gas and oxidation systematically occurred in the WCSS composite powders, impeding the use of this technique in mentioned composition.

.

3.5.2 Dilatometric analysis

The dilatometric characterization was performed to the WC-SS, WC-Cu, WC6SS6Cu powders milled for 20 h. Specimens with a parallelepipedic-shape (14x4x4 mm^3), uniaxially pressed at 300 MPa and isostatically at 350 MPa were used. A homemade vertical graphite dilatometer was used for dilatometric tests [92]. Relative shrinkage was recorded from room temperature up to 1460°C with a heating rate of 10°C/min, under vacuum atmosphere (1 Pa).

3.6. Crystallographic characterization

The crystallographic characterization was performed by qualitative and semi-quantitative approach, X-Ray diffraction (XRD) and Rietveld analysis, respectively. The XRD technique was used to determinate crystallographic phases present in the powders before and after the HEBM, as well as to determinate the phases present in the sintered samples. The Rietveld analysis was used to estimate the weight phase percentage in sintered samples. The XRD spectrum was also used to evaluate the crystallite size of the powders prepared by HEBM, through the Scherrer equation.

3.6.1. Qualitative analysis (XRD)

The XRD analysis was performed in a *Rigaku diffractometer* with CuKα radiation and a characteristic wave length of λ_{cu} = 1.54056 Å. The XRD patterns of the powder samples were recorded in the range 2θ = 10 -60° using a step size of Δ2θ = 0.02° and a counting time of 3 seconds per step. The diffractometer is linked to a system control and data acquisition manages by *Jade 8* software. The sintered samples were converted into fine powder before XRD analysis using a stainless steel mortar and sieving the powder through 75 μm.

3.6.2. Semi – quantitative analysis (Rietveld)

The Rietveld method [93] was used for the phase quantification of sintered samples. The equipment used was a *Panalytical X'Pert Pro diffractometer* with CuKα radiation and a characteristic wave length of λ_{cu} = 1.54056 Å. The *High Score Plus* structural analysis software was applied for the phase quantification.

3.6.3. Crystallite size from XRD line profile analysis

The classic relation used for the calculation of crystallite size is the Scherrer formula:

$$D_{Scherrer} = \frac{K\lambda}{\beta \cos\theta} \quad \textbf{(5)}$$

where $D_{Scherrer}$ is the weighted apparent crystallite size, β the integral breadth of the line profile (XRD peak) caused by small crystallite size, 2θ the diffraction angle, λ the X-ray wavelength (e.g. 0.154056 nm for CuKα1 radiation) and K the (shape-dependent) Scherrer constant (e.g. 0.89 for spherical crystallites) [94]. Crystallite size of the powder material can be quantified from the XRD pattern by application of different line profile analysis (LPA) methods [53, 95, 96]. Peak fitting is one of those methods, and in this work it was found to predict reliable crystallite size values.

The WC crystallite size was determined for the WC – M (M=Cu, Fe, Cr, Ni) composites with the various milling times (2, 4, 6, 8, 10 and 20 hours). The relative small binder content, cause a low binder peaks intensities and in addition, the residual binder stress resulted in

considerable peak broadening, inhibiting the crystallite size measurement of the binder phase.

3.7. Morphological characterization

3.7.1. Scanning electron microscopy analysis (SEM)

Powder morphology was assessed using an *Hitachi SU - 70*, scanning electron microscope operated at 30 kV. As sintered WC– M (M=Cu, Fe, Cr, Ni) composite samples were resin hot mounted using an *Struers LaboPress-3equipment*, followed by the grinding and polishing procedure given in Table 11.

In order to reveal the composite phases, namely eta-phase, it is necessary to make a chemical etching with Murakami's solution (10 g NaOH; 10 g $K_3Fe(CN)_6$, 100 ml distilled H_2O). To analyze the eta-phase, the necessary etching duration is 2 seconds, while to reveal the WC grain boundaries the duration is 2 min. Finally, the samples were removed from the resin, tipped in a carbon pad to an aluminum SEM support and coated with carbon to ensure the conductivity of the sample.

Table 11 - Metallographic preparation technique.

Stages	Time(min)	Disc	Medium
Grinding	10	P350 (silicon carbide)	Water
Grinding	15	P600 (silicon carbide)	Water
Grinding	15	P1000 (silicon carbide)	Water
Polishing	20	Polishing cloths	Etilenogycol, 15 µm diamond suspension
Polishing	20	Polishing cloths	Etilenoglycol, 1 µm diamond suspension
Polishing	20	Polishing cloths	Etilenoglycol, ¼ µm diamond suspension

3.8. Chemical characterization: Energy dispersive X-Ray spectroscopy (EDS)

The chemical characterization was made by energy dispersive X-Ray spectroscopy (EDS *Bruker – Quantax 400*). This system is linked to the scanning electron microscope (SEM *Hitachi SU – 70*) and it is performed simultaneously.
The EDS detector has a detection limit of 1000 ppm, and low precision in the detection of light elements, such as oxygen and carbon. EDS provided rapid qualitative and semi-quantitative analysis of elemental composition. EDS X-rays were also used to form maps or line profiles, showing the elemental distribution present in the sample.

3.9. Mechanical properties characterization

3.9.1. Hardness

The Vickers hardness of the sintered samples, after polishing, were tested using an indentation force of 294.2N (HV30). The equipment used for hardness evaluation was the *Zwick/Roell ZHU*. For each sample, 10 measurements were performed and the hardness calculated using equation 5.
The indentation diagonals were measured as shown in figure 27, using an optical microscope *Zeiss Jenaphot 2000* at a magnification of 200 x, with Vickers hardness (HV30) calculated from Roebuck et al. [97]:

$$HV_{30} = \frac{1.8544\ P}{\left[{(d_1+d_2)}/{2}\right]^2} \quad \textbf{(6)}$$

where P is the applied load (Kgf), and d_1 and d_2 are the indentation diagonals (mm).

3.9.2. Palmqvist toughness

The Palmqvist toughness method is widely used for measuring the fracture toughness of hardmetals. In Palmqvist fracture toughness method, K_{1C}, is obtained by measuring the total

length of cracks coming from the four corners of a Vickers hardness indentation made with a single load of 294.2 N, at room temperature. Each Vickers indentation presented two pairs of radial cracks emerging from the corner. The crack lengths of the 10 indentations performed on each sample were measured using the optical microscope *Zeiss Jenaphot 2000* at a magnification of 200 x.

There are several methods to calculate the Palmqvist toughness and in this work it was used the curve – fitting method described by Ponton [98] (equation 6):

$$K_{1C} = 0.0087 \sqrt{H\, W_G} \qquad \textbf{(7)}$$

where H is the hardness, $W_G = P/L_t$, P is the load applied and L_t is the total crack length. The schematic diagram in Figure 32 represents the measurements of crack length and indentation diagonals.

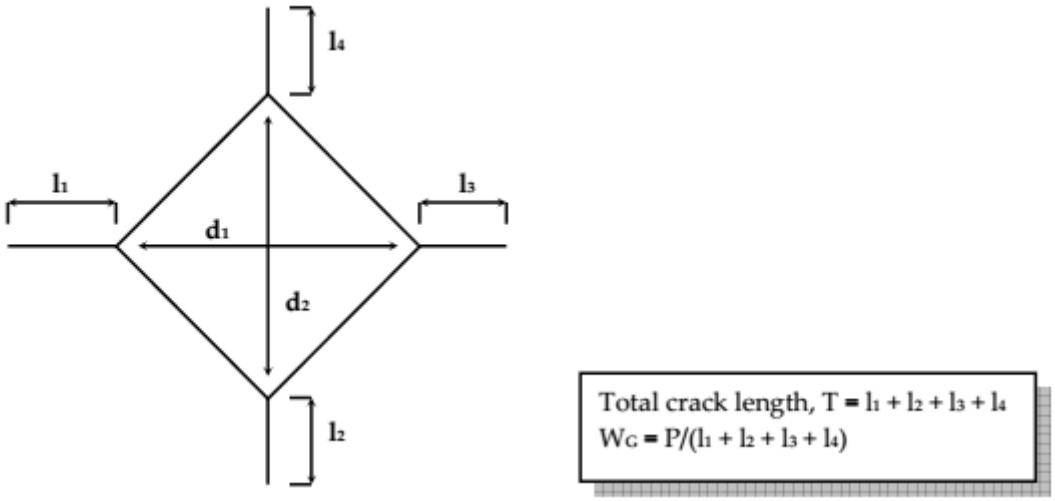

Figure 32 - Schematic diagram and definitions for Palmqvist test method [54].

Chapter 4

Results and discussion

4. Results and discussion

In this chapter the experimental results are described and a critical discussion is made, in order to understand and improve the development of current and future works in this subject.

This chapter is divided into six main sections;

- Initial powder characterization;
- HEBM optimization;
- HEBM powders characterization;
- Powders compaction;
- Sintering process optimization;
- Sintered samples characterization.

4.1. Initial powders characterization

As previously mentioned the raw powder materials used in the preparation of the composites were WC, Cu and SS. It is summarized in Table 12 some characteristics of those powders.

Table 12 – Characteristics of the raw powders

	WC	**Cu**	**SS**
Chemical composition[a] (wt.%)	94.5 (W), 6.13 (C)	99.9 (Cu)	71.15 (Fe), 18.8 (Cr), 10 (Ni), 0.03 (C)
G 50% (<) (μm)	1.1	9.4	5.5

[a] Information provided by the supplier

The powders morphology was attained through SEM, as depicted in Figure 33. The WC powders are constituted by small particles, which form aggregates with an irregular shape, (Figure 33a), while Cu and SS powders (Figures 33 b) and c), respectively) present near spherical particles.

.

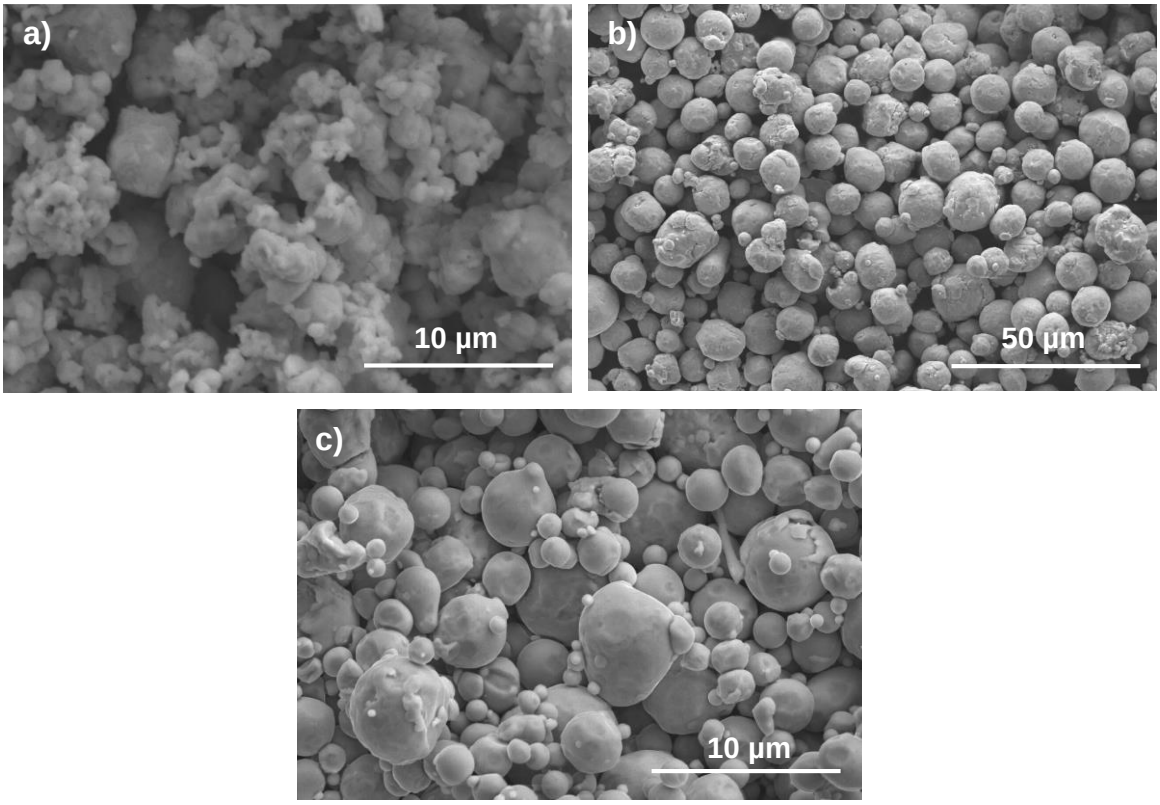

Figure 33 – SEM micrographs of the raw powders: a) WC; b) Cu and c) AISI 304L SS.

The XRD pattern of WC powder is depicted in Figure 34. As mentioned before, WC can exist in three different forms, α–WC (WC), β–WC (W_2C) and γ–$WC_{1-x.}$ Among the possible phases, α–WC is the only detected phase.

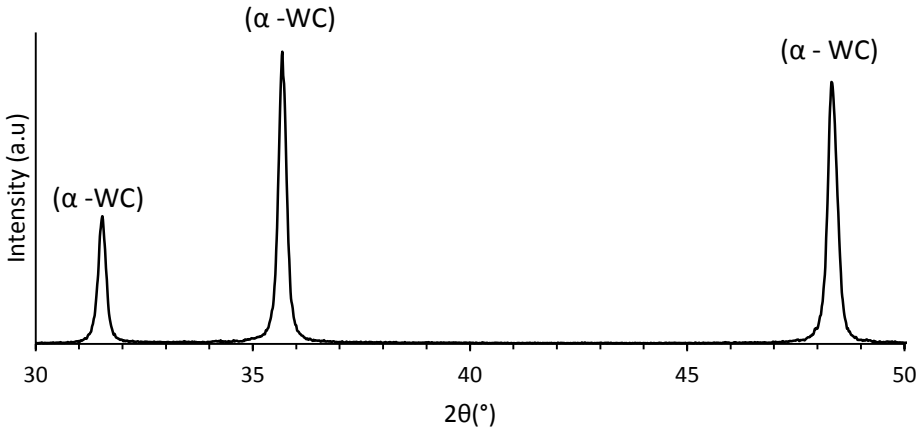

Figure 34 – X-Ray diffraction pattern of WC powder.

The WC powder was used for the formulation of all the compositions and the binder amount was fixed in 12 wt.%. The binders under research are Cu and AISI 304L stainless steel. Compositions of WC and Cu, SS and mixtures of SS+Cu, with SS:Cu ratios of 1:1, 2:1 and 5:1 were prepared (Table 13).

Table 13 – Chemical formulation of the composite powders.

Sample designation	WC (wt.%)	SS (wt.%)	Cu (wt.%)
WC	100	0	0
WCSS	88	12	0
WCCu	88	0	12
WC6SS6Cu	88	6	6
WC8SS4Cu	88	8	4
WC10SS2Cu	88	10	2

4.2. Optimization of HEBM variables

The composite powders were prepared by HEBM. This technique allows the fragmentation of WC hard clusters and transform them into fine particles homogeneously dispersed in the binder phase. This will be important to eliminate the presence of large porosity and other heterogeneities in the sintered samples, as well as to attain a consolidated composite material with fine grain size.

One of the problems frequently mentioned in HEBM process is the contamination of the powders by the surrounding gridding media (balls and container) [52, 53, 99]. In the attempt to avoid undesirable contamination problems it was selected WC–Co balls and an AISI 303 stainless steel container. These two materials are partially composed by the same components of the milled powders and the eventual contamination should not be a problem. The composition of the container was well known (stainless steel AISI 303), but the balls composition is unknown, since they were prepared by mixing new powders with machining burrs, without monitored composition. The average balls composition was carried out by EDS through the cross section analyse of 5 different balls. The mean elemental composition was recalculated assuming the stoichiometric carbon content of WC (Table 14).

Table 14 – Average ball composition assessed by EDS.

Element	wt.%
W	84.4 ± 0.6
Co	9.1 ± 0.9
Ni	0.9 ± 0.5
C[a]	5.6

[a] Stoichiometric carbon content, taking into account the amount of binder phase.

In order to evaluate possible powder contamination coming from the balls and the container it was made a "weight loss" test as described in the previous chapter. This test was performed in Argon (Ar) atmosphere to prevent oxidation and without any powders inside the container to induce severe wear of the gridding media.. For such a purpose, 400 g of WC-Co balls submitted to 350 rpm were weighted from 2h up to 20h of milling time.
After 20 hours of milling, the balls weight loss was c.a.2.5 wt%, (Figure 35), while no significant variation in the weight loss of the container was detected.

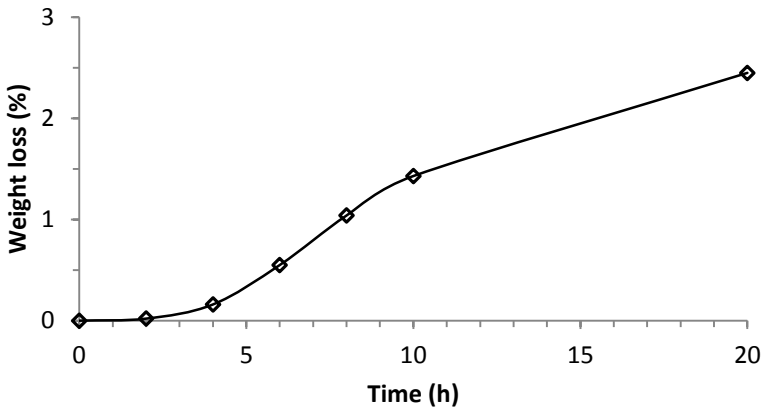

Figure 35 –Weight loss variation with milling time.

The same milling test was performed with WC powder, in order to determine Co and/or SS contamination coming from the gridding media. After 20h of milling it was not detected by XRD or EDS, contamination elements in WC powder, under the detection limits of these techniques. The existence of powder in the gridding media system decreases the energy developed in the collisions of ball-to-ball and ball-to-wall, due to the less free space in the container. It can also be formed a coating of fragmented powder on the surface of the balls and the container walls which prevents the wear of the gridding system [53].

The enhancement of HEBM variables was performed in compositions with and without metallic binder, WCSS, WCCu and WC, respectively (Table 13). The milling variables parameters as rotation speed, ball to powder ratio and time (Table 15) were adjusted, in order to define the best conditions for each composition. The results of crystallite size, calculated from XRD diffraction pattern and the particle size, determined from the DLS technique, were used to assess the evolution of the powders during milling and optimize the HEBM variables.

Table 15 –Variables studied in HEBM optimization.

Milling rotation (rpm)	Ball-to-powder ratio	Time (h)
200	10:1	2,4,6,8,10,20
350	20:1	

XRD diffraction patterns of the HEBM WC powder under the milling conditions of 350 rpm, 20:1, 2 h up to 20 h, are presented in Figure 36. The XRD patterns reveal that with increasing the milling time, the peaks are broadened, indicating a finer crystallite size and/or micro-strain in the milled powder [96].

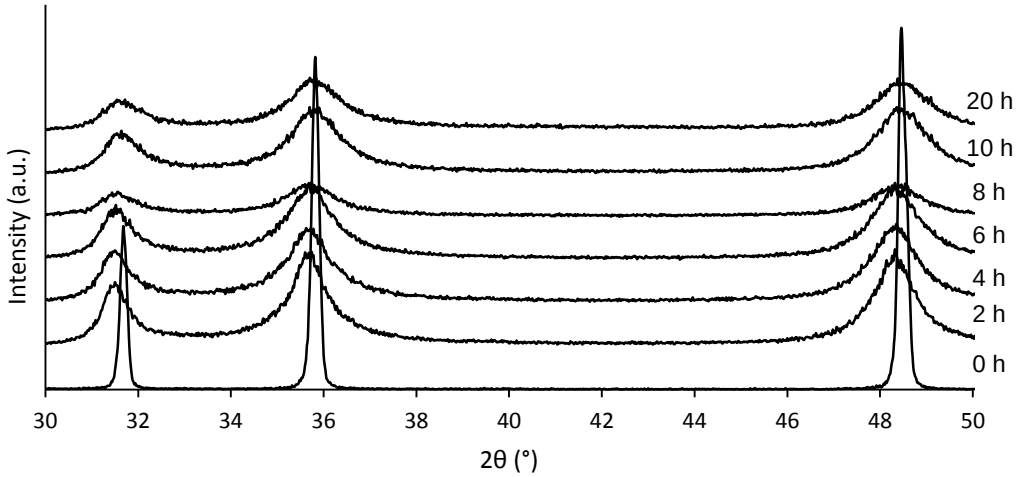

Figure 36 – Evolution of the diffraction patterns of the WC powders with different milling times, at 350 rpm with a ball-to-powder weight ratio of 20:1.

The increase of the milling rotation speed from 200 to 350 rpm and ball-to-powder weight ratio from 10:1 to 20:1 induces the decrease of the crystallite size (Figure 37).

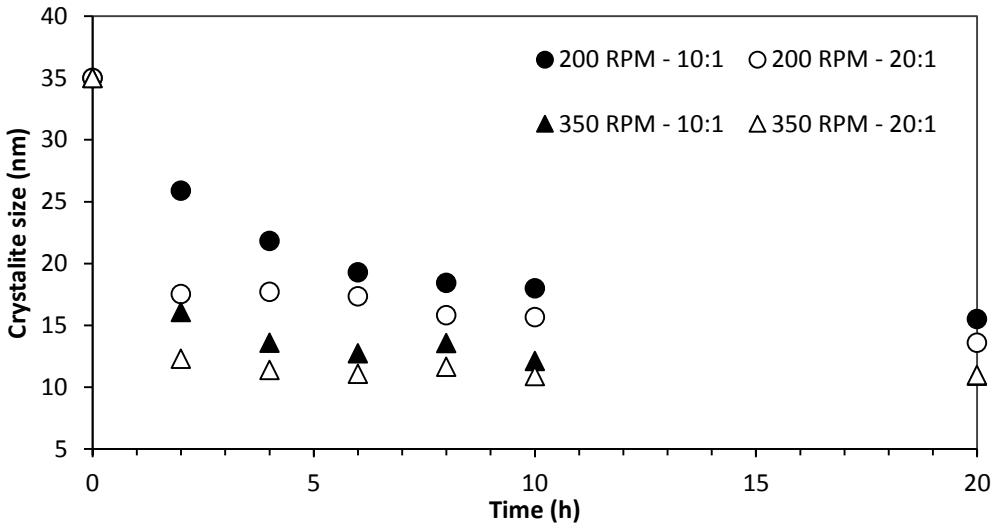

Figure 37 –WC crystallite size evolution under different milling conditions for the composite powder WSS.

The rotation speed has a greater influence on the crystallite size reduction than the ball-to-powder ratio (BPR). As shown in the Figure 37, even for the maximum milling time used in this work (20 h), the powders submitted to a rotation speed of 200 RPM only attained 14-16 nm of crystallite sizes, whereas it is attained a value of ~11 nm when a speed of 350 rpm is applied, independently of the BPR. The combination of 200 RPM of rotation speed and 10:1 ball-to-powder ratio proved to be the less effective in the refinement of the crystallite size. Furthermore, to achieve a reduced crystallite size with those conditions, a longer time is needed, i.e. 20 h to attain 15.5 nm.

It is also noticeable in Figure 37 that the time required to achieve the finest crystallite size is lower in the conditions of 350 rpm, 20:1, i.e. , after 4h a stabilized crystalline size is attained. This trend was visible in all the tested compositions, as exemplified at Figure 38. Therefore, the rotation speed and ball-to-powder weight ratio, chosen to apply to all compositions was 350 rpm and 20:1, respectively.

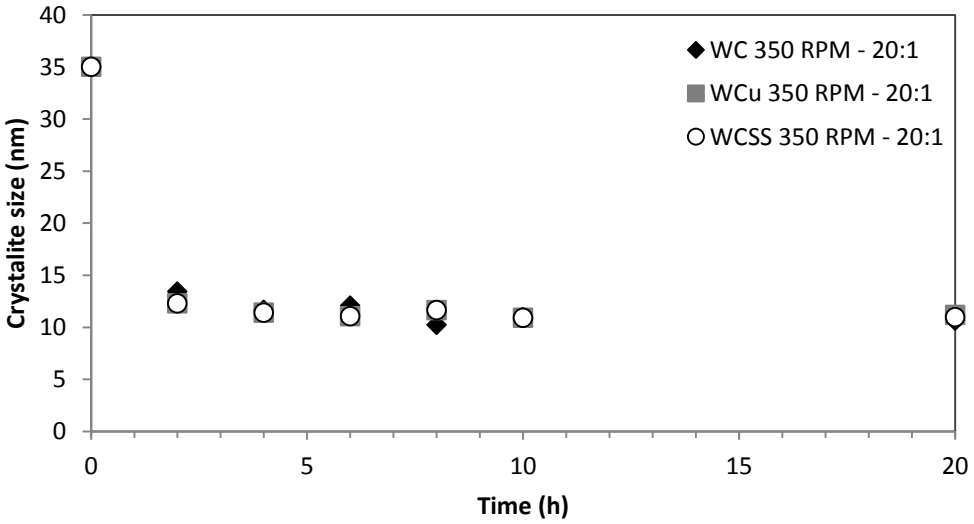

Figure 38 – Variation of the crystallite size with the milling time, attained under the conditions of 350 RPM and 20:1 BPR for different powders composition.

With the established conditions of rotation speed and BPR (350 rpm, 20:1), it was characterized the particle size of the composite powders WC, WCSS and WCCu in function of the milling time. Figure 39 resumes the particle size evolution with the milling time.

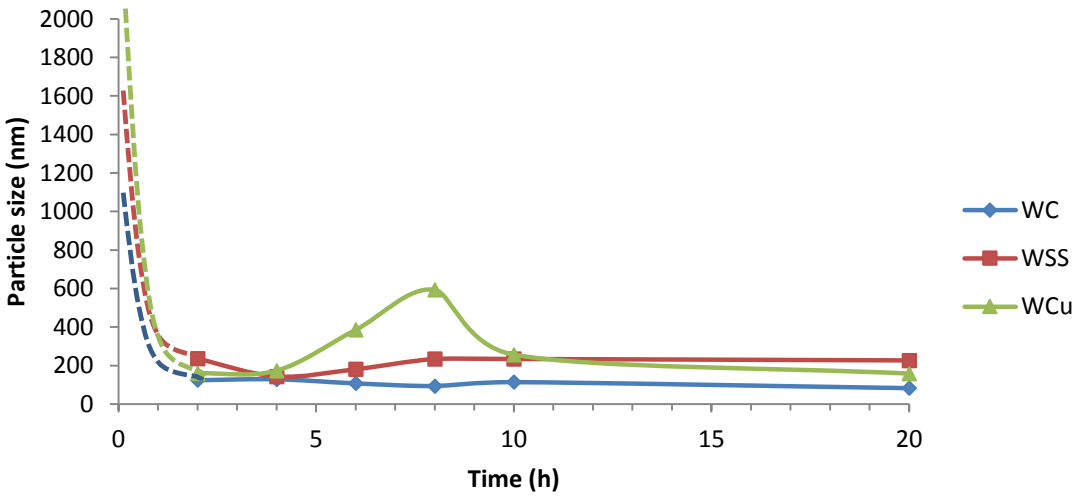

Figure 39 – Particle size evolution during milling (conditions; 350 RPM, 20:1 BPR).

It is shown that after 2 hours of milling the WC powder particle size decreased from ~1100 nm to c.a. 100 nm and no considerable variations are detected for higher milling times (Figure 39).

The behaviour of a mixture of powders composed of a brittle phase (WC) and a ductile phase (SS or Cu) is significantly different. In the initial stages of milling, the ductile metal powder particles are flattened by the ball-powder-ball collisions, while the brittle particles are fragmented, resulting in initial decrement of the particle size, as was firstly reported by Benjamin [100]. With further milling, the ductile powder particles get work hardened, the ductile phase acquires a lamellae shape being the brittle particles localized between the lamellae [53] (as described in chapter 2). Here we reach the state were the particles present the bigger particle size (Figure 39). After that, with continued milling, the lamellae get further refined, the interlamellar spacing decreases, and the brittle particles get uniformly dispersed into the ductile phase [53].

It is also shown in Figure 39 that after 8 hours of milling, the composite powders reached the larger particle size. Another feature that also seems to affect the particle size at this point, is the ductile character of the metal used in the composite powders, the higher ductile binder metal will have the coarser particle size, as is here the case of WCCu.

The milling time was chosen taking into account the results of crystallite size together with the particle size. As pointed before, after 4 hours of milling at 350 rpm, 20:1 BPR, there was no measurable changes in the crystallite sizes of the studied compositions. Nevertheless, there are some important changes in the particle size of the composite powders (Figure 39) which determine the choosing of longer milling time:

i- For the binder compositions with higher Cu content, i.e. WCCu, WC6SS6Cu, WC8SS4Cu, it was selected 10h of milling time (Table 16), because, as observed in figure 39, for composite powders with Cu binder, the particle size increases between 4 and 8 hours of milling stabilizing after 10h;

ii- In the case of composite powders with higher SS content, WCSS and WC10SS2Cu, 8 h of milling time was chosen. As observed in Figure 39 an initial decrement of the particle size occurs, mostly due to the fragmentation of the brittle phase (WC) [100], after that the ductile phase (SS) covers the brittle fragments and the particle size tends to increase. This was observable between 4 and 8 hours of milling, after that there was no mentionable further reduction in the particle size.

Table 16 – Optimized conditions for the investigated compositions.

Composition	Rotation speed (RPM)	BPR	Time (h)
WCSS	350	20:1	8
WCCu	350	20:1	10
WC6SS6Cu	350	20:1	10
WC8SS4Cu	350	20:1	10
WC10SS2Cu	350	20:1	8

4.3. Characterization of the milled powders

The ball milled powder compositions under conditions established in Table 17 were characterized.

Table 17 – Characteristics of the milled powders (350 rpm, BPR 20:1).

Composition / milling time (h)	G 50 (nm)	Crystallite size[b] (nm)
WCSS / 8h	234	11.65
WCCu / 10h	257	11.60
WC6SS6Cu / 10h	241	11.92
WC8SS4Cu / 10h	211	10.47
WC10SS2Cu / 8h	223	10.92

[b] Obtained from XRD diffraction patterns

The influence of the HEBM process in the structure of the WCCu and WCSS powders is shown in Figure 40. It can be seen that copper and iron binder phases are detected in the un-milled powders. However, theses phases are not detected after milling. As explained above, the milling process induce the refinement of crystal structure and the broadening of the peaks in the XRD patterns, reducing the detection limit of minor phases, as is the case of copper and iron.

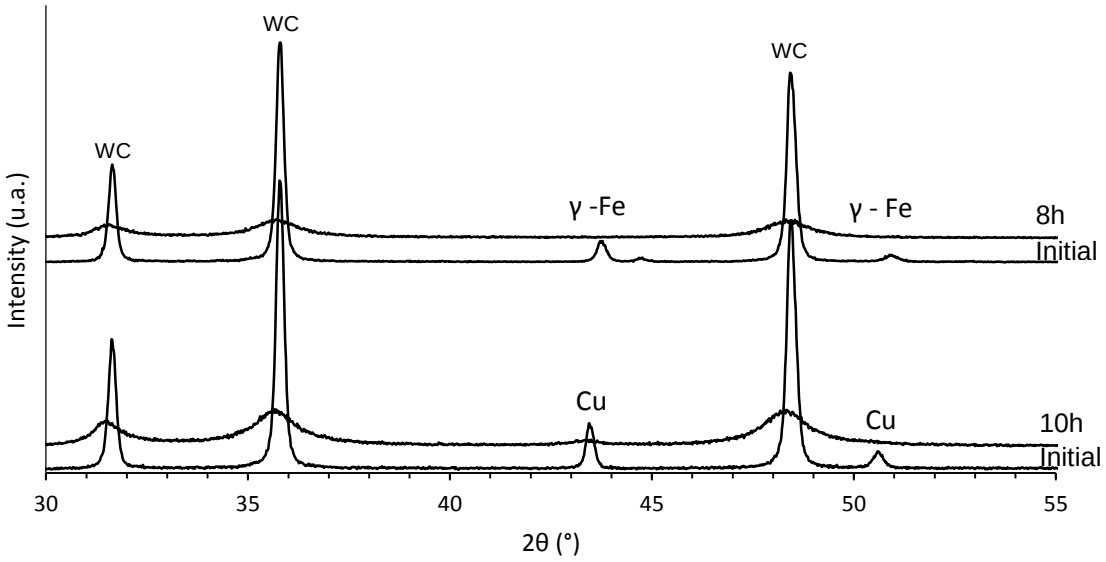

Figure 40 – Influence of the HEBM in the XRD patterns of the WCCu and WCSS powders.

To confirm the presence of the metallic binders in the composite powders after milling, it was realized an EDS map. It was confirmed in all compositions the presence of the binders. Moreover, it was also observable that the binder homogenization is well achieved with the HEBM process, as depicted in Figure 41a for the WCSS composite powders. Comparing the Fe distribution on the WCSS powders milled in similar conditions (200 rpm, 20h) by HEBM and by conventional wet milling (Figure 41b), it is perceptible the larger homogenization achieved in HEBM powders. The HEBM, as expected, allows higher particle size reduction than conventional milling, as well as a greater homogeneity in the binder distribution in the composite powders. These two factors are from the technological point of view very important, since they may have a great impact in the powder processing and therefore in the final mechanical properties of the sintered samples.

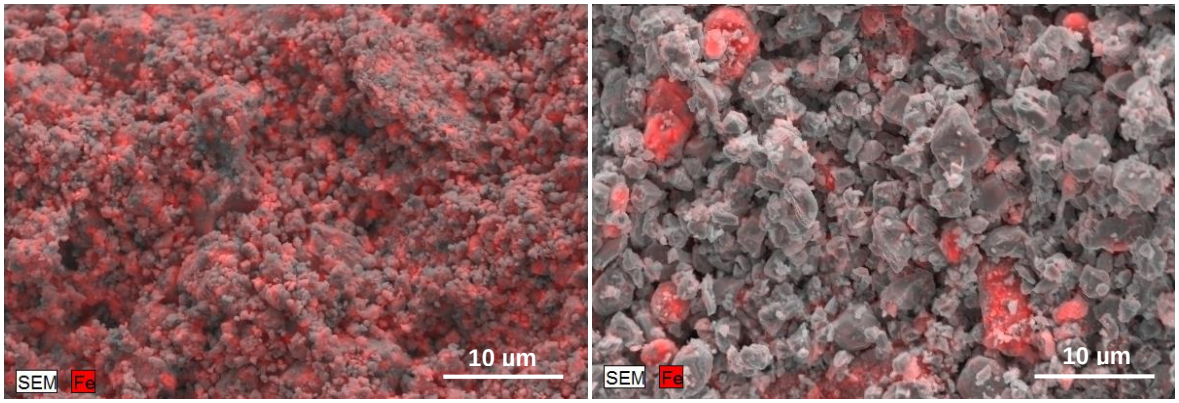

Figure 41 – SEM micrographs and their respective iron x-ray maps **a)** WCSS powder at 200 rpm, for 20 hours. **b)** WCSS powder conventionally wet milled at 200 rpm for 20 hours.

Since different binders compositions were used, the influence of the binder composition in the samples compaction was investigated and it is presented in Figure 42 the compaction behaviour of the WCSS, WCCu and WC6SS6Cu powders.

The uniaxial pressing was performed at four different pressures; 200, 250, 300 and 350 MPa. As expected, the compaction trends were different for the studied powders (WCSS, WCCu and WC6SS6Cu) (Figure 42a) The WCSS composite powder shows an increase of 2% in the relative green density within the range 200 to 300 MPa, after that it stabilizes in the c.a. 59 % of relative density. The same powder composition prepared by conventional wet milling [7] achieved a more efficient packing, 63% of relative density, under the same pressure conditions. The smaller particle size (c.a. 200 nm) reached with HEBM contrasting with 2-3 μm attained by Marques et al [7] could explain the packing difference. The low pressing ability of nanopowders is conventionally explained by adhesive interaction between individual particles, which leads to the formation of strong aggregates. Possible features responsible for the size effect also include the attractive van der Waals forces [101], the absence of plastic deformation of nanoparticles [102], the formation of chemical bonds, electrostatic interactions, and some others [103].

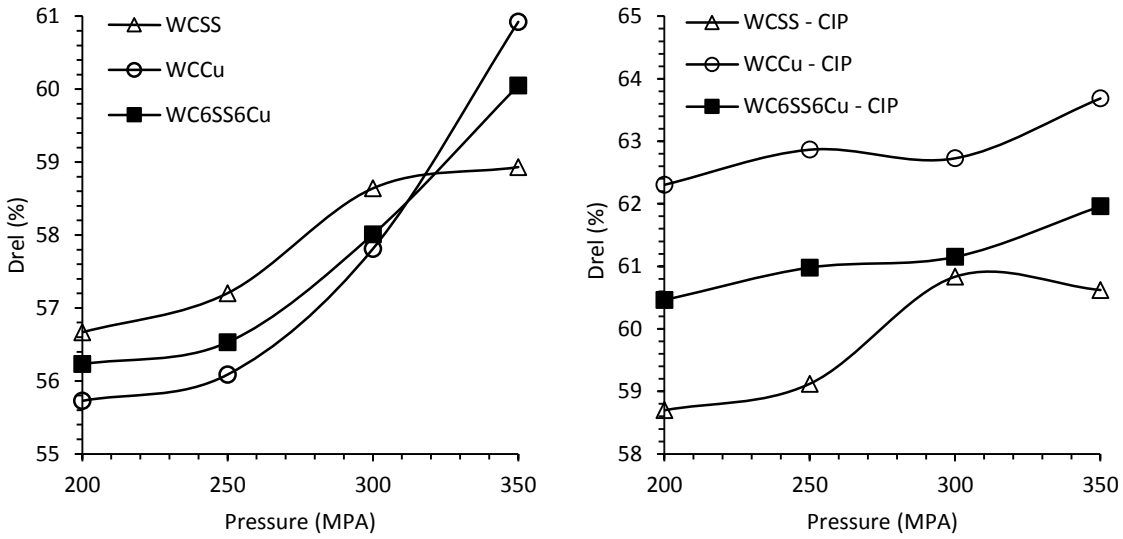

Figure 42 – Variation of relative density as a function of the applied uniaxial pressure in the WCSS, WCCu and WC6SS6Cu powders. **a)** after uniaxial pressing; b) after uniaxial and CIP (350 MPa – 15 min).

The relative green density of WCCu increases until 350 MPa (c.a. 61%) whereas the WCSS powders shows no variation of packing after 300 MPa. (Figure 42a). Indeed, an increment of 5 % in the relative density was discernible between 200–350 MPa, for WCCu and this value is significantly higher than the exhibited by the WCSS powders, mostly due to the superior ductile character of the copper when compared to the SS.

The WC6SS6Cu uniaxially pressed powders shows a compaction behaviour similar to the WCCu powders, as can be seen by the respective curve trends (Figure 42a), denoting the higher influence of the copper in the compaction process, although the presence of SS in the mixture decreases the density attained in the pressure range of 310 – 350 MPa when compared to the WCCu powder, being the highest relative density attained of c.a 60 % at 350 MPa.

After uniaxial pressing, the samples were additionally submitted to cold isostatic pressing (CIP), at 350 MPa for 15 min. This procedure allowed the improvement of the green density in all compositions (Figure 42b). Thus, in WCSS composite powders the increment was c.a. 2% in all the tested range. However, in WCCu powders this value was much higher, 7% for the lower uniaxial pressure, 200 MPa, and 3 % at 350 MPa. In the WC6SS6Cu powders the increment of relative green density was c.a. 5 % for the lower pressure and 2% at 350 MPa, showing once again the same trend of the WCCu powder (Figure 42b). The maximum

relative density attained was 61% for WSS, 64% for WCu powders and 62% for WC6SS6Cu.

Based on the study carried out, the pressing conditions for the different powder compositions were established and are summarized in Table 18. For the powders with higher SS content, WC10SS2Cu and WC8SS4Cu it was selected the same conditions as WCSS powders, due to the predominant amount of SS. For the WC6SS6Cu it was selected the same conditions of WCu powders.

Table 18 – Selected compaction pressures.

Composition	Uniaxial pressing (MPa)	CIP[a] (MPa)
WSS	300	350
WCu	250	350
WC6SS6Cu	250	350
WC8SS4Cu	300	350
WC10SS2Cu	300	350

[a] Pressure applied for 15 minutes.

4.5. Sintering

The sintering process was a challenging step during the progress of this work, due to the different reactive sintering behaviour of the studied powders (Table 13), and the goal to maintain the nanocrystallinity.

In order to predict the thermal behaviour of the composite powders during sintering, it was performed two thermal analysis, DTA/TG and dilatometry.

4.5.1. Thermal analysis

Thermodilatometry (TD) was performed in a graphite furnace dilatometer with a heating rate of 5ºC/min from room temperature until 1450 ºC, and at a constant vacuum pressure of 1 Pa. The linear shrinkage and shrinkage rates were obtained by TD analysis for the WCCu, and WCSS.

The thermal behavior of the WCSS composite powders are showed in Figure 43. In Figure 43a, it is visible two different sintering stages: (I) slow but pronounced densification step

due to the particles rearrangement, characteristic of the solid state sintering; (II) densification due to the mechanisms of solution and precipitation in the liquid phase sintering.

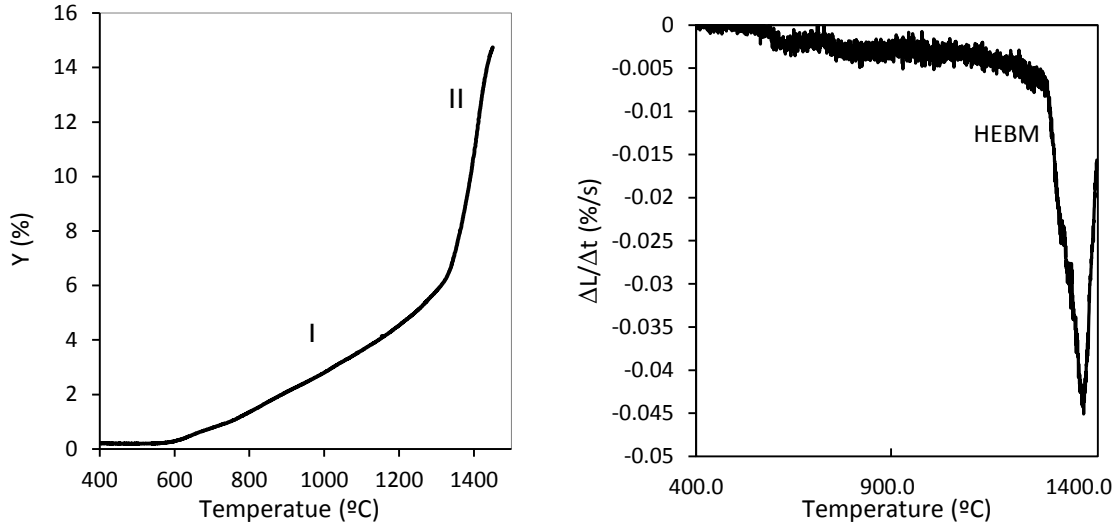

Figure 43 - Thermodilatometric analysis (TD) of WCSS HEBM powders: **a)** Linear shrinkage percentage; **b)** Shrinkage rate.

Comparing the thermal behaviour of HEBM powders (Figure 43) with WCSS conventionally prepared by Marques et al. [7] (Figure 27), it is perceptible significant differences. As mentioned the HEBM WCSS is sintered in two stages while conventional WCSS is sintered in three. It is also perceptible a less pronounced rearrangement step in the conv. WCSS.
The shrinkage of the HEBM WCSS composition starts at 600 ºC, instead conventional milled powders starts at c.a. 900 ºC. As can be seen in Figure 27 the pronounced shrinkage peak attributed to the liquid phase formation occurs in the temperature range 1200–1250 ºC for the conventional WCSS and 1330–1450 ºC for HEBM powders, matching in this case the shrinkage rate peaks visible in Figure 43b. It is thought that, in the HEBM WCSS composites the liquid phase formation is delayed to higher temperatures, beginning as mentioned at 1330ºC, which is higher than the eutectic temperature (1230 ºC), in WC-Fe-Ni system, (the reported phase diagram with the closest similar composition of WCSS). The marked rearrangement step (between 600 ºC and 1330 ºC) of the HEBM WCSS powders increased the decarburization, affecting the carbon content. Therefore, a carbon content dislocation to lower amounts in WC-Fe-Ni phase diagram is expected, increasing the liquid temperature formation (Figure 43).

It was observable that the shrinkage rate of conventional WCSS is higher than in the HEBM WCSS. There are two possible factors that can help to understand this phenomenon. One is the large rearrangement step that can promote the neck formation between the powder particles and decrease their mobility, reflecting in a slower shrinkage rate. Other possible explanation is the higher reactivity of the HEBM WCSS powders that, can react at low temperatures for the formation of eta – phase. Therefore, the SS binder elements are consumed in that phase formation, being unavailable for the liquid phase formation. This behaviour does not occurs on conv. WCSS [7], since the powder reactivity is lower than HEBM, consequently is noticeable a pronounced shrinkage rate at 1220 ºC, (Figure 27).

In Figure 44 is shown the linear shrinkage and shrinkage rates of HEBM WCCu powders. As can be seen the shrinkage of this powders stars at 620 ºC and continues until 1450 ºC. The TD analysis of this powders recorded three distinct sintering stages: (I) small increase of density, attributed to the solid state sintering; (II) sharp increase in density endorsed to the liquid phase formation; and (III) slow densification due to the mechanisms of solution and precipitation in the liquid phase sintering.
Comparing the thermodilatometric curves of WCSS and WCCu (Figure 44 a) and b) it is perceptible that the shrinkage rate of the WCSS is much higher. The higher sinterabillity attained by WCSS powders is expected since copper present poor wettability in WC surface [104].

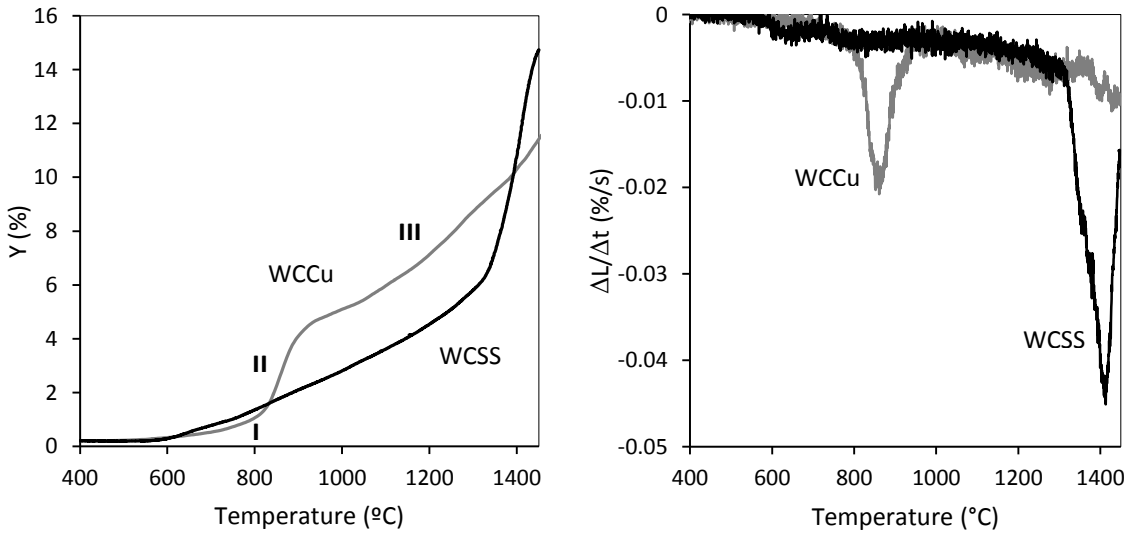

Figure 44 - Thermodilatometric analysis (TD) of HEBM WCCu and WSS powders: **a)** Linear shrinkage percentage; **b)** Shrinkage rate.

The pronounced shrinkage rate peak at 860 ºC matches with the liquid phase formation that is depicted in Figure 45 (DTA analysis) were the beginning of the first endothermic peak also stars at 860 ºC. In WCCu composite powder it is also showed a second endothermic peak at 1080 ºC (Figure 45). During the HEBM the powder particle size was severely reduced until the nanometric size, changing their reactivity and shifting the formation of liquid phase to lower temperatures [105]. Nevertheless, the presence of some remaining copper particles above the nanometric size can explain the existence of the second endothermic peak that occur at the copper melting temperature (1083 ºC).

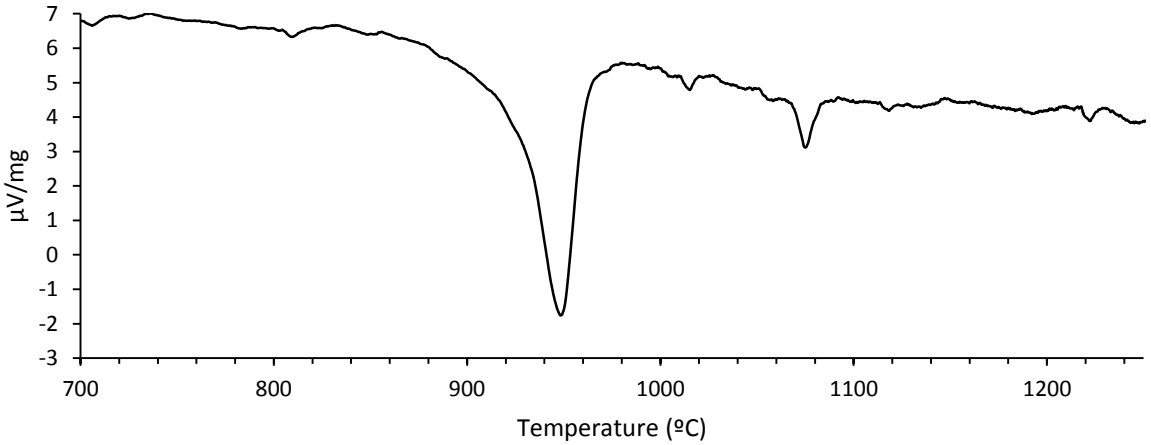

Figure 45 – DTA WCCu analysis.

4.5.2. Sintering optimization

As mentioned before the sintering process was performed in a vacuum furnace using a graphite crucible. It was adjusted for each composition the heating and cooling rates, maximum sintering temperature, dwell time at the maximum sintering temperature and vacuum pressure. The sintering process was developed with the intent of avoiding grain growth; therefore, it was tested two different sintering methodologies, two-step sintering and conventional sintering with short permanence at the maximum temperature and abrupt cooling rate.

Table 19 summarizes the enhanced sintering conditions of conventional sintering for all the studied compositions. It was verified that maximum sintering temperature and vacuum pressure are the principal parameters influencing the weight loss. The combination of low vacuum pressures and excessive temperature revealed to be the most responsible

parameters for higher weight loss, due to metallic binder volatilization. This effect is more noticeable for the samples with higher copper content (WCCu).

The lower melting temperature of copper (1083 ºC) and its insolubility with iron to form a solid solution, directed to a sintering temperature decrease and in other hand a dwell time and vacuum pressures increase, to control the weight loss. In those conditions it was possible to densify until 94% the WC10SS2Cu, while only 78% was achieved for WCCu (Table 19).

In the sample without copper (WCSS) it was attained 99% of relative density at 1450 ºC with the smallest dwell time, 15 min, reflecting the good wettability and sinterability of these powders. Comparing the sintering cycles of HEBM and conventional milled WCSS [7] it is observable a significant reduced holding time at the maximum temperature, from 2 hours in the case of conventional milled WCSS to 15 min in the HEBM WCSS, without prejudice of the sintered relative density (99%).

Table 19 – Results of the conventional sintering technique

Composition	ρ_{green} (%)	Sintering temp. (ºC) / Holding time (min)	Pressure (Pa)	ρ (%)	Weight loss (%)
WCSS	58.9	1450 / 15	20	99	3.0
WCCu	65.2	1300 / 30	40	78	4.1
WC6SS6Cu	60.4	1500 / 15	40	89	3.6
WC8SS4Cu	55.3	1350 / 60	40	91	3.4
WC10SS2Cu	60.8	1380 / 30	30	94	2.8

In order to close some remaining porosity and attain relative densities above 96%, the samples were submitted to HIP (hot isostatic pressing). In this stage it was used 60 MPa of pressure, at 1400 ºC for 1h. Table 20 shows the values of the relative densities before and after HIP. It is observable that the HIP process increases the relative density from 1 up to 8%. All compositions were densified above 96% excepted WCCu composition (79 %), what was really expected taking the high porosity of the sample in the first sintering cycle and the poor wettability of copper in WC.

Table 20 –Relative density before and after sintering of studied compositions.

Composition	$\rho_{before\ HIP}$ (%)	$\rho_{after\ HIP}$ (%)
WCCu	78	79
WC6SS6Cu	89	96
WC8SS4Cu	91	99
WC10SS2Cu	94	100
WCSS	99	100

Other feature that is possible to analyse in Table 20 is the correlation between the relative densities and the copper content. (Figure 46). The increase of copper content decreases the almost proportionally the relative density before HIP, while this effect is only observed for copper contents larger than 4% after HIP.

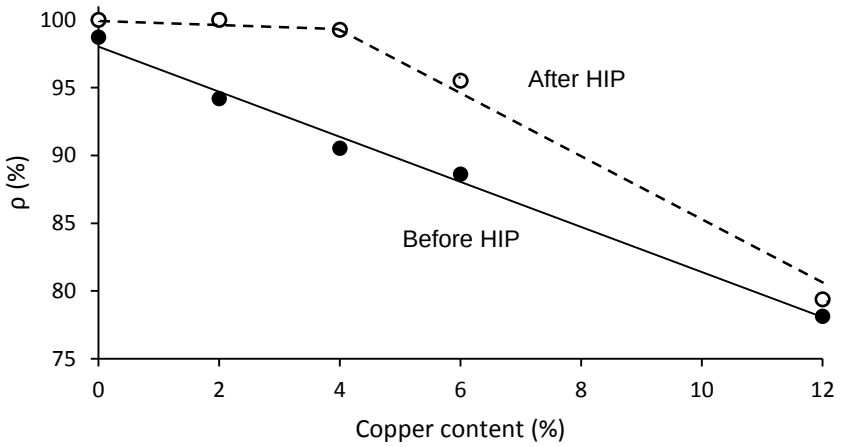

Figure 46 – Correlation between relative density before and after sintering with the copper content.

The two-step sintering (TSS) was selected due to the large time of permanence in temperatures below the liquid phase formation, as depicted in Figure 47, maximizing the rearrangement step. As shown in the thermodilatometry analysis (Figure 43a) and reported by Froschauer et al. [61] the rearrangement in the solid state is the main densification process of nanometric – ultrafine powder compacts.

A faster cooling rate (15 ºC/min) when compared with the heating rate (5ºC/min) was selected for the TSS cycle (Figure 47).

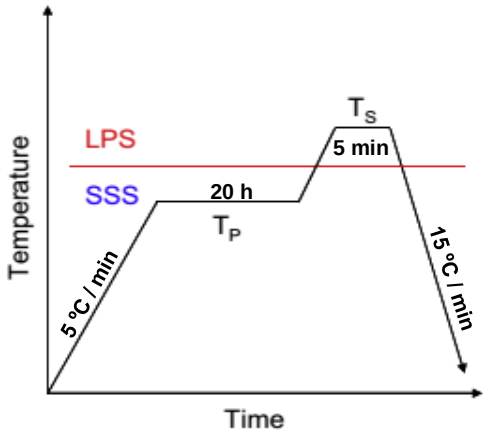

Figure 47 – Two - step sintering thermal cycle.

After reaching the maximum temperature, the grain growth is fully developed. Abrupt temperature decrease and short permanence at this point will decrease the effect of the fast diffusion mechanisms contributing to grain growth. The solid state sintering temperature (TP) and the liquid phase sintering temperatures (TS) were set using the thermodilatometric and TGA analysis data obtained for WCSS and WCCu (Table 21) and the residence time at that temperatures were kept as showed in Figure 47, TP – 20h and TS – 5 min.

Table 21 – Results of two step sintering technique.

Composition	ρ_{green} (%)	TP / TS (ºc)	Pressure (Pa)	ρ (%)	Weight loss (%)
WCSS	58.7	1410 / 1450	20	95	3.5
WCCu	65.0	850 / 1250	40	79	3.1

4.6. Sintered samples characterization

In this work the structural, morphological, chemical and mechanical characterization of the sintered samples was assessed and subjected to critical discussion.

4.6.1. Structural characterization

The structural characterization was performed by XRD, after deagglomeration of the sintered samples into powder. This technique allowed to identify and quantify (Rietveld method) the crystalline phases. In Figure 48 it is depicted the diffraction patterns of WCSS.

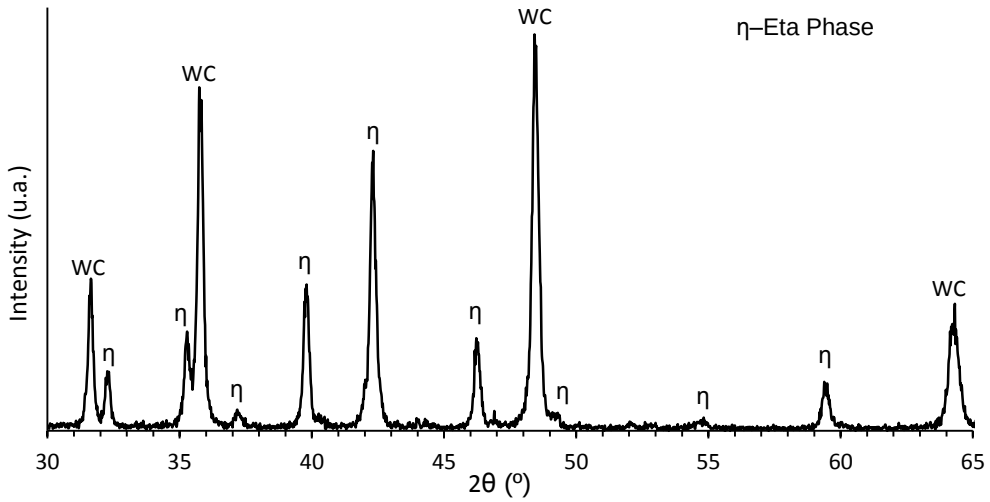

Figure 48 – Diffraction pattern of WCSS.

In this composition two different phases WC and $(M,W)_6C$ (η – phase) were identified. However, it must be mentioned that the detection limit of this technique is 2 wt.%, therefore the presence of phases below this value are not identified or quantified.
The detection of η – phase was expected, since the formation of this phase is predicted in the phase diagram WC-Fe-Ni (Figure 12). The Fe – γ (phase characteristic of the austenitic stainless steel) was not detected and if present it must be in very low quantities, less than 2 wt% (Table22), since it was largely consumed during the formation η – phase.

Comparing the results for the amount of η–phase determined in this WCSS sample, 48%, (Table22) with the amount of 11% reported by Marques et al. [7], (WCSS conventionally prepared), it is noticeable a significant difference despite the similar sintering temperatures in both works. This fact points to the great influence of the particle size in the reactivity of the powders during sintering and in the final phase composition, as well as in the expected mechanical properties of both composites, as will be seen ahead in this work.
In Figure 49 it is depicted the diffraction patterns of WCSS and WC6SS6Cu.

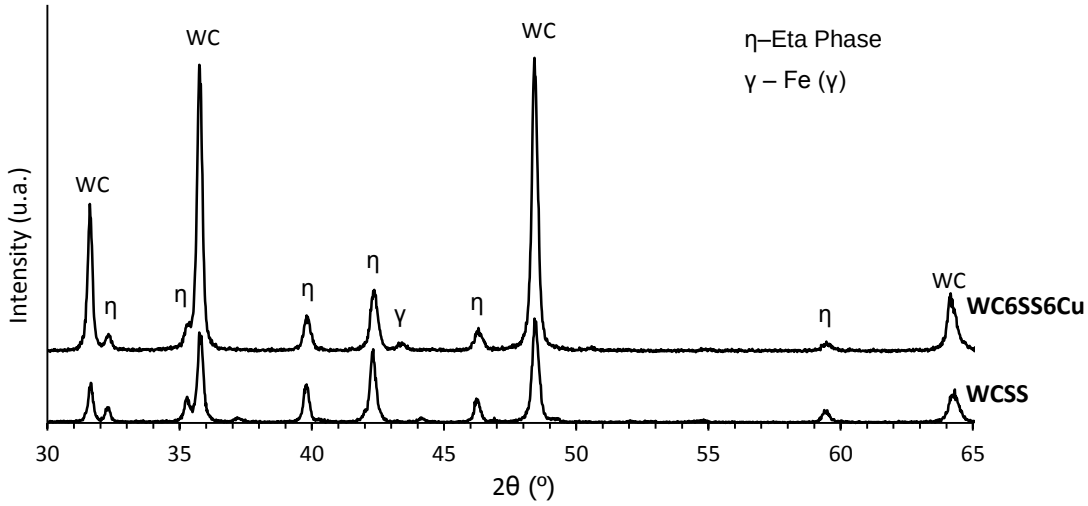

Figure 49 – Diffraction pattern of WCSS and W6SS6Cu.

Comparing the two diffractograms it is noticeable in both compositions the presence of the two characteristic phases of WCSS (WC and eta-phase) and the appearance of a third one in the WC6SS6Cu, Fe (γ). The presence of copper in the WC6SS6Cu powders lead to the segregation of iron during sintering [106] forming small "lakes" of unreacted iron (Figure 50), detectable by XRD. This effect explains not only the presence of Fe (γ), but also the decreasing of the η – phase amount, 19% instead of 24% (since the amount of SS in the composition is one half that of the WCSS, Table 22).

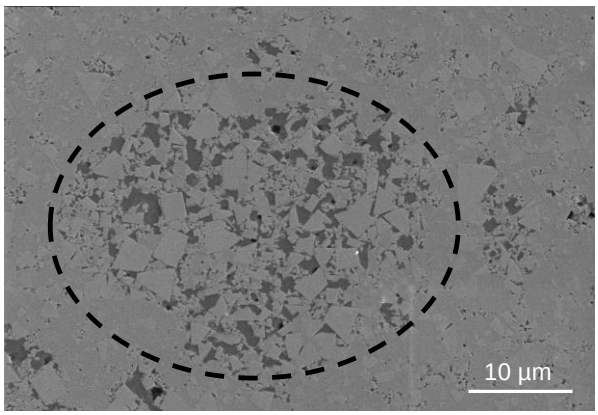

Figure 50 – SEM micrograph **of** WC6SS6Cu composition.

The XRD patterns of the conventionally sintered and TSS WCCu samples are depicted in Figure 51 and it can be observed different crystalline phases.

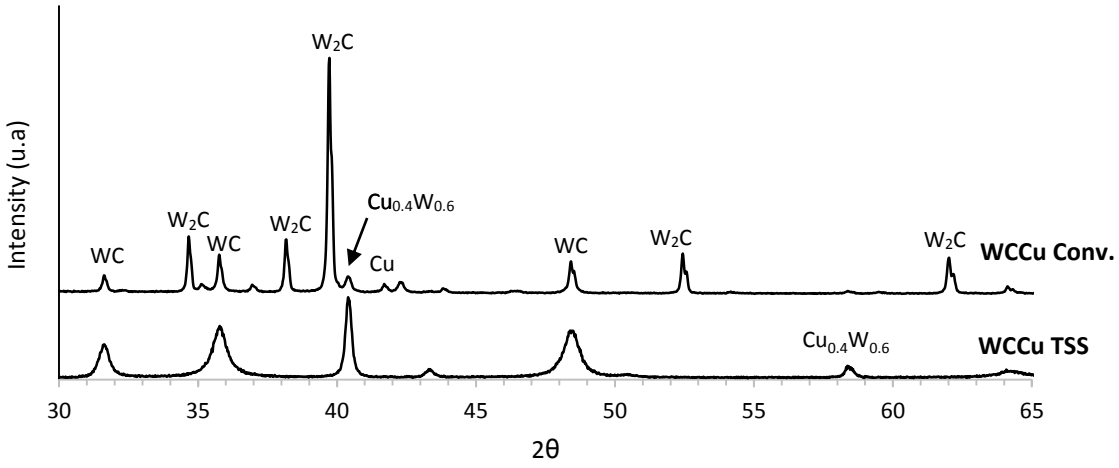

Figure 51 - X – Ray pattern of the conventional and TSS WCCu sample.

The major phase in WCCu conventionally sintered is W_2C (80%) and in the WCCu sintered by TSS is WC (56%), closely followed by $Cu_{0.4}W_{0.6}$ phase (42%) (Table 22). In both sintering techniques decarburization occurs, however the sintering temperatures and times are considerably different (Table 19 and 21). In the conventionally sintered WCCu the temperature/dwell time used was 1300 ºC/30 min, and recurring to the W-C phase diagram (Figure 3), it is understandable that at this temperature W_2C phase is thermodynamically stable. On the other hand, the TSS sample remains at the first dwell (850 ºC) for 20h, and at this temperature the stable phases are W+WC (Figure 3). It is possible that the permanence at this temperature for so long time, allows the establishment of bonding connections between the W and Cu atoms and formation of the $Cu_{0.4}W_{0.6}$ phase, that remains stable since the maximum sintering temperature doesn't exceed 1250 ºC (region of the W_2C formation).

Table 22 – Rietveld phase quantification after sintering.

Composition	Cu (%)	γ (%)	η- Phase (%)	$Cu_{0.4}W_{0.6}$ (%)	W_2C (%)	WC (%)
WCSS	-	0	48	-	0	52
WCu Conv. Sint	2	-	-	0	80	18
WCCu TSS	2	-	-	42	0	56
WC6SS6Cu	0	3	19	0	0	78

4.6.2. Microstructural characterization

After gridding and polishing, the samples were submitted to Murakami's chemical etching and subsequent SEM (scanning electron microscopy) analysis. The microstructures of the sintered samples are shown in Figure 52.

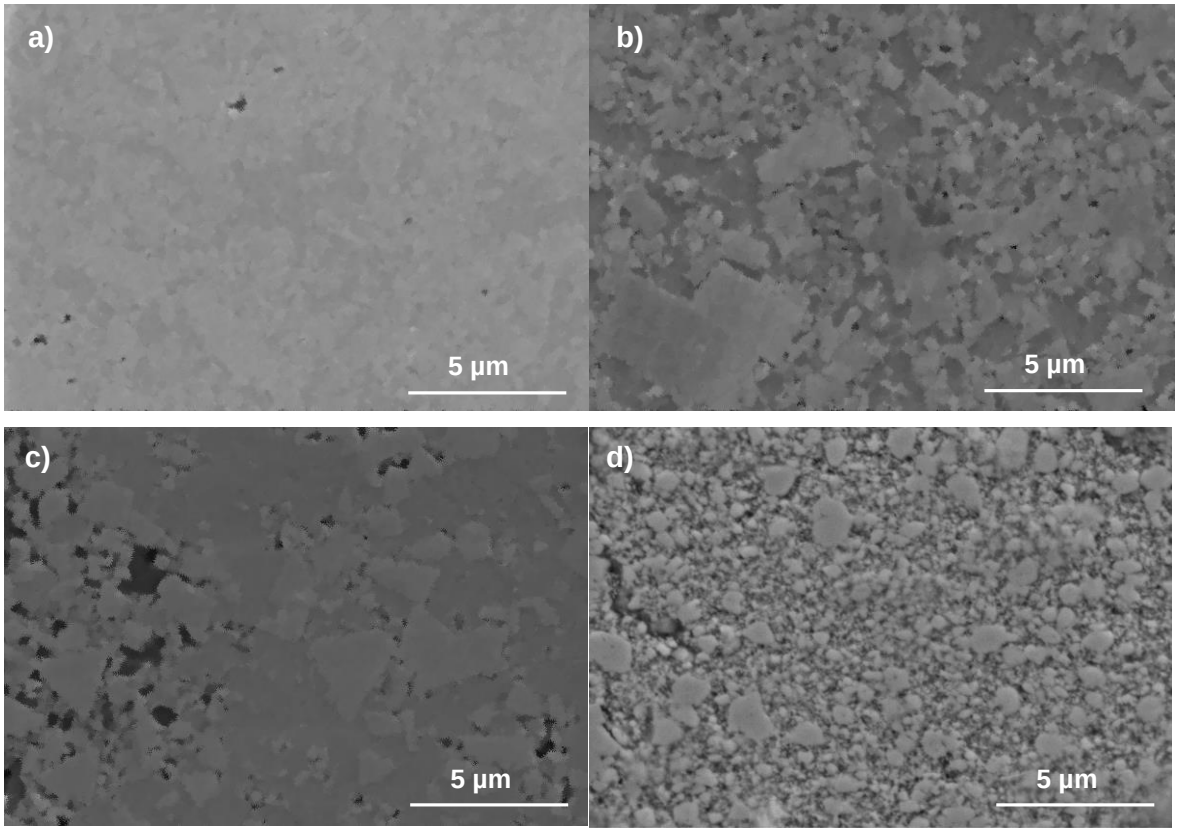

Figure 52 – SEM micrographs **a)** WCSS; **b)** WC10SS2Cu; **c)** WC6SS6Cu; **d)** WCCu.

There are two distinct phases in WCSS and WC10SS2Cu SEM micrographs (Figure 52 a) and b)). The light grey phase is attributed to WC grains and the dark grey phase is mainly η-phase, spread among the WC grains.

The WC grains are mostly characterized by their trigonal and parallelpipedic shape, also observable in the WC8SS4Cu and WC6SS6Cu composites (Figure 52c). It is also noticeable in these micrographs the presence of some larger grains amongst small ones. The average WC grain size and the grain size range are quantified in Table 23.

The WCCu composite was also morphologically characterized (Figure 52d). In this case the light grey colour corresponds to the W_2C grains (phase detected by XRD, Table 22). It can be seen that the W_2C grain shape is rounded and no abnormal grain growth is verified.The

W_2C grain size is the smallest of all the composites (Table 23), however it was not possible to fully densify this sample and the sintered relative density was 79%, due to the poor wettability of copper in WC.

Table 23 – Gain size quantification.

Composition	Grain size range (nm)	Average grain size (nm)
WCSS	50 - 4000	151
WCCu	100 - 1000	153
WC6SS6Cu	50 - 5000	638
WC8SS4Cu	50 - 4000	235
WC10SS2Cu	50 - 3000	161

There is a wide grain size distribution, ranging from some ten nanometers until the micrometric size, but due to the large amount of small grains, the average grain size values are small, within the nanometric/submicrometer range. This bimodal grain size distribution is normally referred as “abnormal grain size growth” (AGG) and is common to arise in hardmetals sintered from ultrafine and nanosized powders [107]. There is no concordance in literature about the explanation of this phenomena. Park et al. [108] suggested that AGG could occur only in the system with singular solid/liquid interface. In such a system, only a few grains larger than a minimum size, which have enough driving force, could grow fast by two-dimensional (2D) nucleation, leading to abnormally large grains. Another mechanism proposed by Ryoo et al. [109] is based on atomic adsorption mechanism and the AGG could be explained by coalescence of two or several prism-shaped WC grains. Sommer et al. [110] attributed this phenomenon to the chemical reactions in the carbon deficiency area at the outer areas of the sample, resulting in twin boundaries facilitating the fast grain growth. In Table 25 it is also visible that the smallest grain size found is c.a. 50 nm, it is though that the existence of such small grains, is due to the partial consumption of the WC grains for the formation of eta–phase during sintering, causing the size decrease.

Figure 53 a) and b) shows the microstructure and EDX maps of WC8SS4Cu and WC6SS6Cu composites. The dark grey phase (see signalled regions in Figure 53) is proved to be the iron rich binder phase.

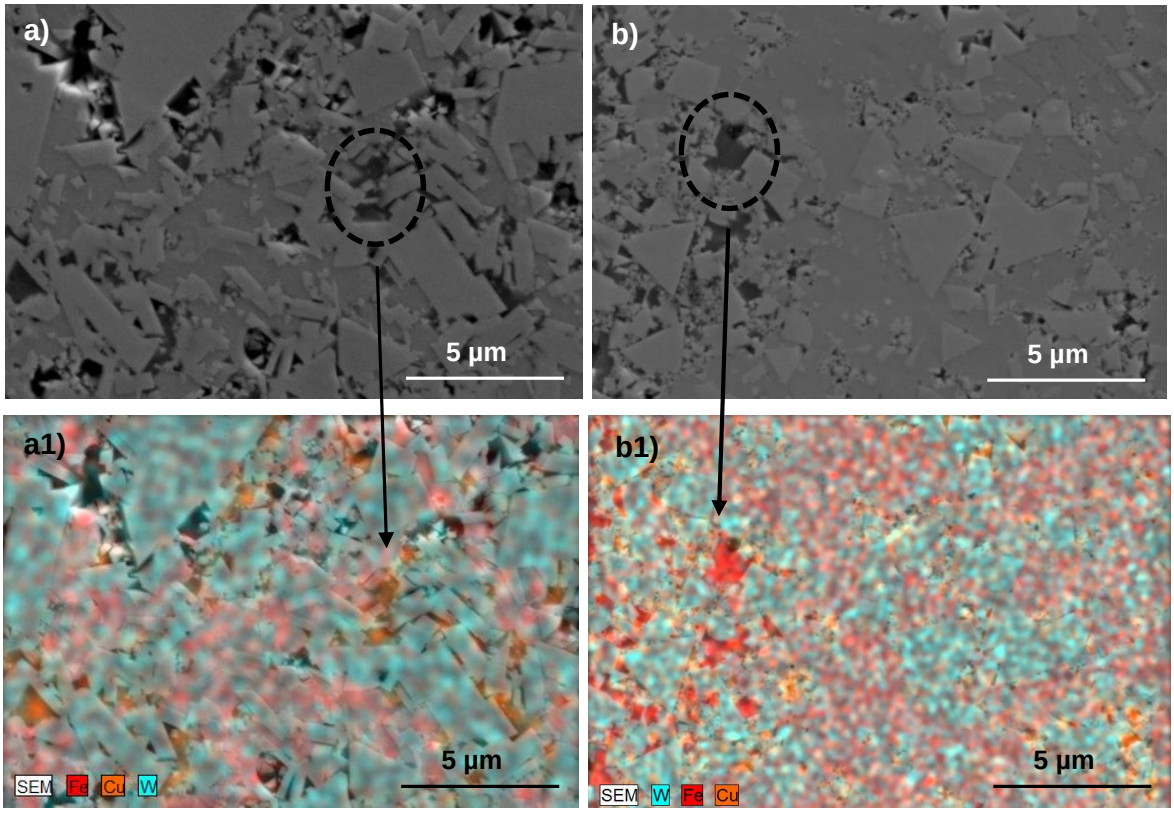

Figure 53 – a) WC8SS4Cu micrograph; **a1)** WC8SS4Cu X – Ray map; **b)** WC6SS6Cu micrograph; **b1)** WC6SS6Cu X – Ray map.

It was also performed an EDS analysis to confirm the presence of Cu in the WC10SS2Cu (phase not detected by XRD). The copper content detected in this composition was c.a 0.5 wt.%, below the XRD detection limit.

4.6.3. Mechanical characterization

In this work it was measured two of the most important mechanical properties of cemented carbides, i.e. hardness and fracture toughness (K_{1C}) (Table 24). The mechanical properties of WCCu sample were not measured since the attained densification is very low. In Figure 54 it is depicted an indentation image of the WCSS composite.

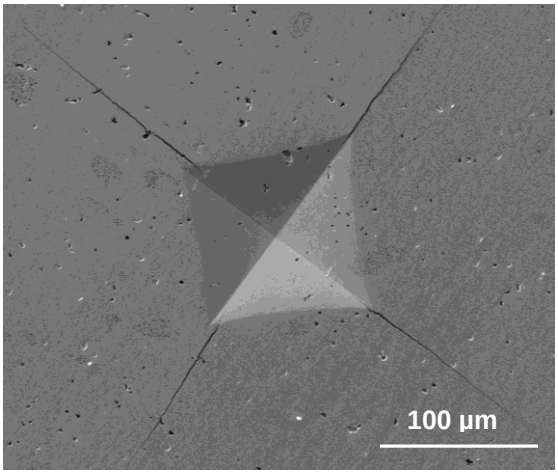

Figure 54 – WCSS indentation image.

Analysing the Table 24 it is possible to affirm that WCSS has the highest hardness (1850 HV30) and the WC6SS6Cu the lowest value (1029 HV30) of all the investigated compositions. In terms of fracture toughness (K_{1C}) the WCSS and the WC8SS4Cu presents similar values, 8.2 and 8.1 respectively, lower than those of WC6SS6Cu and WC10SS2Cu, 11.3 and 11.1, respectively. The value achieved for WC8SS4Cu composition is deviated from the fracture toughness expected trend.

Table 24 - Mechanical properties of sintered samples.

Composition	$\rho_{after\ HIP}$ (%)	Average grain size (nm)	Hardness (HV30)	K_{1C} (MPa.m$^{1/2}$)
WCSS	100	151	1850	8.2
WCCu	79	153	-	-
WC6SS6Cu	96	638	1029	11.3
WC8SS4Cu	99	235	1456	8.1
WC10SS2Cu	100	161	1610	11.1

Correlating the two mechanical properties, hardness and fracture toughness with the copper ratio in the binder phase it is possible to obtain Figure 55.

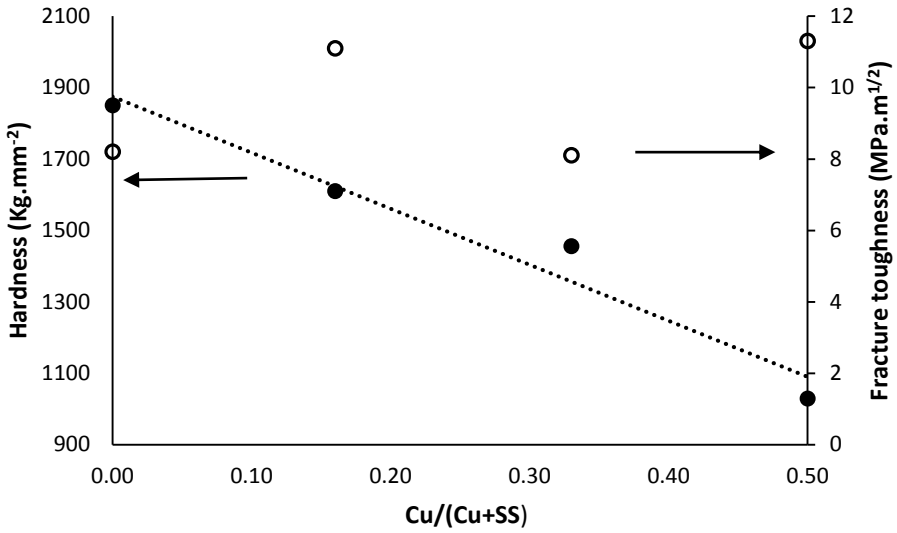

Figure 55 – Correlation of hardness and fracture toughness with the copper ratio in the binder phase.

Figure 55 shows that the copper increase in the binder leads to the hardness decrease and fracture toughness increase. However, due to different phases, grain sizes and relative sintered densities of composites, this relation appears to have some deviations from the ideal behaviour (linear increase of fracture toughness with hardness decrease).

Figure 56 shows the correlation between fracture toughness and hardness of sintered samples prepared by HEBM and conventional milling. The WC-Co composites are represented by green dots, while WCSS are represented by blue dots (conventional milling). The WCSS and WCSSCu composites in this work are pointed in red (Figure 56).

These two major groups (Conv. and HEBM) show distinct mechanical behaviours. The higher fracture toughness belongs to the conventional milled powders and the harder materials to the HEBM powders. Comparing the mechanical properties achieved by HEBM with the attained by Marques et al. [7] using conventional milling, it is observable that a great hardness improvement was reached.

However, the fracture toughness was sacrificed. It was expected a decrease in this property since the grain size was considerably reduced and significant eta-phase (brittle phase) amounts are formed.

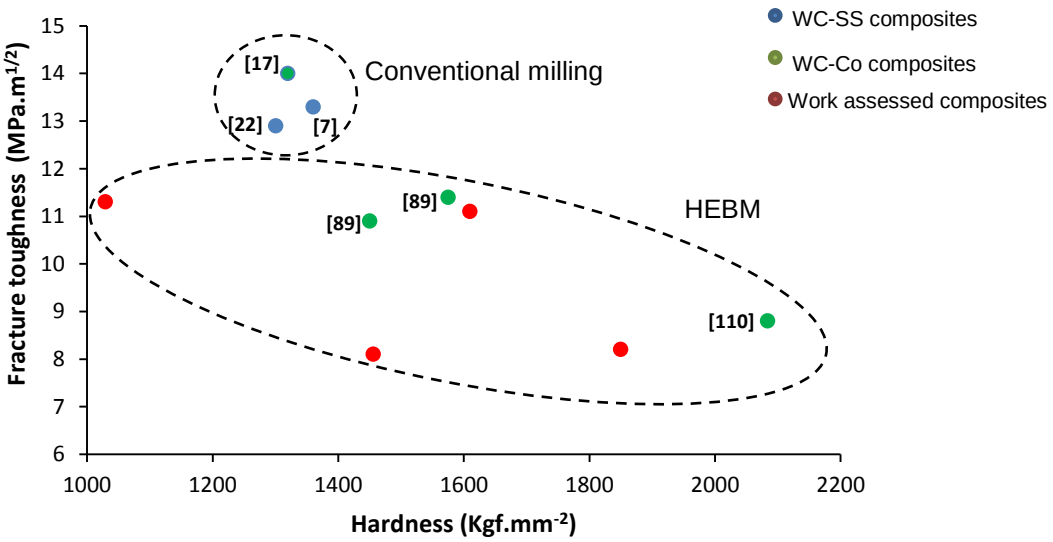

Figure 56 – Representation of the fracture toughness vs hardness. Compilation of the mechanical properties of HEBM (ellipse) and conventional milled (circumference) cemented carbides. The red dots represent the values obtained in the current work.

Comparing the mechanical properties attained for each tested composition in this work, with the commercially available WC-Co grades, several applications can be inferred, as is summarized in Table 25.

Table 25 – Possible application for the developed composites

Composition	Hardness (HV30)	K_{1C} (MPa.m$^{1/2}$)	Applications
WCSS	1850	8.2	Wire drawing, metal cutting and composite machining
WCCu TSS	-	-	Electrical applications
WC6SS6Cu	1029	11.3	Metal forming, can tooling, rolls, mineral and ground tools
WC8SS4Cu	1456	8.1	Wire drawing and metal cutting
WC10SS2Cu	1610	11.1	Composite machining, wire drawing and metal cutting

Therefore, manipulating the composition, milling and sintering conditions, it is possible to attain WCSS and WCSSCu composite materials, with a wide array of mechanical properties (hardness and fracture toughness). Making them suitable for a vast range of applications and in some cases can stand as an available alternative to the WC-Co based composites.

Chapter 5

Conclusions and future work

5. Conclusions and future work

In this work the feasibility of replacing cobalt by copper (Cu), and stainless steel (SS) binders in tungsten carbide based cemented carbides was investigated. In order to achieve WC-SS, WC-SS-Cu and WC-Cu composites with 12wt% of total binder amount, some processing variables of the high energy ball milling (HEBM) and sintering processes were investigated, taking into account structural and morphological parameters of powders and sintered samples, respectively. Finally, the composites mechanical characterization was performed.
The most important general conclusions are here schematically presented:

- **HEBM and powder characterization**

The study of the effect the milling time, ball-to-powder weight ratio and milling rotation speed in HEBM process allowed to select the rotation speed of 350 rpm, a ball-to-powder weight ratio of 20:1 and milling times between 8-10 hours as the best conditions to obtain homogeneous powders with nanometric sizes in the studied compositions. Using these conditions, composite powders of WC-SS, WC-Cu and WC-SS-Cu with reduced particle and crystallite sizes, ~200 nm and 10 nm, respectively, were obtainedHEBM proved to be a successful technique for the homogenization of the SS, Cu and SSCu distribution in the mixtures with WC, especially when compared to the conventional wet milling. Moreover, this process is a more environmentally friendly technique, since it does not use solvents.

- **Powders sintering and reactivity**

It was possible to densify HEBM composite powders at low temperatures and reduced sintering times. However, significant changes in the structure of the compacted powders occurred during sintering for the three studied cases, WC-SS, WC-SS-CU and WC-Cu.
For the WC-SS composite powders, the sintering takes place in two different stages: (I) slow but pronounced densification step starting at low temperatures, ~ 600ºC, in solid state sintering; (II) Densification due to the mechanisms of solution and precipitation in the liquid phase sintering. It is thought that, in the WC-SS composites the liquid phase formation is delayed to higher temperatures, due to the high reactivity of the precursor powders that reacts at low temperatures for the M_6C formation. Therefore, the amount of the binder phase

(SS) available for the liquid phase formation is reduced, perturbing the sintering shrinkage rate.

The WC-Cu sintering process occurs in three distinct stages: (I) small increase of density, attributed to the solid state sintering; (II) sharp increase in density endorsed to the liquid phase formation; and (III) slow densification due to the mechanisms of solution and precipitation in the liquid phase sintering. It was found that the liquid phase formation in the WC-Cu composites occurs in temperatures below the typical melting temperature (1083ºC), due to the nanometric size of Cu powder particles.

Besides WC, the WC-Cu sintered samples revealed two distinct major phases, W_2C and $Cu_{0.4}W_{0.6}$. Their formation depends on the sintering technique, namely conventional or two stage sintering, respectively. The $Cu_{0.4}W_{0.6}$ phase appearance was not expected since it was not predicted in the W-Cu phase diagram. The addition of Cu to the SS to form WC-SS-Cu composites is viable up to 30% of Cu, without substantial decrease of the sintered relative density. Moreover, adding Cu to the SS proved to be an effective way to decrease the M_6C formation.

- **Mechanical properties characterization**

The mechanical characterization revealed that the hardness of the obtained WCSS compacts is similar to the reported values in the literature for WC-Co, despite of the high amount of eta-phase formed. Nevertheless, the fracture toughness showed a significant deterioration.

Adding copper to the SS binder phase promotes the hardness decrement but, on the other hand, the fracture toughness values were improved. The mechanical properties of the WC-Cu composite were not evaluated since full densification of this composition was not reached.

- **Future work**

For future work, it is desirable the control of the composition and grain size through the addition of carbon and grain growth inhibitors (i.e VC, Cr_3C_2).

Further samples characterization such as, wear, corrosion, oxidation and transversal rupture strength should be also addressed.

Bibliography

1. C. M. Fernandes, A. M. R. Senos, and M. T. Vieira, *Versatility of the sputtering technique in the processing of WC–Fe–Ni–Cr composites.* Surface & Coatings Technology, 206: p. 4915 - 4921, (2012).
2. A. T. Santhanam, P. Tierney, and J. L. Hunt, *ASM Handbook, Cemented Carbides*Ohio, ASM international (1992).
3. [12/06/2013];Available from: http://www.indexmundi.com/minerals/?product=cobalt
4. A. Maximenko, O. V. D. Biest, A. Zavaliangos, and A. Laptev, *Recent developments in computer modeling of powder metallurgy processes*Kiev, IOS Press, (2001).
5. R. G. Cornwall, *Think bigger! the future is bright for MIM.* Metal Powder Report, 59: p. 8-11, (2004).
6. C. Suryanarayana and N. A. Aqeeli, *Mechanically alloyed nanocomposites.* Progress in Materials Science, 58: p. 383 – 502, (2013).
7. B. J. Marques, C. M. Fernandes, and A. M. R. Senos, *Sintering, microstructure and properties of WC-AISI304 powder composites.* Journal of Alloys and Compounds, 562: p. 164–170, (2013).
8. B. J. Marques, *O aço inoxidável como ligante no metal duro*, in *Departamento de Materiais e Cerâmica*Unversidade de Aveiro, (2010).
9. Y. Shinoda, Y. Yanagisawa, T. Akatsu, F. Wakai, and H. Fujii, *Development of Creep-Resistant Tungsten Carbide Copper Cemented Carbide.* Materials Transactions, 6: p. 1250 – 1254, (2009).
10. G. E. Totten, *Steel Heat Treatment: Metallurgy and Technologies*Portland, Taylor and Francis Group, (2006).
11. C. Wu and S. Zhang, *Ferrous Materials*Beijing, Metallurgical Industry Press, (1992).
12. K. Buss, *High temperature deformation mechanisms of cemented carbides and cermets*, École Polytechnique Fédérale de Lausanne, Lausanne, (2004).
13. O. H. Pierson, *Handbook of Refractory Carbides and Nitrides - Properties, Characteristics, Processing and Applications*New Jersey, Noyes Publications, (1996).
14. G. S. Upadhyaya, *Cemented Tungsten Carbides: Production, Properties and Testing*USA, Noyes Publications, (1998).
15. K. Chang-Soo, *Microstructural-Mechanical Property Relationships in WC-Co composites*, in *Materials Science and Engineering Department* Carnegie Mellon University, Pittsburgh, USA, (2005).
16. C. M. S. Fernandes, *Sputtering on the production of tungsten carbide based composites* in *Departamento de Engenharia Cerâmica e do Vidro*Universidade de Aveiro, Aveiro, (2008).
17. [cited 2013 15/06/2012]; Available from: http://www.hardmaterials.sandvik.com/.
18. S. H. Materials, *Cemented Carbide, Sandvik new developments and applications.* (2005).

19. Z. Yao, J. J. Stiglich, and T. S. Sudarshan, *Nano - grained Tungsten Carbide - Cobalt (WC/Co).* Materials Modification: p. 27, (1999).

20. A. S. Kurlov and A. I. Gusev, *Tungsten Carbides and W–C Phase Diagram.* Inorganic Materials, 42: p. 121–127, (2006).

21. P. Rautala and J. T. Norton, *Tungsten-cobalt-carbon-system.* Trans. AIME, 194: p. 1045-1050, (1952).

22. T. Farooq and J. T. Davies, *Tungsten Carbide hardmetals cemented with ferroalloys.* The International Journal of Powder Metallurgy, 27: p. 347 - 355, (1991).

23. A. S. Personnel, *The Atlas Steels Technical Handbook of Stainless Steels*Australia, Atlas Steels Technical Department, (2010).

24. *ASM Speciality Handbook, Stanless Steels*, ASM International, (1994).

25. *Engineering Properties of Steels* Metals Park, Ohio, American Society of Metals, (1982).

26. G. E. Totten, *Steel Heat Treatment: Metallurgy and Technologies* Portland, USA, Taylor and Francis Group, (2006).

27. D. R. Joseph, *Copper and copper alloys*Ohio, ASM International, (2001).

28. P. Skočovský, P. Palček, R. Konečná, and L. Várkoly, *Konštrukčné materiály*Žilina, Slovak republic, EDIS, (2000).

29. R. González, J. Echeberría, J. M. Sánchez, and F. Castro, *WC–(Fe, Ni, C) hardmetals with improved toughness through isothermal heat treatments.* Journal of Materials Science, 30: p. 3435 - 3439, (1995).

30. *Handbook of alloy phase diagrams*. Vol. 3, Ohio, ASM, (1992).

31. J. V. Vibhor, *Microstructure and properties of copper thin films on silicon substrates*, Texas A&M University Texas, (2007).

32. K. Mannersson, *WC grain growth during sintering of cemented carbides*, KTM industrial engineering and management, Stockholm, (2011).

33. R. Cooper, S. A. Manktelow, F. Wonf, and L. E. Collins, *The Sintering characteristics and properties of hard metal with Ni-Cr binders.* Materials Science and Engineering, A 105 - 106: p. 269 - 273, (1988).

34. S. Raghunahan, R. Caron, and P. Sandell, *Tungsten Carbide Technologies.* Advanced Materials & Processes, 4: p. 21 - 23, (1996).

35. A. F. Guillermet, *Thermodynamic properties of the Co - W - C system.* Metallurgical Transactions 20: p. 935 - 956, (1989).

36. B. Uhrenius, *Contribution to the knowlege of phase equilibia in tungsten - carbon based systems.* Scandinavian Journal of Metallurgy 20 p. 93 - 98, (1991).

37. *WC - Co enjoys proud history and bright future*, Metal Powder Report. p. 32 - 36, (1998).

38. C. B. Pollock and H. H. Stadelmaier, *The Eta Carbides in the Fe-W-C and Co-W-C systems.* Metallurgical Transactions, 29: p. 767 - 770, (1970).

39. C. M. Fernandes, A. M. R. Senos, and M. T. Vieira, *Control of eta carbide formation in tungsten carbide powders sputter-coated with (Fe/Ni/Cr).* Int. Journal of Refractory Metals and Hard Materials, 25: p. 310 – 317, (2007).

40. C. M. Fernandes, M. G. Willinger, M. T. Vieira, and A. M. R. Senos, *Interface Exploring of Tungsten Carbide-Stainless Steel Composites through HRTEM.* Microscopy and Microanalysis, 18(109 - 110), (2012).

41. H. Suzuki, T. Yamamoto, and N. Chujo, *Properties of WC-10% (Ni-Fe).* Jap.Soc.of Powder and Powder Metallurgy Journal, 14: p. 26 - 31, (1967).

42. C. Agte, *Entwicklung der Hartmetalltchnik in der DDR.* Neue Hutte, 9: p. 544, (1957).

43. D. Moskowitz, J. M. Ford, and M. Humenik, *High-Strength Tungsten Carbides; Modern Developments.* Powder Metallury, 5: p. 225 - 234, (1970).

44. A. F. Guillermet, *An assessment of the Fe-Ni-W-C phase diagram.* Zeitschrift - fur-Metallkunde, 78: p. 165 - 171, (1987).

45. H. J. Goldschimidt, *The structure of carbides in alloys steels Part II - Carbide formation in high - speed steels.* Journal of the iron and steel institute, 170: p. 189 - 204, (1952).

46. M. Bergström, *The eta-phase in the quaternary system Fe-W-C-Cr at 1250 ºC.* Materials Science and Engineering, 27: p. 271 - 278, (1977).

47. L. J. Kecskes, M. D. Trexler, B. R. Klotz, K. C. Cho, and R. J. Dowding, *Mechanical alloying effects in ball-milled Tungsten-Copper (W-Cu) composites*, U.S. Army Research Laboratory, Aberdeen, (2001).

48. G. G. Lee, G. H. Ha, D. W. Lee, B. K. Kim, and I. S. Ahn, *Synthesis of W/Cu Composite Alloys by Thermochemical Method*, in *TMS Annual Meeting Chemistry and Physics of Nanostructures and Related Non-Equilibrium Materials*TMS Society Press, Warrendale, PA. p. 163 - 170, (1997).

49. M. L. Ovecoglu and B. Ozkal., *Comparison of the Sintering Characteristics of Ball-Milled and Attritor-Milled W-Ni-Fe Heavy Alloy.* Journal of Materials Research, 11: p. 1673-1682, (1996).

50. J. C. Kim and I. H. Moon, *Sintering of Nanostructured W-Cu Alloys Prepared by Mechanically Alloying.* Nanostructured Materials, 10: p. 283 - 290, (1998).

51. T. B. Massalski, H. Okamoto, P. R. Subramanian, and L. Kacprzak, *Binary Alloy Phase Diagrams*, 2nd edNew York, William W. Scott Publishers, (1990).

52. C. Suryanarayana and N. Al-Aqeeli, *Mechanically alloyed nanocomposite.* Progress in Materials Science, (2012).

53. C. Suryanarayana, *Mechanical alloying and milling.* Progress in Materials Science, 46: p. 1 - 184, (2001).

54. S. A. Hewitt, *Consolidation of WC - Co Nanocomposites synthesised by mechanical alloying.* University of Wolverhampton, Wolverhampton, (2009).

55. E.-. Eskandatany, M. S. Sumiyana, K. Aoki, and K. Suzuki, *Reactive ball mill for solid state synthesis of metal nitrides powders.* Materials Science Forum, 801: p. 88-90, (1992).

56. S. J. Campbell and W. A. Kaczmarek, *Mössbauer spectroscopy applied to materials and magnetism*New York, Plenum pres, (1990).

57. J. Missiaen and S. Roure, *A general morphological approach of sintering kinetics: application to WC–Co solid phase sintering.* Acta Materialia, 46: p. 3985 - 3993, (1998).

58. A. Mukhopadhyay and B. Basu, *Recent developments on WC-based bulk composites.* Journal of Materials Science, 46: p. 571–589, (2011).

59. G. G.-. Muginstein, *Sintering study of nanocrystalline tungsten carbide powders.* Nanostructured Materials, 10: p. 795 - 804, (1998).

60. W. D. Schubert, A. Bock, and B. Lux, *General Aspects and Limits of Conventional Ultrafine WC Powder Manufacture and Hard Metal Production* International Journal of Refractory & Hard Metals, 13: p. 281 - 296, (1995).

61. L. Froschauer and R. Fulrath, *Direct observation of liquid-phase sintering in the system tungsten carbide - cobalt.* Journal of Materials Science, 11: p. 142 - 149, (1976).

62. S. Haglund, J. Agren, P. Lindskog, and B. Uhrenius, *Solid state sintering of cemented carbides*. Sintering TechnologyNew York, Marcel Dekker, (1995).

63. E. Soares, *Industrial development of submicron to ultrafine WC-Co hardmetal grades* Universidade do Porto, Porto, (2012).

64. G. Gille, *Submicron and ultrafine grained hardmetals for microdrills and metal cutting inserts.* International Journal of Refractory Metals and Hard Materials, 20: p. 3 - 22, (2002).

65. G. Upadhyaya, *Materials science of cemented carbides: an overview.* Materials & Design, 22: p. 483 - 489, (2001).

66. R. J. Nelson and D. R. Milner, *Densificationprocesses in the tungsten carbide - cobalt system* Powder Metallurgy, 15: p. 346 - 363, (1972).

67. R. M. German, *Liquid Phase Sintering*New York, Plenum Press, (1985).

68. K. Buss, *High temperature deformation mechanisms of cemented carbides and cermets*, in *Institut de physique de la matière complexe*École Polytechnique Fédérale de Lausanne, Lausanne, (2004).

69. W. D. Kingery, *Densification during sintering in the presence of a liquid phase. I. Theory.* Journal of Applied Physics, 30: p. 301 – 306, (1959).

70. G. H. S. Price, C. J. Smithells, and S. V. Williams, *Sintered Alloys. Part I. - Copper-Nickel-Tungsten Alloys Sintered with a Liquid Phase Present.* Journal: Institute of metals, 62: p. 239 - 264, (1983).

71. A. Laptev, *Theory and technology of sintering, thermal and chemicothermal treatment.* Powder Metallurgy and Metal Ceramics, 46: p. 317 - 324, (2007).

72. R. M. German, *Liquid Phase Sintering*New York, Plenum Press, (1985).

73. G. M. Randall, S. Pavan, and J. P. Seong, *Review: Liquid phase sintering.* Journal of Materials Science, 44: p. 1 - 39, (2009).

74. R. J. Nelson and D. R. Milner, *Densificationprocesses in the tungsten carbidecobalt system.* Powder Metallurgy, 15: p. 346 - 363, (1972).

75. Y. Wang, A. Delanoé, S. Lay, E. Pauty, and C. H. Allibert, *Morphology and growth of WC grains in WC-Co cermets. Effect of C/W ratio and Cr addition* Materiaux: p. 1 - 5, (2002).

76. R. Porat, S. Berger, and A. Rosen, *Study of the sintering mechanism of submicron carbides.* Acta Materialia, 7: p. 429 - 436, (1996).

77. L. Sun, C. Jia, and M. Xian, *A research on the grain growth of WC–Co cemented carbide.* International Journal of Refractory Metals and Hard Materials, 25: p. 121 - 124, (2007).

78. A. Petersson and J. Agren, *Sintering shrinkage of WC–Co materials with different compositions.* International Journal of Refractory Metals and Hard Materials, 23: p. 258 - 266, (2005).

79. K. H. Cho, J. W. Lee, and I. S. Chung, *A study on the formation of anomalous large WC grain and the eta phase.* Materials Science and Engineering, 209: p. 298 - 301, (1996).

80. D. Y. Yang and S. J. L. Kang, *Suppression of abnormal grain growth in WC–Co via pre-sintering treatment.* International Journal of Refractory & Hard Metals, 27: p. 90 – 94, (2009).

81. J. Weidow and H. O. Andrén, *Grain and phase boundary segregation in WC–Co with TiC, ZrC, NbC or TaC additions.* International Journal of Refractory & Hard Metals, 29: p. 38 - 43, (2011).

82. C. M. Fernandes, A. M. R. Senos, M. T. Vieira, and J. V. Fernandes, *Composites from WC powders sputter-deposited with iron rich binders.* Ceramics International, 35(4): p. 1617-1623, (2009).

83. C. M. Fernandes, A. M. R. Senos, and M. T. Vieira, *Sintering of tungsten carbide particles sputter-deposited with stainless steel.* International Journal of Refractory Metals and Hard Materials, 21(3–4): p. 147-154, (2003).

84. Z. Z. Fang, X. Wang, T. Ryu, K. S. Hwang, and H. Y. Sohn, *Synthesis, sintering, and mechanical properties of nanocrystalline cemented tungsten carbide – A review.* Int. Journal of Refractory Metals and Hard Materials, 27: p. 288 – 299, (2009).

85. K. Jia, E. T. Fischer, and B. Gallois, *Microstructure, hardness and toughness of nanostructured and conventional WC–Co composites.* Nanostructed Materials, 10: p. 875 – 891, (1998).

86. H. Gleiter, *Materials with ultrafine microstructures: retrospectives and perspectives.* Nanostruct Mater, 1: p. 1 – 19, (1992).

87. M. S. El-Eskandarany, A. A.Mahday, H. A. Ahmed, and A. H. Amer, *Synthesis and characterizations of ball-milled nanocrystalline WC and nanocomposite WC–Co powders and subsequent consolidations.* Journal of Alloys and Compounds, 312: p. 315 – 25, (2000).

88. C. G. Lin, E. Kny, G. S. Yuan, and B. Djuricic, *Microstructure and properties of ultrafine WC–0.6VC–10Co hardmetals densified by pressure-assisted critical liquid phase sintering.* Journal of Alloys and Compounds, 383: p. 98 – 102., (2004).

89. D. Sivaprahasam, S. B. Chandrasekar, and R. Sundaresan, *Microstructure and mechanical properties of nanocrystalline WC–12Co consolidated by spark plasma sintering.* International Journal of Refractory & Hard Metals, 25: p. 144 – 152, (2007).

90. S. A. Hewitt and K. A. Kibble, *Effects of ball milling time on the synthesis and consolidation of nanostructured WC–Co composites.* Int. Journal of Refractory Metals and Hard Materials, 27: p. 937 – 948, (2009).

91. I. J. Shon, I. K. Jeong, I. Y. Ko, J. M. Doh, and K. D. Woo, *Sintering behavior and mechanical properties of WC–10Co, WC–10Ni and WC–10Fe hard materials produced by high-frequency induction heated sintering.* Ceramics International, 35: p. 339 –344, (2009).

92. E. Soares, L. F. Malheiros, J. Sacramento, M. A. Valente, and F. J. Oliveira, *Solid and Liquid Phase Sintering of Submicrometer Carbides with Different Cobalt Contents.* Journal of American Ceramic Society, 95: p. 1822 – 1831, (2012).

93. *Materials Characterization*, 9 ed. ASM Handbook. Vol. 10, USA, ASM Hnternational, (1992).

94. W. Pabst and E. Gregorová, *Characterization of particles and particle systems* Institute of Chemical Technology, Prague, (2007).

95. B. D. Cullity, *Elements of X-ray Diffraction*, 2 ed, Addison-Wesley Publishers, (1978).

96. I. Lahiri, *Compaction and sintering response of mechanically alloyed Cu–Cr powder.* Powder Technology, 189: p. 433–438, (2009).

97. B. Roebuck and E. A. Almond., *Deformation andfracture processes and the physical metallurgy of WC/Co hardmetal.* International Materials Review, 33: p. 90 - 110, (1988).

98. C. B. Ponton and R. D. Rawlings, *Vickers indentation fracture toughness test: Review of literature and formulation of standardized indentation thoughness equations.* Materials Science and Technology, 5: p. 865 - 872, (1989).

99. C. L. Castro and B. S. Mitchell, *The use of polymeric milling media in the reduction of contamination during mechanical attrition.* Journal of Materials Research, 17: p. 2997 - 2999, (2002).

100. J. S. Benjamin, *Mechanical alloying – a perspective.* Metal Powder Report, 45: p. 122 – 127, (1990).

101. R. Vassen and D. Stover, *Compaction Mechanisms of Ultrafine Sic Powders.* Powder Technology, 72(3): p. 223-226, (1992).

102. L. I. Trusov, T. P. Khvostantseva, V. I. Novikov, M. Y. Tanakov, and V. Y. Varyanitsa, *Size Effects of Deformation in Nanocrystalline Ni.* Mechanical Behaviour of Materials-Vi, Vols 1-4: p. C667-C671, (1992).

103. G. S. Boltachev and N. B. Volkov, *Size effect in nanopowder compaction.* Technical Physics Letters, 36(9): p. 823-826, (2010).

104. Z. Mirski and T. Piwowarczyk, *Wettability of hardmetal surfaces prepared for brazing with various methods.* Archives of Civil and Mechanical Engineering, 11(2): p. 411-419, (2011).

105. W. D. Schubert, A. Bock, and B. Lux, *Aspects of ultrafine hardmetal sintering*. Adv. Powder Metallurgy Particulate Materials. Vol. 3, Princeton, NJ, Princeton University Press, (1999).

106. F. Doré, S. Lay, N. Eustathopoulos, and C. H. Allibert, *Segregation of Fe during the sintering of doped W–Cu Alloys.* Scripta Materialia, 49: p. 237 - 242, (2003).

107. T. Li, Q. Li, L. Lu, J. Y. H. Fuh, and P. C. Yu, *Abnormal grain growth of WC with small amount of cobalt.* Philosophical Magazine, 87(36): p. 5557-5671, (2007).

108. Y. J. Park, N. M. Hwang, and D. Y. Yoon, *Abnormal growth of faceted (WC) grains in a (Co) liquid matrix.* Metallurgical and Materials Transactions. A, 27 p. 2809 - 2819, (1996).

109. H. S. Ryoo and S. K. Hwang, *Anisotropic atomic packing model for abnormal grain growth mechanism of WC-25wt.%Co alloy.* Scripta Materialia, 39(11): p. 1577-1583, (1998).

110. M. Sommer, D. W. Schubert, E. Zobetz, and P. Warbichler, *On the formation of very large WC crystals during sintering of ultrafine WC-Co alloys.* International Journal of Refractory Metals and Hard Materials, 20: p. 41 - 50, (2002).